Università Campus Bio-Medico di Roma

Dottorato in Bioingegneria e Bioscienze

XXXII ciclo a.a. 2016-2017

Human-inspired control strategy for hand prosthetics

Cosimo Gentile

Coordinatore:

Prof. Giulio Iannello

Tutor:

Prof. Loredana Zollo

Co-Tutor

Dr. Francesca Cordella

To Carmen.
Without her, this Ph. D. wouldn't be even possible.

To my unlces Peppe and Pippo.
They left this world too early, too young.

Abstract

The hand is the human body part that has always fascinated researchers: several studies have been conducted to understand and explain its perfect mechanism.

The hand is used to learn and to interact with the environment and it is clear that hand loss involves irreparable damage for a person. Besides having suffered hand loss, monolateral amputee subjects need to learn how to perform everyday life actions with only one hand. To overcome this problem, since the ancient Egypt, prostheses have been used for both cosmetic and functional purposes.

The functioning of an active prosthetic hand is guaranteed by a mechatronic device, a decoding system to decode human biological signals in gestures and a control law that translates all the inputs (from the hand and from the user) in the desired movement.

The ambition of this thesis is to design and develop a control strategy able to improve grasp and manipulation capabilities of prosthesis based on the tactile sensorization and on the use of this information in the control strategy. The proposed strategy is divided into 3 levels: low-level to regulate force and slippage during the whole grasp, middle-level, to manage the pre-shaping and the fingers reaching to the object, high-level, to decode the biological human signals in movements and force levels.

The greatest limitation for an amputee subject who uses a prosthesis having no sensory feedback is the difficulty to manage unexpected events in an autonomous way. In grasp and manipulation tasks, the possibility

of the object slippage is high. For this reason, it is necessary to detect the beginning of the slippage and provide control with a fast contrast action. The first contribution of this thesis is the development of a touch-and-slippage detection algorithm for effective grasp control of a prosthetic hand embedding monoaxial, low-cost sensors is proposed.

One of the main problems in the prosthetic hand design is to provide the hand with a reliable system for force and slippage control. To decrease the attention level and the cognitive burden for the user during grasp tasks, an automatic strategy is necessary. The second contribution of this thesis is to propose a force-and-slippage control strategy able to i) regulate the grasping force, ii) prevent the slippage events, iii) coordinate fingers for replicating a human-like behaviour on the prosthetic system. Real-time reaction to slippage events and finger coordination have been achieved by means of i) a force control with inner position loop, ii) a sensorization system giving information about the applied normal forces, and iii) an approach for controlling the fingers in a coordinated manner on the basis of the virtual finger concept.

The middle-level is managed with a proportional position control where the user can actively close or open the hand.

The high-level proposed in this thesis consists of a hierarchical classification system used to simultaneously discriminate hand/wrist gestures and desired force levels. Moreover, a system composed of software for the EMG signals management and virtual reality were ad-hoc developed for upper limb amputees underwent the Targeted Muscle Reinnervation (TMR) to train them to control multiple prosthetic modules in a coordinated manner in a safe environment.

Dexterity and manipulations skills in humans are allowed by complex biomechanics of the hand and a control loop based on a bidirectional communication with the brain, thanks to a sophisticated sensory system. This thesis has contributed to show the possibility to enable real-time

closed-loop control of bionic hands in tasks of fine grasp and manipulation. Force and slippage sensations were elicited in an amputee by means of biologically inspired slippage detection and encoding algorithms, supported by an extended stick-slip model of the performed grasp. Closed-loop control capabilities enabled by the neural feedback were compared with those achieved without feedback.

Table of contents

List of figures

List of tables

Chapter 1

Introduction

The human hand is a complex system studied for thousands of years which still fascinates many researchers in different fields, and replicating its correct functioning on a prosthesis [1] is still an open challenge.

Actual commercial myoelectric prosthesis hands are simple devices that allow the opening and the closing, as a gripper [2], by using two antagonist muscles [3], such as flexion and extension of the wrist [4]. It is an unnatural and not intuitive behaviour and for this reason, many amputees use cosmetic prosthesis [5, 6].

To replicate a human hand on a device is necessary not only the external aspect but also the functions [7]. In the last years, there were several attempts but not taking into account a complete replication of the human hand [8].

Control strategies for active prosthetic hands

In the world, there are 10 million amputees, 30% are upper limb amputees [9]. Traumatism is the first cause of upper limb amputation, followed by neoplasia and vascular or infectious diseases [10]. In Italy and UK, people who underwent upper limb amputations are estimated among 3500 and 5200. The different levels of upper limb loss present an incidence of: 16% trans-humeral, 12% transradial, 2% forequarter, 3% shoulder disarticulation, 1% elbow disarticulation, 2% wrist disarticulation, 61% transcarpal, and 3% bilateral limb loss [11].

Over the years, several studies were performed to return a good hand functioning to amputees. First attempts of control strategies for hand prostheses date back to 60' where different prototypes have been developed with hardware-electronic or logical-programming solutions [12]. Although knowledge of the brain was scarce at that time, it nevertheless

proved sufficient to develop multiple-layers control strategies inspired to the distinct phases of the prehension [13] to replicate the human-hand behaviour on a robotic hand [14].

The Southampton Adaptive Manipulation Scheme (SAMS) [15–18] replicates the behaviour of motor control in the Central Nervous System (CNS). Amputee subjects, through muscle contractions, can choose the grasp to be performed with the prosthesis and then go to various states. Once chosen the hand configuration, with a muscle contraction the hand starts the movement until the object is touched. Hence, the automatic control is activated to regulate the interaction force and to manage slippage, by increasing the force during the whole event. In this phase, the user can squeeze or release the object. This strategy has a limited number of states that allow the user to manage, with a low cognitive burden, force and slippage without feedback. Nevertheless, the transition between states is possible through muscle contraction and co-contraction, that is perceived as an unnatural behaviour.

The strategy proposed in [19] is divided into two phases: the first one is for the high-level control and the second one is focused on the low-level control. The high-level decodes the user intentions from his/her biological signals and, consequently, choices the desired grasp (i.e. cylindrical, spherical, tri-digital or lateral [20]) and force level (high or low). The low-level is composed of two subphases: the pre-shaping and the grasping phases. During pre-shaping, it is possible to choose the fingers involved in the grasp. In the grasp phase, the hand closes the fingers using force control algorithms until a reference global force is reached. The reference global force is calculated as the sum of the desired forces applied by each finger involved in the grasp and it is also useful when some fingers close without touching the object. Each finger can grip the object with the same force (the global force divided by the involved fingers in the grasp) but if a finger closes without touching the object,

the global force is redistributed among the rest of the involved fingers, with a safety margin that stops the finger to avoid a finger break.

The strategy in [21] consists of four parts: pre-shaping, closing, force control and detection stages. In the pre-shaping stage, the user can select the desired hand configuration among four possibilities: cylindrical, tip, lateral and open hand. After this phase, the hand closes with the maximum velocity until the contact with the object. This is the closing stage in which the velocity derivative is computed to determinate the touch and then the activation of the stage. After the contact with the object, the force control is activated and it is possible to modulate the force exerted on the object surface. This stage is alternated with the detection stage. The force reference of 1 N is empirically determined as a trad-off between object deformation and initial slippage. With a force within 5% of the reference value, the motor is turned off to reduce the power consumption, the possible oscillatory behaviour and to prevent overshoots because the response of each finger is slowed down. The detection stage is activated when the stable grasp is reached. In this stage, to detect the eventual object slippage, the information from the derivative of the force sensor resistor signal (FSR, for the detecting disturbance) and resistive flex sensors (RFS, for the detection of the unintended object) signals are used. If the slippage is detected, in the force control stage the reference force is increased (with an empirical increase in force).

The strategy described in [22] is a hierarchical human-inspired architecture. With the Petri net formalism, it is possible to describe tasks: a place represents a motor program, while transitions are action or event that allows the motor program execution. The Human-Machine Interface (HMI) is devoted to measure and to interpret biological signals from the human to identify four types of grip postures (rest, open hand, power grip and tripod grip [23]) to send to the below level. Haptic Perception

(HP) level receives information from the robotic hand sensors and from the HMI and generates information (contact and slip) to the high-level control (HLC). Contact is identified with a minimum threshold to differentiate between signal noise and contact with the object. With a first-order time derivative of the force signal is possible to detect the slip. HLC receives information from HP and HMI and coordinates the execution order of the motor programs for the user task, by sending the commands to the mid-level control (MLC). It also shares information with the learning module that acquires new behaviours and stocks recently learned information. MLC receives information from the above levels and generates a low-level command (LLC). It also shares information with the knowledge database as joint positions, motor primitives and sends newly learned facts to be stored in a memory. The motor programs are: Repose, default state of the hand; Pre-shaping, the hand is configured on a primitive to prepare to grasp the object; Grasping, a PI force control strategy (when the HLC detects the contact) is executed to obtain a stable grip without slippages; Slip, 10 per cent Proportionally force increases to contrast the slippage event (when the HLC detects the contact); Release, hand completely opening; Point finger, hand with the extended index finger; Reaching, forearm movement to reach the object; Wait, standby state in which an action is executed. The LLC level receives information from the hand sensors and generates the commands for the hand actuator and for the patient sensory feedback system. A PID position control is used for the tracking of the trajectories in the pre-shaping phase and a PI control to maintain the desired force in the grasping phase.

These control strategies showed a subdivision in states inspired by the human hand: the choice of the hand initial configuration is managed by the user by means of EMG signals, pre-shaping is possible by using pre-determined forces and positions values [24], touch and control of

force and slippage are completely automatic, lightening the cognitive burden to the amputees.

The analyzed studies have shown common critical points, summarized in the Table 1.1:

- The subject, through EMG signals, can only choose the grasping configuration, but the simplicity of this functionality requires special attention when the hand starts closing because the velocity applied [25] before touch could cause the object to go out of the grasping area [26];
- A reach phase where the subject can voluntarily control fingers during the object approach is missing;
- Without a reaching phase, predetermined configurations are necessary for the pre-shaping phase necessary, that cannot be used with a great number of objects (or shapes);
- Except for the SAMS, in the other ones, it is not possible to increase force during the automatic control.

The contribution of this thesis is to overcome these critical issues by developing and experimentally testing a control strategy, inspired to the human hand [27], able to improve grasp and manipulation capabilities of prostheses based on the tactile sensorization and on the use of this information in the control strategy. The main features addressed in this thesis are: i) to sensorize an active prosthetic hand in order to use this information ii) to detect touch and slippage information during the whole grasp, iii) used to regulate the force and to avoid the slippage during the grasp by using a force-and-slippage control law strategy; iv) to coordinate fingers during the grasp with a strategy based on the virtual finger concept; v) to classify both

Table 1.1 Summary of the reported analysis

Control strategy	Strategy subdivision	Pros	Cons
SAMS [15–18]	1. Automatic loop 2. Intermediate: 2.1. Posture logic 2.2. Force logic 3. Command logic	- A limited number of transintion states - Force and slippage automatically managed - Force increment allowed	- Muscle contraction and co-contraction to change transition states - Lack of a reaching phase - Lack of a fingers coordination strategy
[19]	1. High level: 1.1. Decoding of user intentions signals 1.2. Choosing desidered grasp and forces 2. Grasping task: 2.1. Pre-shaping 2.2. Grasping phase	- Force and slippage automatically managed - User's intervention for the configuration choice	- Limited force and positions choice - Lack of a reaching phase - Lack of a fingers coordination strategy - Force increment not allowed
[21]	1. Pre-shaping 2. Closing 3. Force control 4. Detection stage	- Force and slippage automatically managed - User's intervention for the configuration choice	- Slippage management after the reaching of the stable grasp - Lack of a reaching phase - Lack of a fingers coordination strategy - Force increment not allowed
[22]	1.Human-Machine Interface (HMI) 2. Haptic Perception (HP) 3. High-level control (HLC) 4. Mid-level control (MLC) 5. Low-level command (LLC)	- Force and slippage automatically managed - User's intervention for the configuration choice - Reaching phase	- Reaching phase is the forearm movement to reach the object - Lack of a fingers coordination strategy - Force increment not allowed

gestures and forces by using EMG signal with a hierarchical classification approach, with the aim to assess the desired hand/wrist gestures, as well as the desired force levels to exert during grasping tasks.

The proposed approach

The proposed control strategy presents different levels inspired by the human hand (Figure 1.1).

In the low-level (Figure 1.1), slippage detection to prevent the object fall is important because the amputee has no feedback to apply more force to contrast it [28]. Hence, **the first contribution of this thesis is to propose an algorithm able to detect i) the touch between the sensors embedded in the prosthesis and the object surface, ii) the slippage events, by using the only normal component of the force applied on the sensor.** When the touch between the object and the involved fingers is detected, the automatic control is activated and it is possible to regulate the force during the grasp and avoid the object slippage by using additional information from sensors and/or from algorithms. Hence, **the second contribution of this thesis is to propose a hand force-and-slippage control (Figure 1.1) able to i) reach the object with a position increment until the touch occurs, i) regulate the grasping force, ii) prevent the slippage events, iii) coordinate fingers for replicating**

a human-like behaviour on the prosthetic system. Real-time reaction to slippage events and finger coordination were achieved by means of i) a force control with inner position loop, ii) a sensorization system giving information about the applied normal forces, and iii) an approach for controlling the fingers in a coordinated manner on the basis of the virtual finger concept [29].

In the middle-level (Figure 1.1), once the desired movement is obtained, thanks to the pre-shaping it is possible to activate only the involved fingers and then close them with a gradual increment of the position, up to reach the object surface (i.e. position control performed by the user). In this phase is also possible to open the hand, in the same way.

In the high-level (Figure 1.1), the human biological signals (e.g. electromyographic are typically used [30]) are acquired and processed to extract information about the desired movement, with different techniques, as described in Section 2. In this phase, it is important to correlate the decoded movement with the natural way the user performs it to ensure him the intuitiveness of the gesture. The choice of the movement is obtained by the decoding of human biological signals can be changed in each time and in each phase, to replicate the will from the user to switch the configuration during the grasp. Hence, **the third contribution of this thesis is to propose and test a hierarchical pattern recognition strategy to simultaneously identify desired hand/wrist gestures and force levels starting from EMG signals. In details, a Finite State Machine (FSM) scheme is introduced to manage desired hand/wrist gestures and force levels, following a hierarchical approach. The "hand/wrist gestures classifier" is devoted to identifying the desired hand/wrist class among 7 gestures (rest, spherical, platform, point, tip, wrist pronation, wrist supination). The output of this classifier determines the next classifier used in the hi-**

erarchy. If the output of this classifier is "Spherical" motion class, then the "Spherical force classifier" is used to determine the desired force level (low, medium, high) to exert on an object. This second classifier is conditioned on the decision of the first classifier. The same strategy is adopted if the output of the first classifier is "Tip" motion class. Thus, the classifiers of the second level of the hierarchy discriminate the force levels applied during the related grasping class. If the output of the first classifier is any hand/wrist gestures different from "Spherical" or "Tip" gesture, no force classifiers are activated. Hand and wrist gestures are classified by using the single "hand/wrist gestures classifier". The FSM use allowed the two classifiers of different grades of the hierarchy to work simultaneously. Until the "Spherical" or "Tip" state is classified by "hand/wrist gestures classifier", the "Spherical force classifier" or the "Tip force classifier" intervenes to discriminate force levels. Moreover, i) a software and ii) a virtual reality were ad-hoc developed for upper limb amputees underwent the TMR. The first one aims to identify the movements intention of the user and train him/her to control multiple prosthetic modules in a coordinated manner. The second one provides a safe environment where the amputee can improve his/her capabilities before trying the prosthesis.

Although these actions are automatic, the user can intervene if he wants to increase the force. With a signal derived from the EMG-force classification of the high-level [31], the user adds value to the reference force; the maximum force increment, built on the correspondent maximum human signal performed, is limited in a safe range to avoid the object and prosthetic breaking. The human signal relaxation leads the subtraction of the previous increment until return to the initial reference value when the signal activity is close to zero.

If the user wants to open the hand from the automatic control, he performs the corresponding movement class and the robotic hand opens the involved fingers. After losing the touch signal, the control returns in the middle-level; the opening occurs as the closing, but the user could re-close the hand starting a new grasp. It is not necessary to return to the configuration in which the hand is completely open to choose a new configuration or a new grasp.

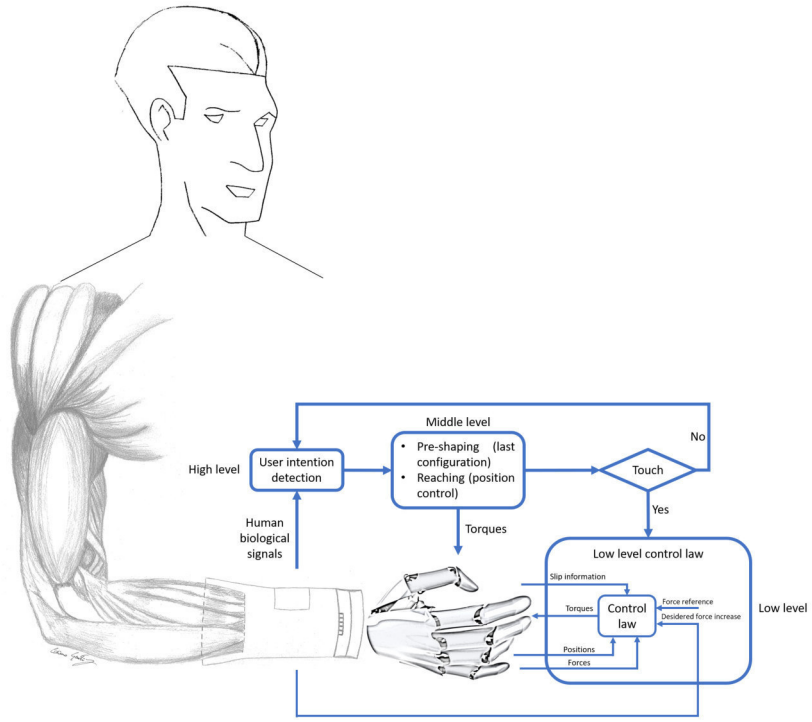

Figure 1.1 The proposed hand force-and-slippage control

Dexterity and manipulations skills in humans are allowed by complex biomechanics of the hand and a control loop based on a bidirectional communication with the brain, thanks to a sophisticated sensory system. The restoration of sensory information to the amputee, through neural

electrodes, allows a physiological motor control of the hand prosthesis. Hence, **the developed modules above described have contributed restoring a real-time force-and-slippage closed-loop control (Figure 1.2) that i) includes an amputee subject in the control loop through invasive neural electrodes, ii) provides close-to-natural force and slippage sensations to improve manipulation skills for the amputees during the prosthesis use, modulating the grasping force level and preventing the object fall through a myoelectric control of the prosthesis.**

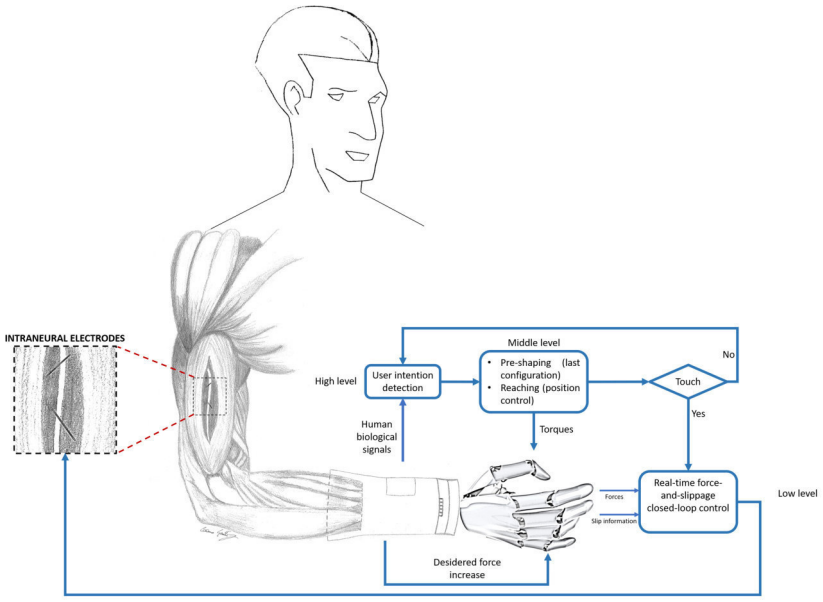

Figure 1.2 The proposed real-time force-and-slippage closed-loop control

Thesis organization

It is fair to point out that some of the contents included in this thesis are taken from conference and journal papers previously published by the author of this work. To summarize, the thesis is structured as follows.

- In Chapter 2, an overview of the evolution of controls for robotic hands is presented. The controls for the prostheses treasure the experience achieved with control of robotic hands, but the needs are different and they have led to the study of the human hand to have a control more similar, in terms of functioning, to the human one.

- In Chapter 3, the state of art on the methods to detect grasped object slippage is analysed and a novel algorithm that overcomes their limitations is proposed. Subsequently, the experimental setup and protocol used to validate the proposed approach are described and experimental results are discussed. Contents are included in the paper submitted in [32].

- In Chapter 4, the literature regarding the control strategies used to drive prosthetic robotic hands are analysed. Then, a novel force-and-slippage control strategy for prosthetic hands is proposed, and the experimental setup and protocol used to validate the approach are described. Moreover, a hierarchical pattern recognition strategy to simultaneously identify desired hand/wrist gestures and force levels starting from EMG signals is presented. Finally, experimental results are discussed. Part of the contents included in this chapter are already published in [31–33].

- In Chapter 5, the state of the art regarding the recent studies on the restoration of sensory feedback in amputees through neural interfaces is presented. Then, the proposed real-time closed-loop control strategy able to recover tactile sensations through neural electrodes to finely control bionic hands during grasp and manipulation tasks is described. Finally, experimental results are shown and discussed. Part of the contents included in this chapter are already published in [34].

- In Chapter 6, conclusions and final considerations are reported.

Chapter 2

The hand

Abstract

The hand is the human body part used to learn and to interact with the environment. The hand loss leads to irreparable damages for a person who needs to learn how to perform everyday life action with only one hand. To overcome this problem prostheses have been developed and used for both cosmetic and functional purposes. Amputees felt these devices as a foreign mechanical equipment and not like the lost limb. Why?

2.1 Introduction

Thousands of years ago, Aristotle described the hand as follows: "For the hands are instruments or organs, and the invariable plan of nature in distributing the organs is to give each to such animal as can make use of it [...] man does not owe his superior intelligence to his hands, but his hands to his superior intelligence. For the most intelligent of animals is the one who would put the most organs to use; and the hand is not to be looked on as one organ but as many; for it is, as it were, an instrument for further instruments" [35]. It was clear to him the superiority of the hand as an instrument, useful for increasing man's intelligence. More recently but however old, a study about the hand has been carried out by Sir Charles Bell in 1834 [36], who analysed the hand starting by a comparison with animal anatomy. The hand has always fascinated many people, from scientists to artists, and several studies have been conducted to understand and explain a perfect mechanism that allows its knowledge. In 1900 two famous anatomists, Frederic Wood Jones [37] and Russell Napier [38], studied the primitive nature of the human hand and the similarity with the other pentadactyl mammals but functions like prehension or dexterity belong only to primates and humans [39].

The hand is the most important part of the human body used to learn and to interact with the environment and it is clear that hand loss represents irreparable damage for a person. Life is upset and activities of daily living (ADLs) are compromised. Besides having suffered hand loss, monolateral amputee subjects need to learn how to perform everyday life action with only one hand. To remedy this problem, since the ancient Egypt, prostheses have been used both for cosmetic and functional purposes [40]. The first documented amputee who used a prosthetic limb is General Marcus Sergius, lived in Ancient Roman times [41]: "In his second campaign Sergius lost his right hand. [...] He had a right hand made of iron for him and, going into battle with this bound to his arm, raised the siege of Cremona, saved Placentia and captured twelve enemy camps in Gaul - all of which exploits were confirmed by the speech he made as praetor when his colleagues tried to debar him as infirm from the sacrifices." [42]

The prosthesis development is a process lasting 2000 years, but the first externally powered prosthesis has been made only in 1919, using pneumatic and electric power sources [43]. The first myoelectric prosthesis was born in 1948 [44]: a simple device that powered the actuators by using the amplified superficial EMG signals (sEMG). This idea did not have future either in clinical or commercial acceptance. It has been forgotten until 1969 when the idea has been reinvented [45].

Nowadays, the use of EMG signals is the most common approach to actively control prosthetic hands [46]. After 1948, many research units developed myoelectric control in complete autonomy, reaching comparable results among them. A simple solution thought to use EMG signals is the on-off control, where the overcoming of the threshold by the signal generates a high output sent to the prosthetic hand [47]. In [48] two electrodes have been placed on agonist and antagonist muscle pairs, in which a single motion (opening and closure) is associated with

a single muscle. Another solution envisaged the use of EMG dynamic to proportionally modulate force or speed [49, 50]. The number of degrees of freedom (DoFs) is clearly small; a solution to overcome these limitations is offered by pattern recognition [51–53]. This technique extracts several features from different time segments of sEMG and uses them as input to the classifier to predict different grasps. The classifiers output can be used to control a prosthetic device.

A study carried out in [11] analysed real needs for the amputee subjects to provide a focus to researchers to develop prosthesis, with sensors and control laws, that are more similar to the human hand. Several questions have been asked to amputee subjects that used both cosmetic and myoelectric prosthesis. Thanks to their answers it emerged the necessity to have a limb like the lost one. Fundamental points from this study are: performing ADLs; having sensory feedback; regulating force during grasp, lightening the visual attention and the cognitive burden for the user; avoiding slippage of the grasped object [28]; manipulating an object; handling small objects.

Unfortunately, the actual commercial prostheses are typically driven with proportional or on/off control [47], with a limited number of grasping configurations. Commonly, they only allow the opening and closing of the prosthetic hand, by using sEMG signals related to the flexion and the extension of the wrist [54]. In the last 30 years, technologies and functioning of commercial prosthetics have not changed [55], resulting in devices abandonment [56, 57]. Many amputee subjects do not use myoelectric prostheses because they are unnatural and not intuitive [58].

These devices are felt as a foreign mechanical equipment and not like the lost limb [59]. Why?

2.2 Why is control important?

The functioning of an active prosthetic hand is guaranteed by a mechatronic device, with sensors and actuators; a system that decodes human biological signals in gestures; a control law that translates all the inputs (from the hand and from the user) in the desired movement [60].

A control law that replaces human hand functions and makes a prosthesis acceptable and simple to use by the amputee [61] is the real challenge. What is the best control law for an active prosthetic hand?

2.3 Control laws for robotic hands: an overview

Research on robotic hands dates back to 1960s. In [62] and in [63] the first computer-operated mechanical hand and a robotic hand that can be considered the first dexterous multi-finger hand are presented, respectively.

To develop a control for grasping and manipulation for a robotic hand is necessary to divide the process into 3 phases: task selection, planning and motion control. In task selection is possible to choose a hand shape and the grasp type. Then, it is possible to determine the initial grasp points and motions during the manipulation in the planning phase. In the last phase, the desired motion is performed to realize the selected task. A generic task is chosen based on the hand taxonomy [43, 64–67]. These studies have a common characteristic: a very small number of primitive grasping configurations.

Once the object, in a stable grasp, is moved due to disturbance, a control system is necessary to allow the robotic hand to avoid the loss of the contact point between the hand and the grasped object. The successive step is applying the correct force on the object to be grasped and manipulate it guaranteeing grasping stability.

The development of robotic hands and of control strategies has travelled in parallel: in [63] in addition to the robotic hand, a control strategy has been developed to mimic human reflexes and in [68] a sequential controller, performed with relay circuits, has been realized to drive a three-fingers hand. These control methods emphasize reaction rather than stability.

Sensors play a significant role in control development because of return information about positions, forces and torques. Robotic hands mount several sensors, becoming sophisticated devices. Thanks to the information from positions, forces and torques it is possible to realize control strategies to regulate forces during grasping and to avoid slippages [69]. In the last 50 years, many control strategies have been developed, exploring several scenarios.

A joint servo error has been used to preserve the internal force and to realize a planned joint motion generated by motion planners [70]. In this case, contact stability is not strictly guaranteed.

In [71] a hybrid force/position control has been employed to ensure position and orientation of the object in the hand. In [72] an impedance control uses the mechanical impedance has been used to regulate the contact force. Many algorithms based on these methods were developed under mainly quasi-static assumptions.

A model-based technique [73] has been used to manipulate an object by using the contact points between fingers and object as input to the model. These kinds of controllers generally require precise a-priori knowledge of the dynamic parameters.

To avoid a-priori knowledge, in [74] an adaptive grasp controller under frictional contact points has been proposed. This control is theoretically very sophisticated, but most of the implementations are just simulations, because of the development of computer technology for graphical simulations and the difficulty in obtaining precise modelling.

Until the '90s, hardware and control strategies were developed without considering the human hand as an inspiration but around 2000s there was a counter-trend. The properties of the human hand, such as the opposition of the thumb [75] or the synergies [76], have been introduced to develop controllers and hand structure [77].

Empirical approaches based on the imitation of human grasping strategies have been proposed [78] to reduce the computational burden of grasp control for robotic hands. In particular, it has been investigated whether humans use a combination of basic grasp configurations to facilitate the replication of a human-like behaviour on robotic devices [79].

Myoelectric prosthetic hands treasure the experience achieved with control of robotic hands as previously discussed and as reported in [80, 81, 11]. On the other hand, they have a limited number of actuators to keep the hand weight and size low, and the computational burden of myoelectric control. This leads to lower performance than in robotic hands, which are characterized by a high number of actuators and consequently by many active DoFs.

The physiological reaction time of the human hands, useful to perform a simple task, is between 50-100 ms [82–87]. Then, the increase of the controller performance, such as cycle velocity, does not make natural the use of prosthesis.

It is clear that the human hand must be the base for the development of a control strategy.

Therefore, the first step to develop an active prosthetic hand inspired by the human hand is to understand how the neural system works to control the hands [88]. Thanks to the evolution of neurosciences, the study of the hand functioning has been intensified.

2.4 Human hand functioning

A study performed by analysing the brain can well describe, with more details, the real functioning of the hands. Unfortunately, free access to the human brain in order to acquire and to analyse the brain activity is not ever possible, for ethical reasons.

Another way is studying the primates brain to find some similarities with that of humans. These studies have been conducted on macaques with invasive techniques like the physiological recording of brain activity [89–91].

Subsequently, it has been possible to study neural activity without invasively accessing to brain thanks to neurophysiological technique, like positron emission tomography (PET) and functional magnetic resonance imaging (fMRI) that detect variation in blood flow properties due to the increment or the decrement of the neural activity [92–94]. Another technique is the transcranial magnetic stimulation (TMS), to cause a temporally disrupt or to stimulate a particular area of the brain. TMS is used to understand if an area is involved in a task, inhibiting it [95].

Thanks to these and other innovative techniques, non-invasive studies have been carried out on humans, and it has been possible to find similitudes and differences in brain activity in macaque and humans [96–100] from which it emerged that the grasping mechanism is based on the properties of the object to grasp [97], by also investigating weight, surface, etc [101–106]. Furthermore, the choice of the grasping configuration is affected by the task to perform with the grasped object [107–110]. Information, as electrical impulses, travel from a region to another of the nervous system through a series of connected nerves formed by axons that make synapses among neurons [111].

The flow of information related to the various phases of prehension is allowed by two pathways: the dorsolateral, that codes the grasping, and dorsomedial, that codes the reaching (Figure 2.1).

The first one connects the anterior part of the intraparietal sulcus (AIP) [112] until the inferior parietal lobule (IPL) and area F5 until the ventral premotor cortex (PMv) [113, 114]. This pathway is involved in the motor commands for the hand pre-shaping, by transforming the grasped object proprieties, derived by the visually guided grasping [115].

The second one, connects two regions within the posterior parietal cortex (PPC), area V6A [116] and MIP [117], with the dorsal premotor cortex (PMd [118]). This pathway integrates somatosensory and visual information [113] for planning and controlling arm position during the transport phase.

However, a specific pathway subdivision is not possible because the functioning of each phase happens with an overlapping of the different areas [119–122]. Core region in dorsomedial pathway codes information for the grasp and not only for the reach. In the same way, some regions between the two pathways code reaching information. The areas forming the pathways are highly distributed and the overlapping moves, with a gradient, to the desired hand movement [123]. Nevertheless, nowadays many studies are focused on this mechanism to find how the prehension works in humans.

2.4.1 Grasp stability

To move and manipulate an object, the fingers involved in a grasp apply tangential forces to the object surface while they apply normal forces on it to ensure grasp stability [124–129]. The grip force control is based on the prediction of the dynamical properties of the objects' that influence the mapping between motor commands of the arm and resultant tangential forces and torques [130–133]. Dexterous manipulation involves balancing grip and load forces to object surface properties, a capacity that is lost with an amputation.

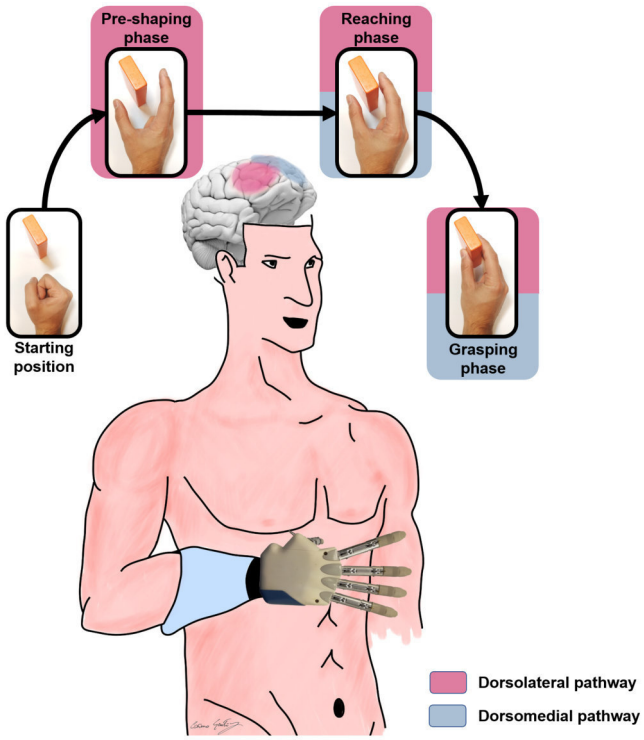

Figure 2.1 Prehension neurophysiology

Indeed, healthy people regulate grip and load forces to different frictional conditions, using high grip forces with more slippery surfaces [124, 128, 134]. In a similar manner, people adjust grip and load forces to the shape of the object to ensure grasp stability [125, 135, 136]. The result of these adaptations, excessive grip force is avoided.

The responses of the initial contact in tactile afferents provide information about surface properties. A mismatch between predicted and actual sensory information can trigger corrective actions, leading changes in grip-to-load force ratios after $\sim$ 100 ms from the contact and to an updating of the representation of the surface properties that

Cosimo Gentile

are used in future interactions with the object [86]. Visual cues about the object shape can provide the information required to make these predictions [135, 136], but shape information provided by tactile signals after contact can override predictions based on visual cues.

2.5 Conclusions

The hand loss is a traumatic event implying a radical changing of life. To overcome this problem, prostheses have been developed and used by amputees. Unfortunately, the prosthesis abandonment is common because amputees don't feel them as part of their body but like an external device.

The real needs of amputees are: performing ADLs; having sensory feedback; regulating force during grasp; lightening the visual attention and the cognitive burden for the user; avoiding the slippage of the grasped object; manipulating an object; handling small objects. Then, amputees would like a prosthesis that reproduces the functions performed with the losing hand.

From the study of the human hand functioning, it emerged that a control strategy for grasp and manipulation tasks must be divided into levels: high to decode the human biological signal, middle for the reaching to the object of the involved fingers, low for the force regulation. A further parameter is related to the force adaptability during the whole grasp when there are friction changes between fingers and object surface or in presence of slippages.

Chapter 3

Touch-and-slippage detection algorithm

Abstract

The greatest limitation for an amputee subject who uses a prosthesis having no sensory feedback is the difficulty to manage unexpected events in an autonomous way. In grasp and manipulation tasks, the possibility of the object slippage is high. For this reason, it is necessary to detect the beginning of the slippage and provide the control with a fast contrast action. In this thesis, a touch-and-slippage detection algorithm for effective grasp control of a prosthetic hand embedding monoaxial, low-cost sensors is proposed. The algorithm has a low computational burden and is capable of detecting slippage events using only the normal force component. Two experimental sessions were performed to validate the touch-and-slippage algorithm. In the former, the variation of the normal force component provided by a Force Sensing Resistor (FSR) sensor was compared with the tangential force component measured by a triaxial force sensor. In the latter, the threshold for detecting slippage events was obtained and applied to study the dependence of the number of slippage events on sliding velocity and force applied to the sensor.

The low computation time of the algorithm, i.e. 4.9 ms, and the high success rate in terms of detected slippage events (99.4%) suggest that the algorithm applicability in real systems is feasible.

3.1 Introduction

The control of the prosthesis is possible by using information from the efferent pathway, where the subject intention of movement can be extracted from muscular (EMG) or neural (ENG) signals.

The extraction of neural signal, then the EMG, always requires an invasive technique to implant neural interfaces. Then, to command a prosthesis, the use of EMG signals is preferred.

Over the years growing interest has been addressed to grasping and manipulation actions performed by active prosthetic hands. One of the main aspects to be taken into account in the evaluation of grasping and manipulation is the stability of the grasped object which could be guaranteed by estimating and preventing object slippage.

Different approaches have been proposed in the literature to obtain information about object slippage during grasping and manipulation actions.

It is possible to distinguish among approaches that use sensors providing the three force components, solutions utilizing the information about vibration, and methods relying only on the normal force component. All these approaches have been proposed for commercial and ad-hoc developed sensors.

To detect both the tangential and the normal force components, complex sensors such as load cells or 6-axis force/torque sensors have been largely adopted. In these cases, the methods for slippage detection mainly rely on the Coulomb friction model, Kalman filters, machine learning, Fast Fourier Transform and threshold models. In [137], the Coulomb friction model has been applied to tangential and normal forces obtained from a 6-DoFs force/torque sensor positioned on the wrist of a robotic gripper. In [138], Coulomb friction model has been applied on the output of three different sensors, i.e. a 10N single-axis tension load cell sensor, a load cell and an optical encoder. In [139], the torque necessary to contrast the slippage event has been computed from the ratio between the tangential force and friction coefficient. In order to identify the slippage onset and to filter the high-frequency noise, the residual of a Kalman filter has been added to the obtained torque. In [140], a 6 axis Force/Torque sensor has been mounted on a parallel gripper and a cascade of machine learning algorithms has been adopted to control which parts of the grasped objects are in contact with the instrumented

surface of the gripper. The object slippage has been provided as a binary value by using a Support Vector Machine algorithm. In [141], the slippage is detected when the normal force value is lower than a threshold that depends on the tangential force, the torque and the translational and rotational friction coefficients. A silicon-based tactile sensor has been proposed in [142] to measure normal force and tangential force simultaneously. A pre-sliding is detected when the tangential force, measured by the sensor positioned on the hand fingertips, is smaller than the surface shear traction. Contrariwise, a gross slip is identified. In [143], a Fast Fourier Transform (FFT) has been used to examine the slip and nonslip events from six strain gauges located on the thumb of the Motion Control Hand. It has been verified that, during object slippage, the vibrations in the range 25 - 60 Hz are amplified.

The main drawbacks of the sensors providing the three force components are that their expensiveness, complexity (especially the electronics for signal acquisition and processing) and susceptibility to noise [144]. Furthermore, the approaches adopted with these sensors for detecting slippage events are characterized by a high computational cost (e.g. Fourier or wavelet transform have to be applied to big sample windows of the force signals [145]).

Other solutions use the information about vibrations induced by slippage itself for detecting it. A characterization of vibrations caused by slippage events has been performed in [146], where it has been found that vibrations are stochastic, non-Gaussian white noise processes and that their magnitude depends on the relative velocity of sliding. Starting from these findings, in [147] an algorithm based on the covariance among the vibration information from the tactile sensors placed on a gripper has been developed. Slippage detection has been associated with a threshold, i.e. when the covariance is smaller than a threshold, slippage is not present, contrariwise, object slippage happens. In [148], the pressure

response from a biomimetic tactile sensor array [149] has been analyzed with a Short Time Fourier Transform (STFT) with a time window of 80 ms, to mimic biological grip reflex response times [85]. The range of frequencies between 30 Hz and 200 Hz has been considered since it has been verified that slippage events are located in this range. In [150], the ThimbleSense has been adopted to detect slippage from vibrations by using Discrete Wavelet Transform in static conditions. In [151], a method that uses a biomimetic fingertip that integrates piezoresistive MEMS sensors to detect, from the vibrations measured from the normal force component, the ON/OFF signal related to the presence or absence of slippage has been developed.

Other methods use low-cost commercial sensors, such as the Force Sensing Resistors (FSR). In [152] two methods for detecting slippage have been proposed and tested on a tactile sensor array attached to gripper fingers under silicone rubber. The first method uses the rank correlation for detecting both translational and rotational slippage, the second one adopts the 2-D cross-correlation to detect slippage velocity. In [153], the forces acquired from an FSR sensor are used to build a dynamical model of initial slip on the basis of the theory of friction-induced vibration at near-zero slip velocity [154, 155]. The high-frequency component of the grasping force signals is extracted by wavelet transform and the change of wavelet coefficients is used to detect the onset of slip. Fuzzy logic controllers have been also applied to the outputs of an FSR [156] for discriminating among "slow slip" (i.e., the controller detects a slow object slipping), "fast slip" (i.e., the controller detects a rapid change in slip values), and "null" (i.e., the object is either grasped or it has slipped and fallen beyond controller action).

The main drawbacks of the above methods are i) uncertainty about the slippage output when the absolute value of the signal derivative is evaluated (i.e. a force increment could be confused with a slippage

event), ii) the presence of additional noise due to the computation of the signal derivative, which could imply the impossibility of recognizing slippage with respect to noise, iii) the confusion between initial touch and slippage.

Progress beyond the SoA The contribution of this thesis is to overcome the limitations highlighted in the literature by proposing and validating a fast and efficient algorithm, able to detect the touch and the onset of the slippage event by using only the normal component of the acquired signal (i.e. force or voltage). The approach is grounded on the detection of the vibrations due to the sliding between two contact surfaces.

The main purpose of this work is to propose and experimentally test: i) the introduction of the touch identification stage, ii) the discrimination between true positive slippages and false-positive slippages, iii) the adoption of a current loop both for conditioning the signal originating from resistive tactile sensors in order to cancel noise and as a proof of concept for the future implementation of an integrated circuit [157], iv) the introduction of a systematic way for validating the proposed slippage detection, general enough to be used for evaluating other approaches. The steps performed to develop a robust slip detection method will be described in detail to provide general methods for quantitatively evaluating system performance and establishing performance comparisons.

3.2 The proposed approach

In literature, few data are present about the time needed to calculate the slippage or the necessary torque to move the hand fingers starting from the reading of the information from the sensors. The available data showed a high time to obtain the above information: 50 ms to obtain the slippage [151], 350 ms to move the hand fingers [158] and

almost 64 ms [159] to classify movement intention starting from EMG signal. Therefore, the total time useful to decode the user intention and to consequently move the hand prosthesis is over 400 ms. In presence of slippage events, the time increases untill 450 ms. It is evident that this time is far from the biological time needed to react to a slippage event (i.e. $\sim$ 100 ms) [86].

In this section, an algorithm able to detect the touch and the slippage from information about the normal force component measured by a Force Sensing Resistor sensor and a conditioning circuit are described. The proposed approach and conditioning circuit are applied in the following to the output of an FSR sensor, but they can be used with several kinds of sensors providing information about the normal force component, such as resistive, inductive and capacitive sensors.

3.2.1 Conditioning circuit

The Anderson loop [160] was chosen for conditioning signals from the monoaxial tactile sensor. As the classic Wheatstone bridge, the loop performs the subtraction of the voltage drop across the sensor from the one measured on a reference resistor, but differently it relies on active subtraction instead of a passive one. In this work, a strain gauge identical to all others, lodged in the palm, is used as the reference resistor R_{ref}. Since it is affected by the same background vibrations present at fingertips, this noise is simultaneously subtracted from the tactile signals acquired from sensors ($(R_{S1}$-$R_{S5})$.

Main advantages provided by Anderson loop to this work with respect to the bridge are: i) no need of three passive reference elements for each FSR (all elements in the loop are sensors having identical natures, i.e. similar thermal coefficients and drift behavior), ii) fewer connections, and iii) higher tolerance to random variations in wires (since their resistance is not sensed by the subtractors - Kelvin sensing).

As shown in Figure 3.1, the Anderson loop consists of a reference current (I_{ref}), a set of N resistive sensors (R_{S1}-R_{S5}) connected in series, a reference resistance (R_{ref}), and (2N+1) instrumentation amplifiers (IA_0-IA_{51}). The current reference circuit, shown in the blue rectangle of Figure 3.1, consists of a reference voltage (OP1) that sets the input for a second operational amplifier (OP2). OP2 establishes $I_{ref} = V_{ref}/R_{set}$ throughout its feedback loop (pink background area) containing six resistances (R_{ref}, and R_{S1}-R_{S5}). Each resistance is an FSR linearized with a parallel 10 kΩ.

Two layers of active subtractors, depicted in the green area, were implemented with instrumentation amplifiers (AD623). The first layer (IA_0 to IA_5) amplifies total voltage drops across each of the FSR sensors (R_{S1}-R_{S5}), including the reference one (R_{ref}). The second layer produces the output signals (V_{o1} to V_{o5}), which are proportional solely to the resistance variation ΔR_{Si} on each sensor ($V_{oi} = I_{ref}.\Delta R_{Si}$, $i = 1,...,5$).

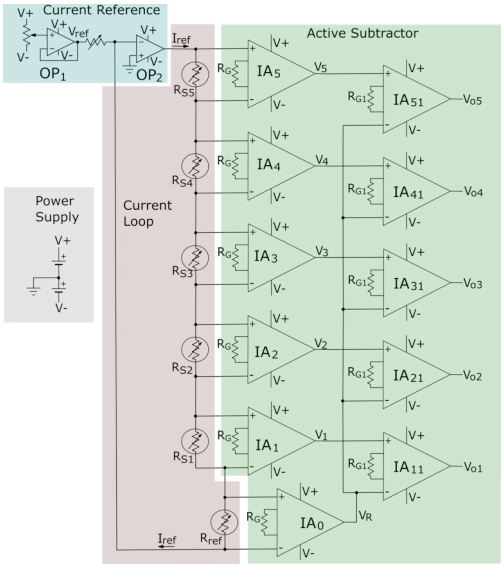

Figure 3.1 The Anderson Loop conditioner circuit.

Cosimo Gentile

3.2.2 Threshold detection for the algorithm output

The ROC curve analysis method originated from the theory of signal detectability [161] has been used in many fields, such as medical diagnosis or algorithm validation [162–164].

Let us first recall some definitions: true positive rate (TPR), or *sensitivity*, is the probability that slippages are correctly classified based on the threshold; true negative rate (TNR), also called *specificity*, is the probability that no-slippages are correctly classified; false-positive rate (FPR) is the probability that no-slippages are falsely classified; false-negative rate (FNR) is the probability that slippages are falsely classified.

The hit rate of a classification process is highly dependent on the function chosen to separate results into each class. In this work, where simple thresholding is adopted, the ROC curve analysis was used for determining the threshold in two confused states yielding maximum *sensitivity*. In particular, for the slippage and no-slippage state classification, a threshold (or cut-off point) was determined to discriminate the algorithm output.

In the ROC curve coordinate system, the x and y of the cut-off point are represented by FPR and TPR, respectively. The area under the ROC curve (AUC) can be used as an index to evaluate the detection capacity of a specific feature. The detection accuracy increases with the AUC increase. If AUC is greater than 0.9, the test is highly accurate [163]. Then, the cut-off point will be in the upper left corner of the ROC curve [162].

3.2.3 Touch-and-slippage detection algorithm

Considerable researches have been performed to understand the sliding process. The stick-slip model describes well the behaviour of the sliding between two contact surfaces: a stick phase, where the system accumu-

lates potential energy, is alternated with a slip phase, where the energy is transformed into a movement, causing vibrations [165–168].

This model is also used to describe the slip coding in epicritic tactile perception (relating to mediating cutaneous sensory reception) because the slip appears discontinuous in space and in time [169]. The vibrations due to the sliding between two contact surfaces [146] represent the key-point of the proposed algorithm.

The algorithm is able to detect i) the first touch between the sensor and an object and ii) the slippage events. The functioning principle is shown in the workflow in Figure 3.2.

With the aim of removing the electronic noise from setup components, mean value v_{mean} of the FSR conditioned signal (i.e. force or voltage), v_i, has been computed for every 5 samples (this value has been experimentally obtained and seemed to be adequate to decrease the noise, by avoiding an increase of the computation time) acquired with a frequency of 2 kHz

$$v_{mean} = \frac{1}{5}\sum_{i=1}^{5} v_i \tag{3.1}$$

The 1^{st} stage of the algorithm is devoted to the identification of the first touch between the sensor and the object surface. The steps of the touch identification procedure are the following:

1) Computation of the average value on 10 samples (acquired with a frequency of 2 kHz) of the voltage signal at resting (calibration) period. In the calibration period, no force variation is detected, and v_{rest} represents the mean of background noise magnitude.

2) Comparison of v_{rest} with v_{mean}, to obtain a mean voltage error

$$\Delta v = v_{rest} - v_{mean} \tag{3.2}$$

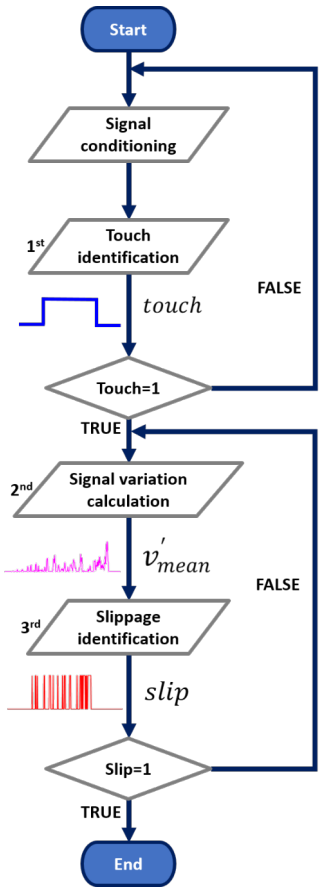

Figure 3.2 Workflow of the touch-and-slippage detection algorithm.

The touch with the object is detected if Δv is greater than the minimum voltage variation (δ) measured by the sensor when pressed

$$\Delta v > \delta, touch = 1; \tag{3.3}$$

In the algorithm 2^{nd} stage, the value v'_{mean}, i.e. the voltage signal positive derivative, is computed. Only the positive derivative is considered since the negative value corresponds to a pressure increment on

the FSR, as shown in the first and the second subplots in Figure 3.3 (to obtain the force value corresponding to the measured voltage, a static characterization of the sensor was performed, as described in Section 3.3.1.1)

$$v'_{mean} = \frac{d}{dt} v_{mean} = \frac{v_{mean}(i) - v_{mean}(i-1)}{cycle\ time} \tag{3.4}$$

The derivative of the mean values between two consecutive 5-samples sets is computed through backward differentiating to have an online working algorithm [170]. In the 3^{rd} stage, the obtained value is compared with a threshold α established by using the ROC curve [161] (as it has been explained in Section 3.2.2). According to Eq. 3.5, a binary value (called $slip$) is set to 1 when v'_{mean} is higher than the threshold (i.e. the slippage occurs), otherwise, it is set to 0.

$$\begin{cases} v'_{mean} \geq \alpha, slip = 1 \\ v'_{mean} < \alpha, slip = 0 \end{cases} \tag{3.5}$$

The proposed approach can be applied both on voltage or force signals, simply choosing the negative or positive derivative of the signal. An example of the signal behaviour is shown in Figure 3.3: at time instant t_0, a variation is observed indicating pressure on the FSR surface. The signals remain steady up to t_1 when slippage occurs. At time instant t_2, the pressure becomes equal to zero.

3.3 Experimental validation

Two experimental sessions were carried out to validate the proposed approach.

In the first experimental session, the correctness of the output v'_{mean} obtained from the 2^{nd} stage of the proposed slippage detection approach was verified. In particular, it was tested if the method was able to detect

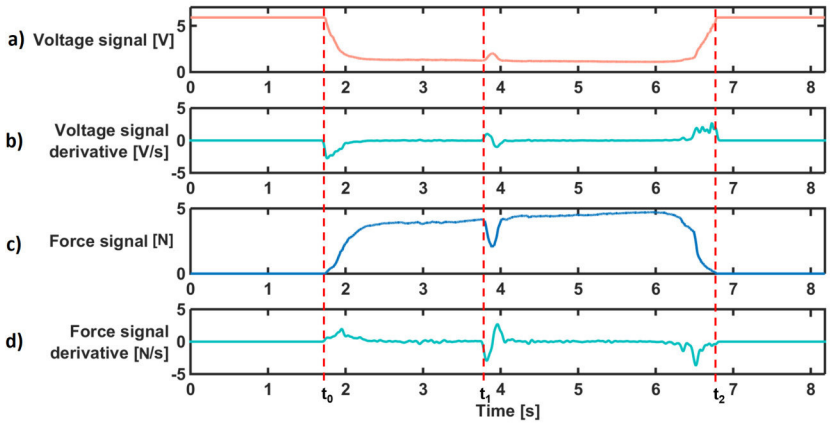

Figure 3.3 a) FSR conditioned signal b) and its derivative. c) Corresponding force signal d) and its derivative.

a variation v'_{mean} of the normal force component, measured by the FSR sensors, only when a tangential force component F_y, measured by a Multi-Axis Force - Torque Sensor (i.e. the JR3 sensor), is present.

In the second experimental session, the value of the threshold α necessary to obtain an algorithm output value equal to 1 if slippage is detected, 0 on the contrary (3^{rd} stage in Figure 3.2) was determined. The obtained threshold value was applied to the data acquired in the first experimental validation to study the dependence of the number of slippage events on sliding velocity (which depends on the sliding duration) and force applied on the sensor.

In the following, each experimental validation is described in detail.

3.3.1 Experimental session 1

3.3.1.1 Experimental setup and protocol

In the first experimental validation, an FSR sensor (Model 402 by Interlink Electronics [171]) was mounted on the top of the JR3 Multi-Axis Force - Torque Sensor, model 20E12A4-M25ES-EF 105N5 [172]. The

FSR 402 can provide information about normal forces up to 20 N with a discriminant threshold of 0.2 N, while the JR3 measures the three force components in a range of $\pm$ 200 N with a resolution of 0.015 N.

An ad-hoc developed probe was positioned on the end-effector of an anthropomorphic robotic arm (i.e. the Kuka Light Weight Robot 4+ [173]) to apply forces on the sensors (Figure 3.4).

The experimental setup can simultaneously record the normal force component from the FSR sensor and the normal and tangential force components from the JR3 sensor. The FSR conditioned signal and the JR3 force components were acquired by a National Instruments (NI) DAQ USB-6210 in a synchronous way.

To establish a relationship between the output signal from FSR voltage value V and the force value F, the FSR sensor was statistically characterized, as explained in [174]. The relation between voltage and force can be modelled as [31]

$$F = p_1 V^4 + p_2 V^3 + p_3 V^2 + p_4 V + p_5. \tag{3.6}$$

To obtain the vector F_{JR3} of the generalized forces (i.e. force and torque) from the voltage values acquired by the JR3 sensor, the JR3 calibration matrix M, provided by the producers, was multiplied by the sensor voltage vector V_{JR3}

$$F_{JR3} = M V_{JR3} \tag{3.7}$$

The proposed touch-and-slippage detection algorithm, implemented in C programming language under Windows 10, was applied to the normal force acquired by the FSR sensor and was tested within its force range.

The robotic arm is characterized by 7 active DoFs and is provided with joint position and torque sensors. It was controlled with a parallel

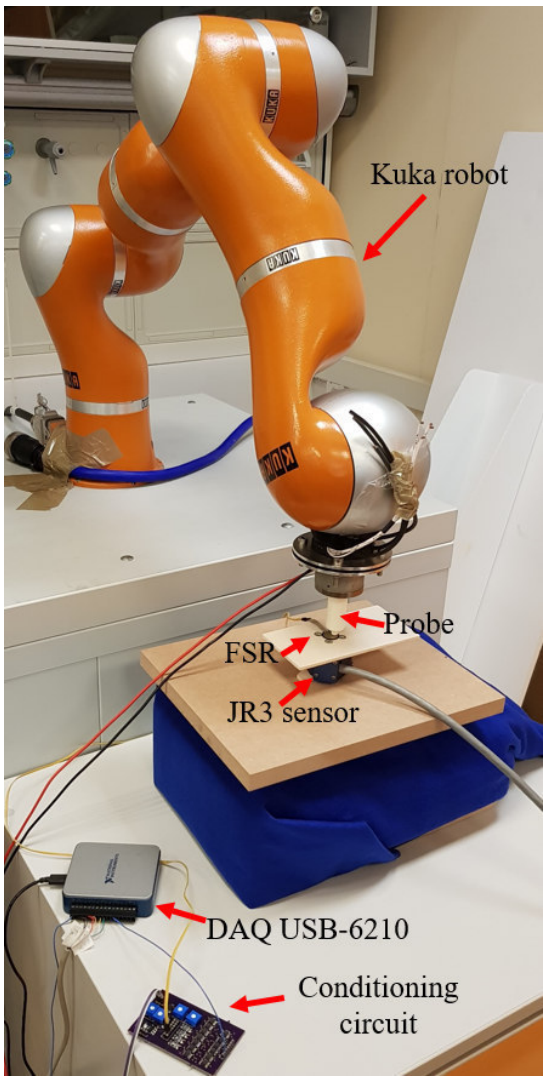

Figure 3.4 Setup for the first experimental validation.

force/position control to pass over the entire surface of the FSR sensor by applying a constant force and simulating a slippage.

v'_{mean} was compared with the tangential force component F_y (Figure 3.5) acquired by the JR3 sensor during the probe sliding. The aim is to verify if the method is able to detect a normal force component variation, due to vibrations caused by the slippage event, when a tangential force (used as ground truth) is present.

To verify the correctness of the method in different conditions of forces and sliding velocities, three force values exerted by the robot arm and 3 durations of the probe sliding were chosen, as shown in Table 3.1 (i.e. Force A Time A, Force B Time C, etc.).

Table 3.1 Parameters used in the first experimental validation: forces and time needed by the robot arm to pass over the FSR sensor surface.

	A	**B**	**C**
Force [N]	1.2	3.6	4.7
Time [s]	5	3	1

The robot arm was controlled to move the probe in contact with the FSR sensor surface (Figure 3.5 a) and apply one of the force values shown in Table 3.1.

3.3.1.2 Resutls and discussion

The experimental results obtained with the 9 force-time combinations are presented in the following.

For the sake of brevity, for each force value, the behavior obtained with only one sliding velocity is reported. In particular, in Figure 3.6, Figure 3.7 and Figure 3.8 *a)* the behavior of the force measured by the FSR sensors, *b)* the corresponding v'_{mean}, and *c)*, *d)* and *e)* the behavior of the 3 force components acquired by the JR3 sensor are shown in the

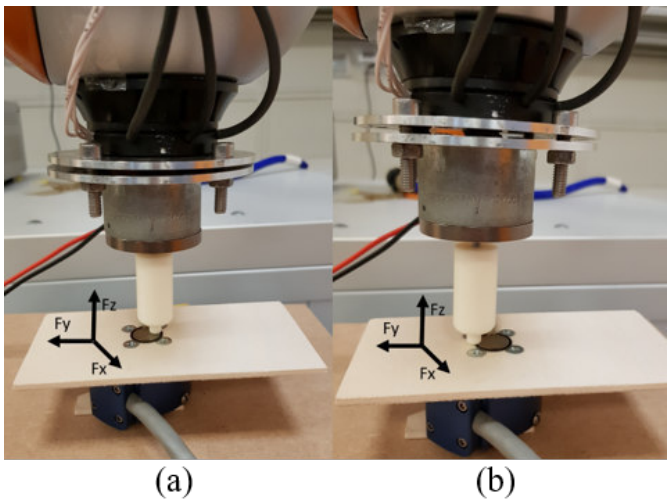

Figure 3.5 a) Initial position, b) Final position for the Kuka-probe. The reference system is for the JR3 sensor.

following 3 force/time combinations: force A time A, force B time B and force C time C (Table 3.1).

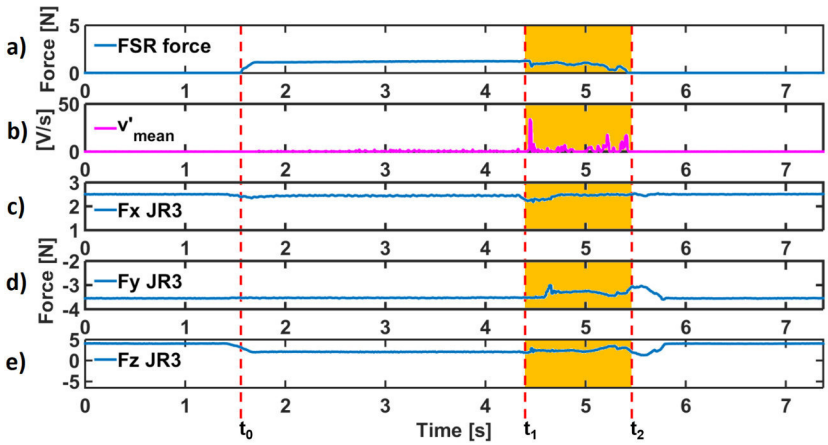

Figure 3.6 Force A Time A. a) The force acquired by the FSR sensor. b) v'_{mean}. The c) Fx, d) Fy and e) Fz force components acquired by the JR3 sensor.

It is possible to notice a force-offset on the three force components measured by the JR3 sensor. It is due to an initial load caused by the presence of a wooden board attached to the JR3 sensor surface. Thanks to this board, the FSR is positioned on a flat surface.

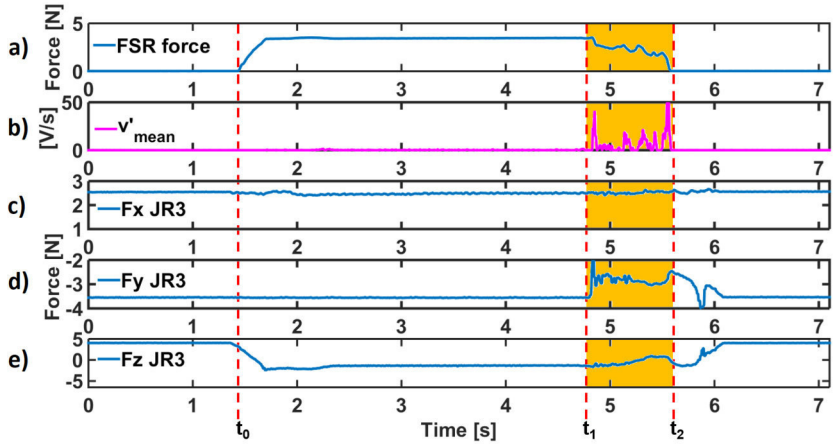

Figure 3.7 Force B Time B. a) The force acquired by the FSR sensor. b) v'_{mean}. The c) Fx, d) Fy and e) Fz force components acquired by the JR3 sensor.

At the time instant t_0, a variation is observed in all force signals (*a)* FSR Force, *c)* Fx, *d)* Fy, *e)* Fz) indicating that the probe was in contact with the FSR surface. The probe remains steady up to t_1, when it begins to slide in the Y direction of the JR3 reference system (Figure 3.5), stopping when it overcomes the FSR surface. For this reason, forces are still applied on the JR3 sensor after t_2.

The variations on Fx and Fy in the time range $t_0 - t_1$ are due to the robotic arm vibrations caused by its motors.

The intervals highlighted in yellow represent the part of the acquisition corresponding to the sliding of the probe across the full surface extension of the FSR sensor.

By comparing the signal shown in *b)*, *c)* and *d)* of Figure 3.6, Figure 3.7 and Figure 3.8 it is possible to note that, during the probe sliding

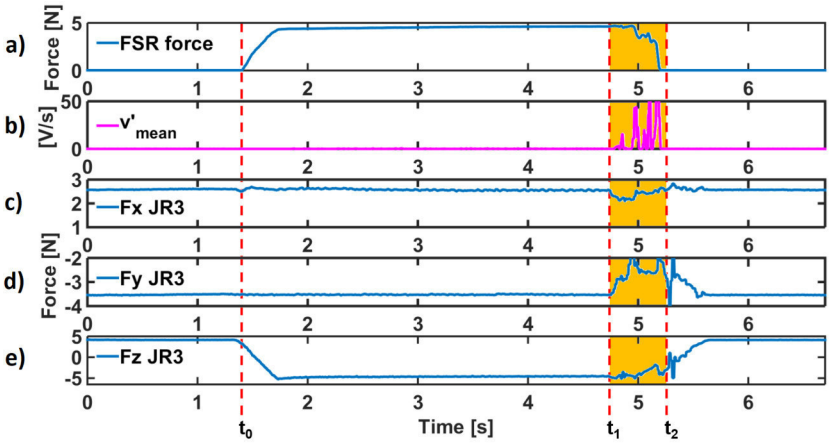

Figure 3.8 Force C Time C. a) The force acquired by the FSR sensor. b) v'_{mean}. The c) Fx, d) Fy and e) Fz force components acquired by the JR3 sensor.

time, highlighted in yellow, v'_{mean} (showed in pink in *b)*) is different from zero throughout the time in which the tangential force component F_y is present. These findings confirm that the presence of the output v'_{mean} generated from the algorithm 2^{nd} stage (i.e. a signal variation due to vibrations) corresponds to the presence of a tangential force value, measured by the JR3 sensor.

In Figure 3.11, *b)* the positive derivative of the voltage was compared with *c)* the acceleration variation and by *d)* the displacements to make sure that the number of the calculated slippages were the same of the ones inducted and detected by the accelerometer and by the optoelectronic system.

3.3.2 Experimental session 2

3.3.2.1 Experimental setup and protocol

The IH2 anthropomorphic robotic hand [175], is a 5-finger robotic hand with a weight (640 g) and a size similar to the human ones. The hand has

11 DoFs, of which 5 are active. Each underactuated finger is composed of two phalanxes and a tendon wrapped around the pulley placed in the joints. The F/E (i.e. Flexion/Extension) angles of the MCP (i.e. MetaCarpo-Phalangeal) and PIP (i.e. Proximal InterPhalangeal) joints (i.e. q_{mcp} and q_{pip} respectively) are linked to the slider position x by means of the joint pulleys radii (r_{mcp} and r_{pip}) and the starting joint angles ($q_{0_{mcp}}$ and $q_{0_{pip}}$, supposed equal to 0) [176]:

$$x = r_{mcp}(q_{mcp} - q_{0_{mcp}}) + r_{pip}(q_{pip} - q_{0_{pip}}) \tag{3.8}$$

The long fingers kinematic chain is the one of two-link planar manipulators, whereas the thumb kinematic chain is equal to the one of an anthropomorphic manipulator. The dynamic model of the manipulators is given by

$$B(q)\ddot{q} + C(q,\dot{q})\dot{q} + g(q) + T_{el} = \tau \tag{3.9}$$

where $B(q)$ is the joint inertia matrix, $C(q,\dot{q})$ is the vector of centrifugal and Coriolis torques, q, $\dot{q}$, $\ddot{q}$ are respectively the joint position, velocity and acceleration vectors, $g(q)$ is the gravitational torque vector.

Two FSR sensors were placed on the thumb and index fingertips of the IH2 Azzurra hand. The robotic hand was controlled to grasp a cubic object (33 x 33 x 33 mm, weight = 15.32 g) equipped with a magnetoinertial sensor (M-IMU, XSENS MTw) to measure the acceleration components caused by slippage. The optoelectronic system BTS SMART-D Motion Capture System (www.btsbioengineering.com/it/) was used to track markers positioned both on the robotic hand index and on the cube in order to measure the object displacement due to slippage. Displacement was calculated as the euclidean distance between the marker positioned on the cube and the marker positioned on the robotic hand index finger. The BTS SMART-D Motion Capture System

is a 7-camera motion analysis with an acquisition rate of 60 Hz and an accuracy less than 0.1 mm over a 2 x 2 m area. The information provided by the M-IMU and by the optoelectronic system were used to verify the algorithm performance in terms of false positives and negatives and true positives and negatives.

To ensure repeatability of the experimental conditions, a moving-object system was developed (Figure 3.9). The system is a manipulator with 4 passive DoFs and a gripper like end-effector. In this way, the hand can hold the grasped object always in the same position; then the gripper releases the object and changes its orientation without interfering with the task. After each activity, the object support comes back into the initial position.

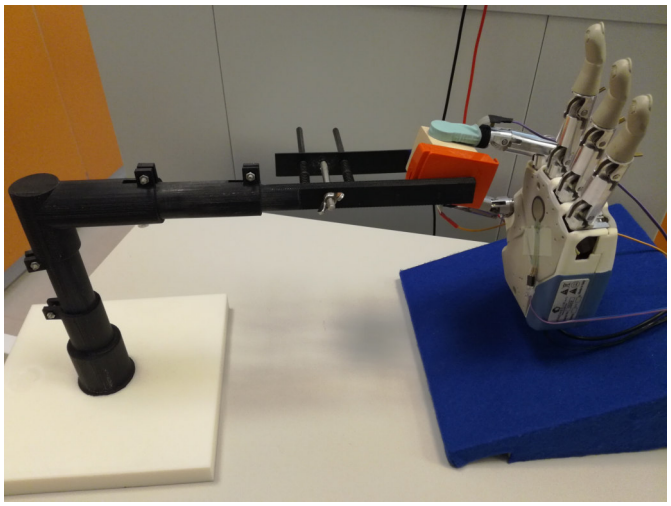

Figure 3.9 The IH2 robotic hand grasping the cube equipped with the M-IMU from the moving-object system.

The KUKA robotic arm provided with the probe was used to apply an impulsive force to the grasped object and induce slippage (Figure 3.10). Data acquired by the M-IMU and by the optoelectronic system represent our ground truth.

Two signals were used to calculate the threshold: the first one is the positive derivative and the second one is the binary signal related to the induced slippage. The binary signal is built as an array made of 0 and 1, where 1 is added when the slippage was induced and a corresponding displacement was measured.

To determine the threshold α (eq. 3.5), different values of α were tested and the corresponding parameters described in Section 3.2.2 (i.e. TPR, TNR, FPR, FNR) were evaluated. The threshold was determined on data acquired by the FSR sensor attached on the index fingertip of the prosthetic hand during the pinch grasp of the cube. When the cube was firmly grasped, 30 slippage events were induced by the probe attached to the robotic arm end-effector. The ROC curve was constructed on the acquired data and the value that yields to the largest Area Under the Curve (AUC) was chosen as the threshold α. Furthermore, the obtained threshold value was applied to the data acquired in the first experimental validation to analyze the dependency of the output of the algorithm 3^{rd} stage (i.e. $slip$) on applied force and sliding velocity.

3.3.2.2 Results and discussion

As reported in Section 3.2.2, $sensitivity$ and $specificity$ were computed and the AUC was analyzed to provide the threshold for identifying slippage.

As described in Section 3.3.2.1, a single test was performed where the probe attached to the KUKA robot end-effector induced 30 slippages to the cube, equipped with the M-IMU, grasped by the robotic hand (robotic hand index and cube were equipped with markers).

In Figure 3.11 *a)* force, *b)* positive derivative of the voltage, *c)* acceleration and *d)* displacements related to the above task are shown.

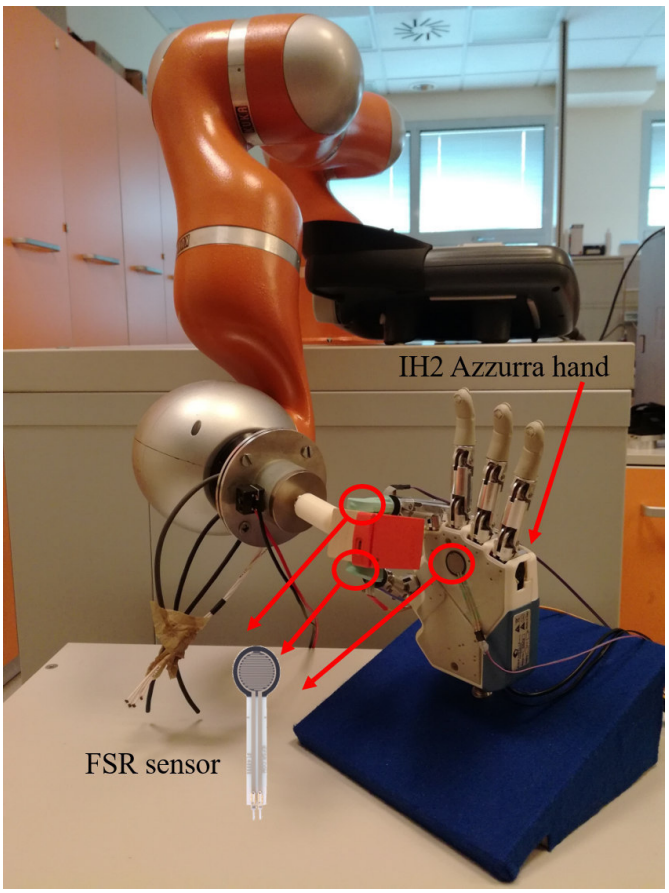

Figure 3.10 Setup for the second experimental validation.

In Figure 3.12 the ROC curve is shown. The AUC brown curve corresponds to the case in which true slippages are not discriminated from true no-slippages, namely no discrimination.

Once the threshold was established, it was applied to the output of the algorithm 2^{nd} stage (i.e. v'_{mean}) obtained during the first experimental validation to compute the output of the 3^{rd} stage (i.e. $slip$). In particular, we want to verify if the amount of slippage events is influenced by the

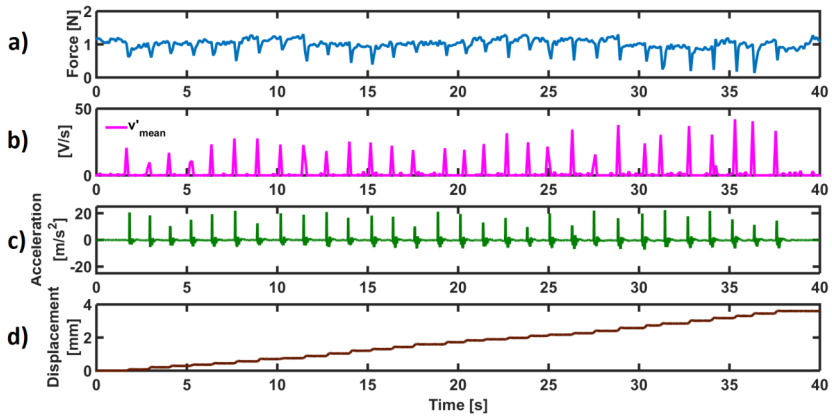

Figure 3.11 a) The force acquired by the FSR on the thumb and b) the positive derivative of the voltage. c) The acceration and d) the displacements caused by the slippages.

force applied on the sensor surface and by the time needed by the probe to pass over the FSR sensor surface.

In Figure 3.13, Figure 3.14 and Figure 3.15 the same results of Figure 3.6, Figure 3.7 and Figure 3.8 are reported with the following three differences: i) only the results related to the data from the FSR sensor are shown; ii) in the second subplot, the threshold has been added in light blue; iii) in the last subplot, touch and slippage signals are shown in blue and in red, respectively.

From the data analysis, it emerged that there is a trend that binds the number of slips with the change of the force applied to the sensor and the sliding velocity of the probe. In particular, it is possible to notice that the number of slips decreases when speed increases, keeping the force constant, whereas it increases when force increases, at a constant velocity. This behaviour is confirmed by the literature findings according to which when velocity and force increase, the friction coefficient decreases and therefore, also vibrations decrease since there is a loss of contact between the surfaces [177]. Since the proposed approach grounds on variations, a

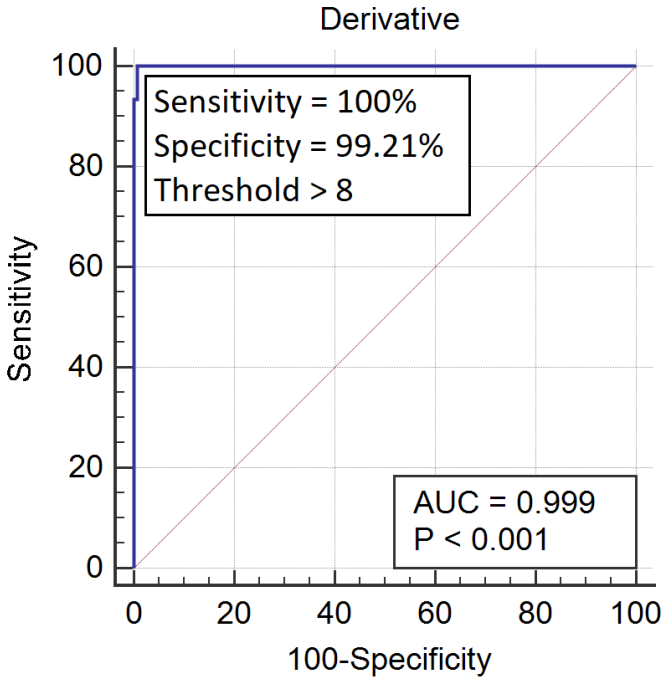

Figure 3.12 ROC curve for the threshold detection.

decrease in the number of vibrations implies a decrease in the number of slippage events. In Table 3.2, the average and the standard deviation of the number of slippages for each force-time combination are reported.

The algorithms computation time, i.e. from the acquisition of the first voltage sample to the binary output (i.e. 1 slip, 0 no slip), is 4.9 ms. This time was obtained using an Intel Core i5-4570 @ 3.20 GHz processor with 4 GB of RAM. By using a dedicated device a lower computation time could be obtained.

As evident from the results shown in Figure 3.12, the best AUC equal to 0.999 is obtained using a threshold value α equal to 8, with a *sensitivity* of 100% and a *specificity* of 99.21%. Therefore, a threshold α equal to 8 represents the value for obtaining the binary output of the

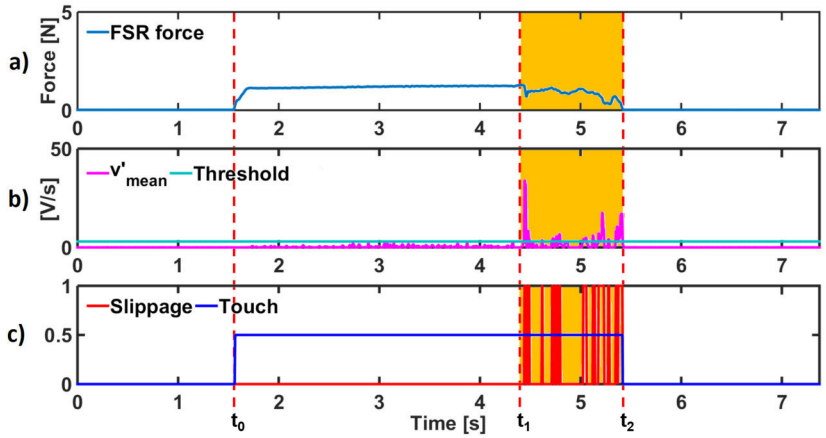

Figure 3.13 Force A Time A. a) The force acquired by the FSR sensor. b) v'_{mean}. c) The 1/0 slip and the touch signals are shown in red and blue.

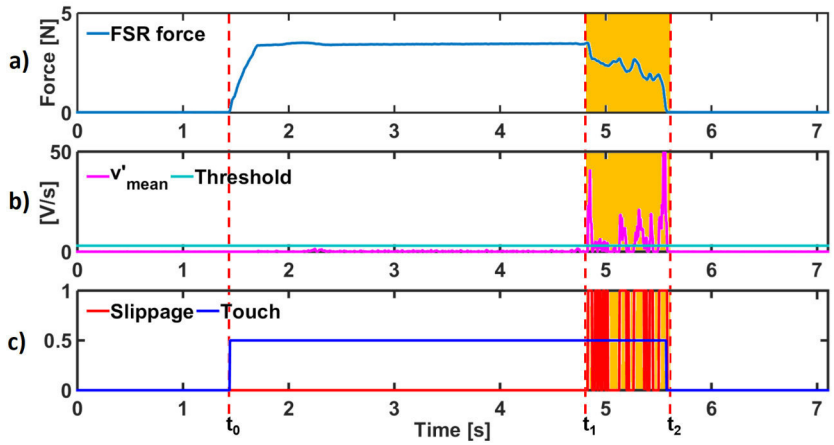

Figure 3.14 Force B Time B. a) The force acquired by the FSR sensor. b) v'_{mean}. c) The 1/0 slip and the touch signals are shown in red and blue.

algorithm 3^{rd} stage in Figure 3.2. The obtained threshold is valid in the whole functioning range of the FSR sensor, as shown in Figure 3.16 in which a single slippage has been inducted with the Kuka-probe system.

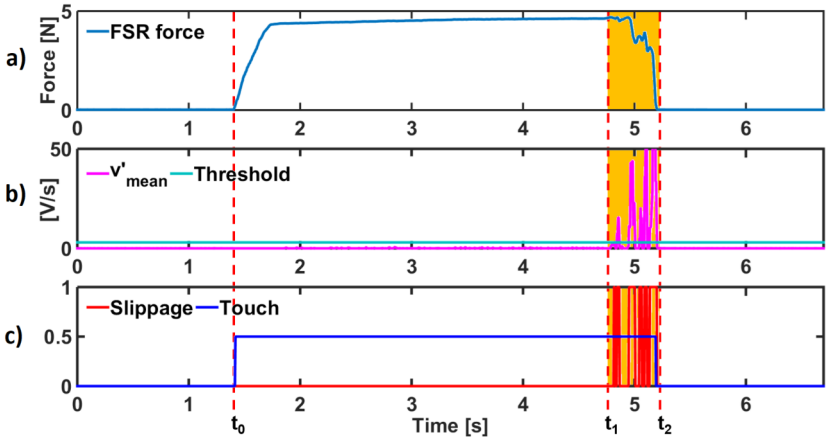

Figure 3.15 Force C Time C. a) The force acquired by the FSR sensor. b) v'_{mean}. c) The 1/0 slip and the touch signals are shown in red and blue.

Table 3.2 Average and standard deviation of the number of the slips for the tasks performed in the first experimental validation and calculated in the second experimental validation, as a function of the force and time.

Force \ Time	5 s		3 s		1 s	
	Aver.	**St. dv.**	**Aver.**	**St. dv.**	**Aver.**	**St. dv.**
1.2 N	37.6	2.45	22.9	8.15	17.4	5.72
3.6 N	42.3	8.17	31.2	5.42	22.1	4.68
4.7 N	55.7	9.71	44.6	9.84	28.4	7.66

The found threshold α was applied to the output of the algorithm 2^{nd} stage obtained during the first experimental validation (i.e. v'_{mean}). When the obtained v'_{mean} (shown in pink in *b)* of Figure 3.13, Figure 3.14 and Figure 3.15) is higher than the threshold α, an output equal to 1 was generated by the algorithm 3^{rd} stage. It is shown in red in *c)* of Figure 3.13, Figure 3.14 and Figure 3.15 together with the touch signal (outlined in blue).

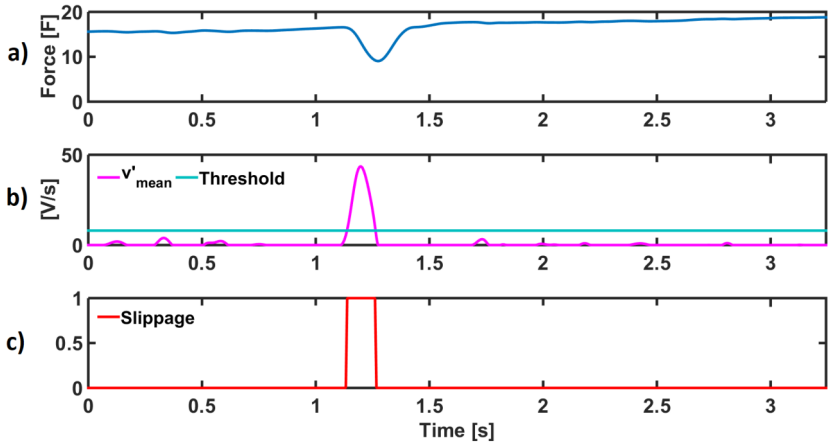

Figure 3.16 a) Force signal, b) the positive derivative of the voltage and c) slippage behaviour when the maximum force (i.e. 20 N) measured by the sensor is applied.

These results confirm that the threshold determined with the ROC curve, applied to the performed tasks, is optimal for correctly detecting slippages (i.e. generates a $slip$ value equal to 1 in correspondence of the probe sliding in tangential direction). The threshold α was applied to all the tasks performed in the first experimental validation; the results have demonstrated that the algorithm works independently by the applied force-and-velocity combination and that the number of slippage events depends by the force applied on the sensor and by the sliding velocity.

Moreover, a further task was performed to demonstrate that the algorithm does not generate false positives. By using the same setup used for the ROC curve determination, 50 impulsive external disturbances were induced on the cube by the Kuka-probe system. The impulsive external disturbance was set in order to not generate a slippage and then an object displacement. As evident from Figure 3.17, the disturbances induced force reductions and, then, force variations. These variations

did not overcome the threshold value and, then, did not generate false positives.

Anyway, since the approach is conceived to be integrated in a complete prosthetic system composed of the peripheral interface responsible for sending motor command to the prosthesis (e.g. surface electromyography) and the control subsystem driving the commands for the prosthesis actuation system, the voluntary reduction of the grasping force that could be considered a slippage is not directly managed by the proposed touch-and-slippage detection algorithm but it is directly handled by the control system.

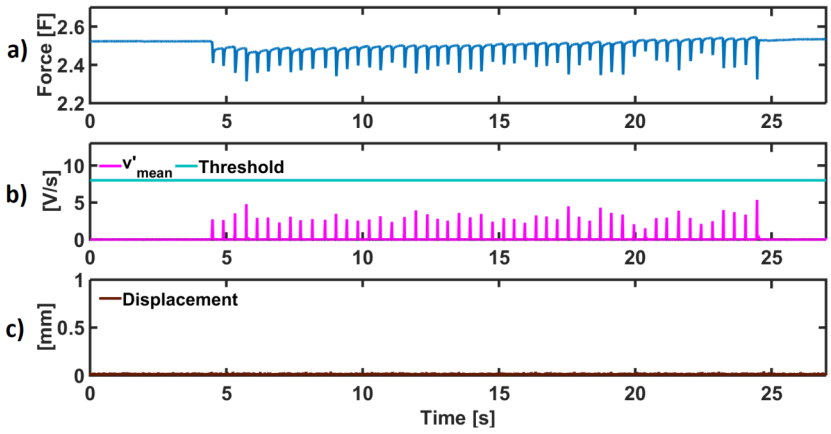

Figure 3.17 a) Force signal, b) the positive derivative of the voltage and c) object displacement when 50 impulsive external disturbances were induced on the cube.

3.3.3 Comparison with other approaches

With respect to methods where the threshold for detecting slippage is empirically derived [178, 148] or is identified with a demanding off-line training [179], the proposed method has the advantage to have a short training time. In fact, a small number of acquisitions, i.e. less than 30

events, need to be available to determine the optimal threshold for a wide range of measures (in Section 3.3.2.2, it has been demonstrated that the obtained threshold is valid in the whole functioning range of the FSR sensor).

Information about the initial touch is not differentiated from slippage in no one of the reviewed paper. For instance, in [151], touch is considered as false positive, but it is not distinguished from the other false positives.

Although some literature approaches demonstrated to obtain good results, no one of them adopts a rigorous performance evaluation of the proposed method. Although papers [151] and [152] evaluate true and false positives (in [151] true positives were detected in 100% of the cases and false positives in no more than 1.01%; in [152] 100% of true positive rate and 93% of true negative rate were obtained) they do not adopt a rigorous method to evaluate algorithm performance. In fact, they do not adopt a ground truth to recognize effective slippage events, therefore the reader cannot verify the correctness of the obtained results. In this work, not only the performance is evaluated in terms of false positives and negatives and true positives and negatives outperforming the values obtained in the literature (the true positive rate is 96.25%, the true negative rate is 100%, the false positive rate is 0% and the false-negative rate is 3.75%), but the correctness of the results is guaranteed by the adoption of a ground truth obtained with an optoelectronic system.

One significant contribution of this work is to provide a systematic way for validating the proposed slippage detection approach, by determining the threshold with the ROC curve, by adopting a probability-based approach to determine false positives and negatives so as true positives and negatives, and by introducing different ground truths to verify the correctness of each part of the method.

3.4 Conclusions

Force information is not sufficient to control a prosthesis to avoid the object falling. For this reason, a touch-and-slippage detection algorithm for robotic/prosthetic hands has been presented and experimentally validated. The proposed approach relies only on the normal force component (or on the corresponding voltage raw signal) to detect the slippage events. The touch with the object surface has been also computed and adopted as a trigger to start the slippage detection.

It has been verified that the 2^{nd} stage (v'_{mean}) of the developed algorithm, based on the signal variation, produces an output only in presence of a tangential force component (measured by a JR3 Multi-Axis Force - Torque sensor).

A ROC curve has been adopted for the detection of the threshold in order to generate a value equal to 1 only if the output of the 2^{nd} stage is higher than the threshold α.

From the data analysis, it is possible to conclude that the number of slips is dependent on the change of the force applied on the sensor and on the sliding velocity of the probe. Further, the developed algorithm works independently by the force applied to the sensor and the sliding velocity of the probe.

The results obtained in papers presenting alternative algorithms, mentioned in our literature survey, were compared with the ones obtained with our method, demonstrating the high performance reached and the rigorous evaluation procedure adopted.

Each step performed to develop the approach proposed in this paper has been described in detail and validated in a rigorous manner. This made it possible to define general methods for quantitatively evaluating system performance.

Chapter 4

Hand force-and-slippage control

Abstract

One of the main problems in the prosthetic hand design is to provide the hand with a reliable system for force and slippage control. To decrease the attention level and the cognitive burden for the user during grasp tasks, an automatic strategy is necessary. The contribution of this thesis is to propose a force-and-slippage control strategy able to i) regulate the grasping force, ii) prevent the slippage events, iii) coordinate fingers for replicating a human-like behaviour on the prosthetic system. Real-time reaction to slippage events and finger coordination have been achieved by means of i) a force control with inner position loop, ii) a sensorization system giving information about the applied normal forces, and iii) an approach for controlling the fingers in a coordinated manner on the basis of the virtual finger concept. The approach has been validated on a real prosthetic hand, i.e. the IH2 Azzurra, on which tips FSR sensors have been placed. The preliminary experimental results have demonstrated the feasibility of the combined use of the force-and-slippage control with the touch-and-slippage detection algorithm, and have shown that the prosthetic hand is able to perform stable grasps of different objects guaranteeing fingers coordination.

The high-level proposed in this thesis consists of a hierarchical classification system used to discriminate simultaneously hand/wrist gestures and desired force levels. In details, the highest NLR classifier, i.e., the "hand/wrist gestures classifier", is devoted to identifying the desired hand/wrist class among seven gestures. The output of this classifier determines the next classifier used in the hierarchy. If the output of this classifier is "Spherical" motion class, then the "Spherical force classifier" is used to determine the desired force level to exert on an object. This second classifier is conditioned on the decision of the first classifier. The same strategy is adopted if the output of the first classifier is "Tip" motion class. In this case, the "Tip force classifier" lower in the hierarchy is used to determine the desired force levels.

4.1 Introduction

Raising the attention level and the cognitive burden for the user to obtain an automatically controlling grasp also avoiding object slippage is a very important issue in hand prosthetic systems. To firmly grasp the objects, the prosthesis users need to provide constant visual attention during the task execution to adjust the grasping force and to prevent object slippage. The studies on prosthesis user needs have outlined the discomfort in this situation, where the possibility to perform actions in a more coordinated manner with a low visual attention level is always pointed out [11, 56].

The integration in the prosthesis of a control system able to drive hand actuators, managing the forces acquired by an embedded tactile system could guarantee the grasp and the stability of different objects with less visual attention (as described in Section 2.4.1) with respect to most of commercially available prosthesis hands where the force regulation during grasping is managed only by a visual control from the user.

The literature highlighted the importance of a force control strategy to ensure stability during grasp. In [180], a PI force control was implemented with a velocity inner loop, while in [26] an inner loop based on fuzzy position control was proposed keeping a PI force control as the outer loop. In [21] a force control strategy based on a neural network, aimed at compensating sensors and hardware non-linearities, was developed.

The main limitations of these approaches are that they cannot hinder the possible object slippage. In [145], improvements on grasp stability by introducing slippage prevention algorithms in the control was obtained. In particular, the results obtained with a slip prevention controller based on an integral sliding mode was compared to the results obtained with a Proportional-Derivative (PD) shear force feedback control and with a sliding mode control with no-slip prevention. The former produced

the least amount of deformation with respect to the latter controllers, simultaneously guarantying a stable grasp. The controller proposed in [156] was divided into a pre-shaping phase relying on position control and a further fuzzy logic algorithm phase to prevent the object from slipping.

Progress beyond the SoA The contribution of this thesis is to propose and experimentally test (i) a control strategy for grasping force regulation and slippage prevention and (ii) a finger coordination method for replicating on the prosthesis system a human-like behaviour.

A human-like behaviour was achieved by means:

- a low-level, for the management of the force and the slippage information, and for the voluntary force increase.
- an approach for controlling the fingers in a coordinated manner was achieved by means of the virtual finger concept [29];
- a high-level, in which a hierarchical classification approach with the aim of assessing the desired hand/wrist gestures, as well as the desired force levels to exert during grasping tasks.

4.1.1 Low-level control law

For modelling the hand fingers opposing forces on the grasped object, the concept of the virtual finger [181] was introduced. In particular, considering pad opposition grasp configurations [24] (i.e. the hand postures where the thumb pad as opposed to the long finger pads), the long fingers (i.e. the index, middle, ring and little) were modelled as a single (virtual) finger opposing forces to the thumb [29]. The choice of combining the behaviour of different fingers by modelling them as a single finger has the twofold purpose: replicating the behaviour of the human hand during grasping on the prosthetic hand (i.e. the normal

force applied by the virtual finger should be equal and opposite to the normal force applied by the thumb [29]), and reducing the prosthetic control need, handling different fingers and different grasp configurations identically.

The low-level control law block scheme of the thumb and of the virtual finger is shown in Figure 4.1.

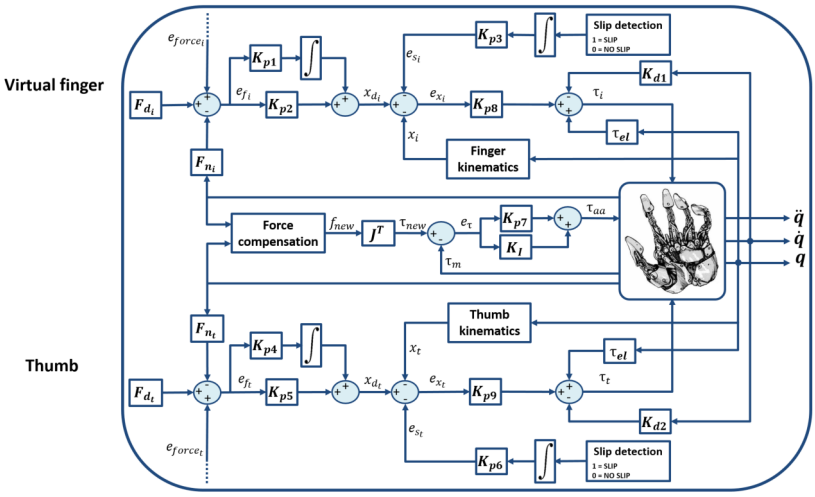

Figure 4.1 Low-level control law block scheme of the thumb and the virtual finger

The control architecture is composed of the virtual finger control, the thumb control and the coordination among the two fingers achieved by the force compensation block. This approach was adapted for under-actuated fingers, but it is extensible to other transmission systems. The fingers were controlled with a force control with inner position loop.

The reference grasping forces of the thumb F_{d_t} and of the virtual finger F_{d_i} were determined by starting from the human study performed in [33]. It is clear that a force reference for each unknown grasped object is hard to obtain, especially in real-time. The slippage information

allows a control adjustment for each grasped object, increasing force until a stable grasp is achieved. Therefore, a specific force reference for each object and for each grasp type was not necessary [182, 183].

The normal forces, F_{n_t} and F_{n_i}, acquired by the force sensors and applied by the prosthetic hand fingers tips on the object surface were subtracted to the reference force to obtain a force error, e_{f_t} and e_{f_i}, that have to be minimized by the control. Then, the reference position x_{d_i} for the $i-th$ finger slider was obtained from a Proportional-Integrative (PI) force control

$$x_{d_i} = K_{p1} \int_0^{t_f} (F_i - F_{n_i} + F_{increase_i}) dt + K_{p2}(F_i - F_{n_i} + F_{increase_i}) \quad (4.1)$$

and was compared with the actual position x_i derived from the hand position sensors. K_{p1} and K_{p2} are the controller gains and t_f is the final integration time. Two additional contributions were considered: $F_{increase_i}$ to increase the force during the grasp and e_{s_i} to manage slippage events [145]. Therefore, the position error of the $i-th$ finger is

$$e_{x_i} = x_{d_i} - x_i - e_{s_i} \quad (4.2)$$

where

$$es_i = K_{p3} \int_0^{t_f} \alpha, \quad (4.3)$$

α is the binary signal equal to 0 when slip does not occur and 1 if a slip occurs, K_{p3} is a constant regulating the e_s weight in the control. The integration of this signal will guarantee a smooth increment of the applied grasping force in presence of slippage [145]. Three force levels were managed [31], with a single increasing equal to 0.3 N (total equal to 0.9 N).

The so obtained position error e_{x_i} should be led to zero by a PD control in the slider space described by the equation

$$u = r[K_p(x_{d_i} - x_i - e_{s_i}) - K_D\dot{x} + T_{el}] \tag{4.4}$$

T_{el} is the cable tension compensating for the spring elastic forces due to the underactuated transmission system, r is the vector of the pulley radii and x, $\dot{x}$, $\ddot{x}$ are the slider position, velocity and acceleration, respectively [176]. Under the hypothesis of the rigid object and rigid finger pads, to guarantee the grasp stability, the normal force applied on the object surface by the virtual finger should be equal and opposite to the normal force applied by the thumb, neglecting the force contribution due to the grasped object weight [29].

As described in Section 1, a force compensation block was added to guarantee a fingers coordination, taking in input the normal forces acquired by the sensors on the fingertips.

To be compared, the acquired forces should be expressed in a common reference frame that was supposed coincident with the wrist joint. Therefore, the measured forces applied by the hand tips were computed in the wrist frame

$$F_{TIP}^{wrist} = R_{tip}^{wrist} F_{TIP}^{tip} \tag{4.5}$$

where R_{tip}^{wrist} is the rotation matrix of the fingertip reference frame with respect to the wrist reference frame, F_{TIP}^{wrist} is the force applied by the TIP in the wrist reference frame and F_{TIP}^{tip} is the fingertip force expressed in the fingertip reference frame. Then, the obtained forces of the thumb and of the virtual finger were compared and equalized in the wrist reference frame. By means the transformation matrices, they were brought back to the fingertip reference frame. The application of the desired force on the object was guaranteed by driving the finger motors to apply the corresponding torque τ_{new} obtained by means of the hand finger Jacobian and of the balanced forces:

$$\tau_{new} = J_p^T F_{new_{TIP}}^{wrist} \tag{4.6}$$

where $F_{new_{TIP}}^{wrist}$ is the force the TIP should apply in the wrist reference frame and J_p^T is the transposed Jacobian matrix related to the linear velocity. Only the torque pertaining the thumb A/A was considered and compared with the actual thumb A/A torque τ_m obtained from the hand sensors. A PI controller was added to guarantee the convergence to zero of the torque error e_τ. The so obtained A/A torque was given in input to the thumb dynamics.

4.1.2 High-level strategy for the classification of hand/wrist gestures and forces

A hierarchical pattern recognition strategy was proposed for the classification of the desired hand/wrist gestures (Rest (hand relax), Spherical (hand with all fingers closed), Tip (hand with thumb and finger touching as if picking a small object), Platform (hand completely open and stretched), Point (hand with all fingers closed except for the index finger), Wrist Supination, Wrist Pronation) and force levels (Low, Medium, High) from muscular signals (Figure 4.2). The FSM coordinated the hierarchical activation of the three classifiers.

The highest classifier in the hierarchy was a single classifier able to discriminate seven discrete hand/wrist motion classes. The output of this classifier determined the desired hand/wrist gesture and, in case of "Spherical" or "Tip" class, the force classifier, lower in the hierarchy, to be activated. Thus, the force classifiers were activated for force levels recognition.

The FSM coordinated the three classifiers activation (i.e one for hand/wrist gestures and two for force levels). The FSM approach was characterized by the following key features:

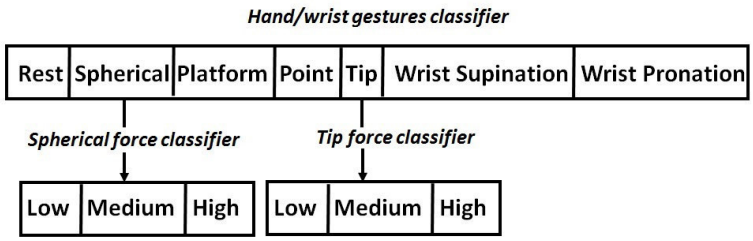

Figure 4.2 Hierarchical classification strategy. "Hand/wrist gestures classifier" allowed the identification of the desired motion class among 7 different gestures. "Tip force classifier", lower in the hierarchy, allowed the classification of 3 force levels for "Tip" gesture. "Spherical force classifier", lower in the hierarchy, allowed the classification of 3 force levels for "Spherical" gesture.

- The FSM can only be in a fixed set of states;
- The FSM can only be in one state at a time;
- A sequence of inputs was sent to the FSM.

The proposed classification system was characterized by three different classifiers (Figure 4.3):

- The "hand/wrist gestures classifier" was able to discriminate seven states, corresponding to seven hand and wrist gestures (blue circle states in Figure 4.3). This classifier was always active and it was the highest classifier in the hierarchy (Figure 4.3).
- The "Spherical force classifier" was able to discriminate three force levels (i.e. Low, Medium and High Level shown in Figure 4.3 in the red box). It was active if the "Spherical" gesture was identified and it was lowest in the hierarchy (Figure 4.3).
- The "Tip force classifier" was able to discriminate three force levels (i.e. Low, Medium and High Level shown in Figure 4.3 in the red box). It was active if the "Tip" gesture was identified and it was lowest in the hierarchy (Figure 4.3).

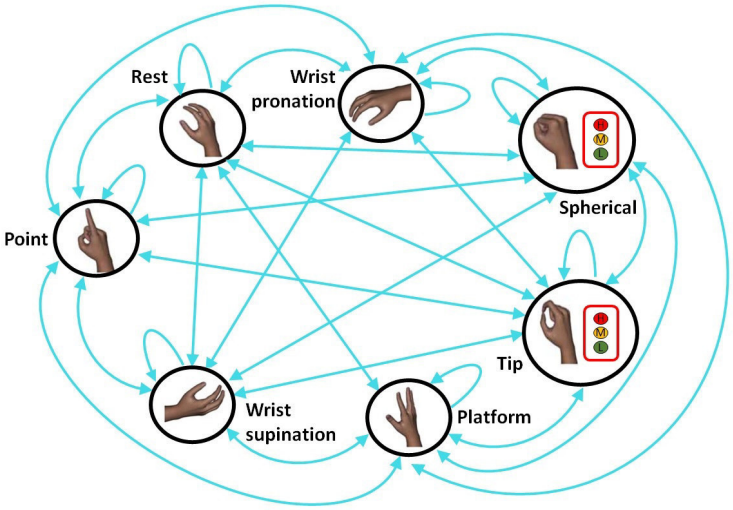

Figure 4.3 FSM strategy for the classification of 7 different hand/wrist gestures and 3 force levels: the blue circle states indicated the hand gestures and wrist motions and they were all classified through the "hand/wrist gestures classifier". Three force levels (Low, Medium, High) can be classified through the "Spherical or Tip force classifier" if the "hand/wrist gestures classifier" discriminated respectively the "Spherical" or "Tip" state. If the "Spherical" or "Tip" state was classified, the hierarchical classification strategy was adopted.

FSM determined the following different scenarios: a single classification approach used "hand/wrist gestures classifier" to recognize 7 discrete hand/wrist motion classes; the classification approach became hierarchical when the output of this classifier was the "Spherical" or "Tip" motion class. In this case, a second classifier (force classifier) was activated. Until the FSM system remained in one of these two states (i.e. "Spherical" or "Tip"), the output of the FSM system provided hand/wrist gestures and the force levels information. Otherwise, if the FSM system was in a different state from the "Spherical" or "Tip", only the single "hand/wrist gestures classifier" was activated and the gesture information was supplied.

The force classifiers managed only a three classes classification problem related to three different force levels (i.e. Low, Medium and High).

4.2 Experimental validation

Two experimental sessions were carried out to validate the proposed approach.

In the first experimental session, the force-and-slippage control strategy with the touch-and-slippage detection algorithm (described in Section 3) was verified in a real case, by using a prosthetic robotic hand, provided with FSR sensors on the thumb and index fingertips, to perform pinch and power grasps. False positives and negatives so as true positives and negatives were identified through an optoelectronic system used to measure the object displacement due to slippage.

In the second experimental session, a hierarchical classification approach with the aim to assess the desired hand/wrist gestures, as well as the desired force levels to exert during grasping tasks was verified. An FSM was introduced to manage and coordinate three classifiers based on the Non-Linear Logistic Regression (NLR) algorithm. The classification architecture was evaluated across 31 healthy subjects.

4.2.1 Experimental session 1

4.2.1.1 Experimental setup and protocol

The IH2 Azzurra hand, described in Section 3.3.2.1, was used with the difference that all the fingertips were equipped with an FSR.

The aim of this work is to validate the strategy independently of the adopted interface with the user. Therefore, the prosthetic hand has not been directly commanded by the user, but it was positioned on support

and commanded by a PC that simulates the movement class and the force levels of the high-level.

Only the index and the thumb fingers were able to detect slippages during the grasps since they are involved in both grasp types.

The starting Abduction/Adduction angle of the thumb was imposed on the basis of the human being behaviour [87]; in particular, for the pinch and power grasp, it was imposed an A/A angle of 86° and 110°, respectively.

The proposed strategy was implemented in C under Windows 10. The communication between the hand and the PC was performed by means of a USB port. Referring to Figure 4.1, the gains of the control strategy were imposed equal to $K_{p1} = K_{p5} = 0.1, K_{p2} = K_{p6} = 1, K_{p3} = K_{p7} = 4, K_{p4} = K_{p8} = 80, K_{p9} = 1, K_{d1} = K_{d2} = 0.004$ and $KI = 10$.

The moving-object system described in Section 3.3.2.1 was used to give the objects to the hand. Both objects and the robotic hand index were equipped with markers; the optoelectronic system, used in Section 3.3.2.1, was employed to measure the displacement due to slippage, as previously described. In particular, a small ball (SB) of diameter ∅ = 35 mm and weight of 17 g, a small cylinder (SC) of ∅ = 19 mm, height (h) = 100 mm and weight 18 g, and a small parallelepiped (SP) 28 x 49 x 100 mm and weight 47.2 g were grasped with a pinch grasp; a tennis ball (TB) of ∅ = 60 mm and weight of 58 g, a big cylinder (BC) of ∅ = 35 mm, height (h) = 150 mm and weight 103 g, and a big parallelepiped (BP) 40 x 67 x 133 mm and weight 255.5 g were grasped with a power grasp. During the grasp types of the objects, the fingers flex until the forces measured by the sensors reach the reference value, as shown in Figure 4.4.

When the object was firmly grasped, 5 slippages were induced by the robotic arm, as previously described. This task was repeated 40 times

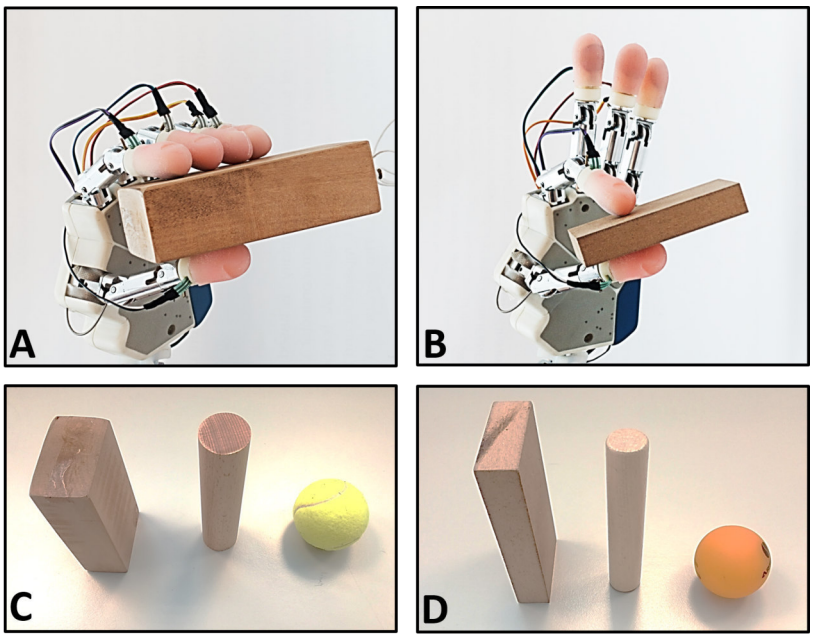

Figure 4.4 Grasp types and objects used during the experimental session. **A** Power grasp of BP. **B** Pinch grasp of SP. **C** Objects grasped with power grasp (BP, BC, TB). **D** Objects grasped with pinch grasp (SP, SC, SB).

for each object for the two grasp types. The forces measured by the FSR sensors were acquired during the whole session.

The performance of the force-and-slippage control strategy in the presence of the touch-and-slippage detection algorithm was evaluated to first verify the feasibility of its application in a real scenario.

4.2.1.2 Results and discussion

To test the approach on a real scenario, the IH2 robotic hand was used to grasp different objects (robotic hand index and each object were equipped with markers) from the moving-object system, while the slippage events

were simulated by applying impulsive forces to the object surface by means of the robotic arm.

For the sake of brevity, in Figure 4.5 the outputs of 5 slippages induced by the robotic arm are shown for a single task both for pinch and power grasps.

Until the time instant t_0, high-level is active and the user can decide the movement to perform. From t_0 to t_1, medium level allows pre-shaping and reaching phases, until the touch with the object is present. Then, low-level is activated until t_2, when the open movement class is sent to the hand by the user. The touch with the object is lost and the medium level allows the hand opening. From the instant t_3, the high-level is again activated.

Subplot *a)* in A. and B. depicts the forces applied by the fingers. Subplots *b)* and *c)* show the touch and the slippage events detected by each finger. In the subplot *e)*, the displacements due to the slippages are presented.

It is possible to observe that the sensor on the thumb detected one slippage event in A. and two in B., whereas the one on the index detected five slippage events for both cases. This information is enough for the force-and-slippage control strategy adopted for controlling the robotic hand since it requires that only one of the fingers detects the slippage, in order to compensate it. In subplots *d)*, the finger joint angles are shown. An increasing of the F/E angles of the involved fingers joints and a variation of the A/A angle of the thumb joint are evident when slippage occurs (in the red box of the subplots *d)* of Figure 4.5 an enlargement of this behaviour is shown).

To verify the correctness of the use of the force-and-slippage control strategy with the touch-and-slippage detection algorithm, the *sensitivity*, *specificity* and *accuracy* (the capacity of the algorithm to detect the slip; it is obtained by the ratio between the correct classified samples

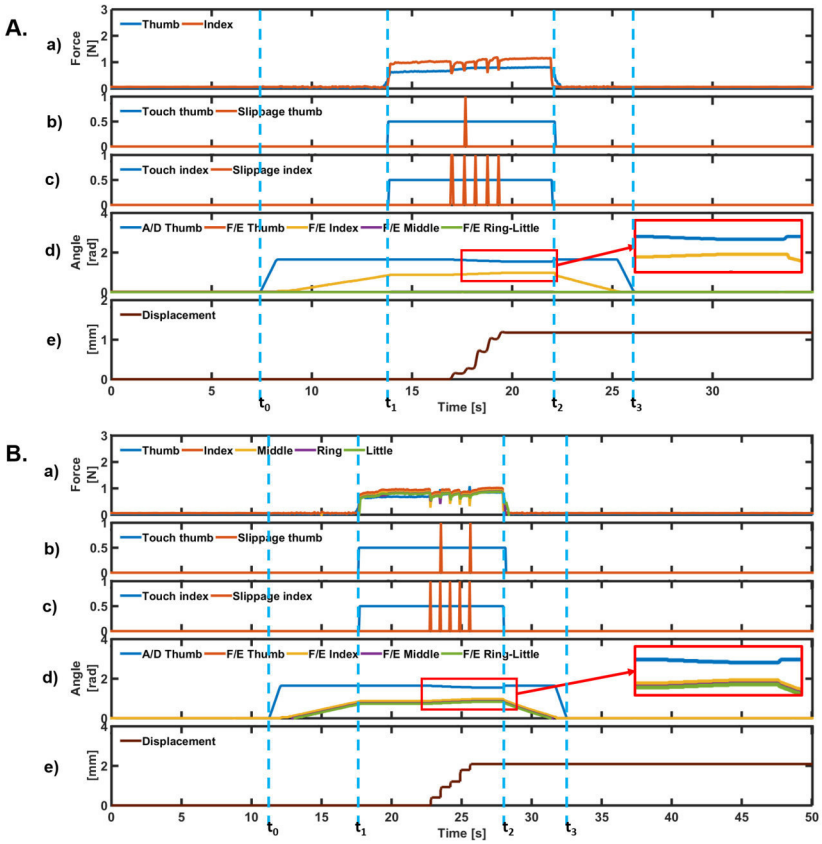

Figure 4.5 Validation in real scenario. A. Pinch grasp of SB. a) The force acquired by the FSR sensors on the thumb and the index. The touch and the slippage events detected by b) the thumb and c) the index finger. d) The joint angles of the robotic hand. The joint angle variations corresponding to the slippage compensation are outlined in the red box. e) The displacements between the markers positioned on the object and on the robotic hand index caused by the slippages. **B. Power grasp of TB.** The only difference with respect to A. is the first subplot in which the forces are acquired by the FSR sensors on all the fingers.

and the total samples) parameters for the 40 tasks for each of 3 objects for the 2 grasp types, listed in Table 4.1. On the total 240 tasks, the true

positive rate is 96,25%, the true negative rate is 100%, the false positive rate is 0% and the false-negative rate is 3,75%.

The low computation time of the force-and-slippage control strategy with the touch-and-slippage detection algorithm, i.e. 20 ms (from the acquisition of the first voltage sample to the sending of the torques values to the fingers motors, including the time to calculate the eventual slippage), lower than the physiological time of 100 ms [86], suggests that the applicability in real systems is feasible.

Finally, in Figure 4.6 it is possible to observe three force increases (at the time instants t_2, t_3 and t_4) during a pinch grasp and then the return to the initial reference value.

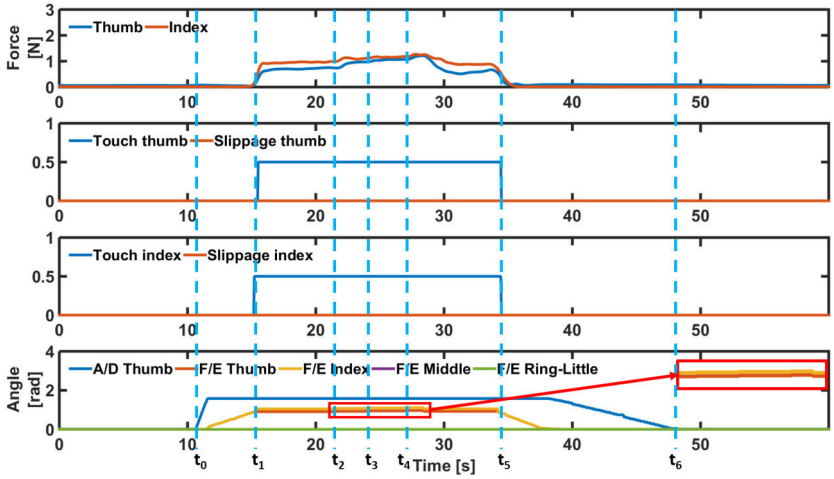

Figure 4.6 Three force increasing during a pinch grasp. The joint angle variations corresponding to the force increasing are outlined in the red box.

As evident in Table 4.1, in most cases the *sensitivity*, *specificity* and *accuracy* are equal to 100%, i.e. all the 5 induced slips were detected; in the other cases only 4 slips were detected with a *sensitivity* equal to 80%, *specificity* 100% and *accuracy* 99.53%.

Table 4.1 Sensitivity, specificity and accuracy parameters for the 40 task performed with the robotic hand for each object and each grasp type.

	Pinch grasp					
	SC		**SP**		**SB**	
	40 total tasks		**40 total tasks**		**40 total tasks**	
	39 tasks	**1 tasks**	**38 tasks**	**2 tasks**	**40 tasks**	**0 tasks**
Sensitivity	100%	80%	100%	80%	100%	-
Specificity	100%	100%	100%	100%	100%	-
Accuracy	100%	99.53%	100%	99.53%	100%	-

	Power grasp					
	BC		**BP**		**TB**	
	40 total tasks		**40 total tasks**		**40 total tasks**	
	37 tasks	**3 tasks**	**39 tasks**	**1 tasks**	**38 tasks**	**2 tasks**
Sensitivity	100%	80%	100%	80%	100%	80%
Specificity	100%	100%	100%	100%	100%	100%
Accuracy	100%	99.53%	100%	99.53%	100%	99.53%

4.2.2 Experimental session 2

4.2.2.1 Experimental setup and protocol

Thirty-one healthy participants (age: 28 $\pm$ 7.6 years) were involved in the experiments. Six commercial active sEMG sensors (Ottobock 13E200=50, 27 mm X 18 mm X 9.5 mm) were equidistantly fixed on an elastic adjustable bracelet and then were placed on the forearm of the able-bodied subjects in order to acquire sEMG signals (Figure 4.7).

The bracelet was located about 5 cm below the subject's elbow, in line with the positioning of the electrodes, commonly used to control a prosthetic hand [184]. The number of sEMG sensors was chosen equal to six because it was considered the highest number that was possible to place into the socket [184]. Moreover, it allowed reducing the data dimensionality and complexity [185].

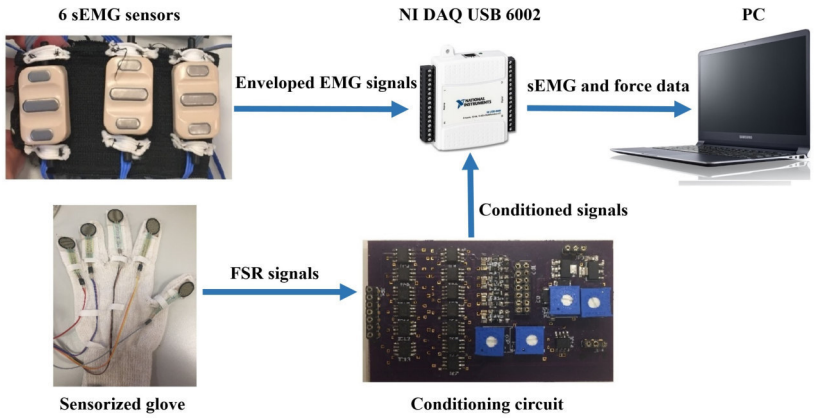

Figure 4.7 The experimental setup was composed by: (i) a sEMG elastic bracelet, (ii) NI DAQ USB 6002, (iii) a conditioning circuit and (iv) glove equipped with FSR 402

Five FSR 402 [171], were placed on a glove to verify the effective forces executed by the subjects. The relationship between the FSR voltage value V and the force value F was established as described in Section 3.3.1.1. The Anderson loop was used as signal conditioning circuit [160]. The EMG and force data were simultaneously acquired at 1 kHz using a DAQ USB 6002 device. The PC (Samsung Intel(R) Core (TM) i7-4500U CPU @ 1.80 GHz 2.40 GHz) and DAQ communicated by means of a USB port.

The subject was sitting in front of a monitor (Figure 4.8) and was asked to perform the above described seven hand gestures: Rest, Spherical, Tip, Platform, Point, Wrist Supination and Wrist Pronation. The participants were asked to produce each of these gestures for six times and hold it for 2 s with an interval of rest state about 2 s between each repetition.

In an initial phase before the training, each subject was asked to produce maximum muscle contractions in order to perform the highest

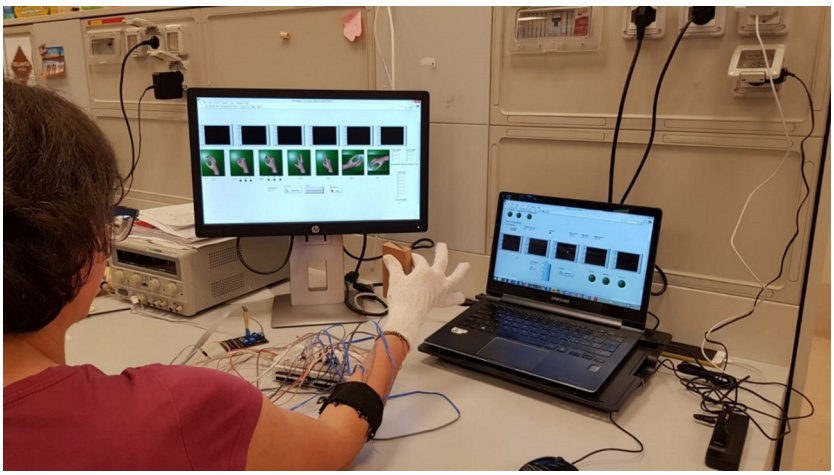

Figure 4.8 Subject positioning and data acquisition during experimental validation of the proposed approach. The subject was sitting in a comfortable chair in front of a PC monitor and was asked to perform six repetitions of each hand/wrist gesture. The subject performed "Spherical" and "Tip" gestures during the grasping of a rectangular object and executed three force levels. Written informed consent for the publication of this image was obtained.

peak of force, while grasping a stiff object of rectangular shape (weight 66 g, dimensions 50 x 100 x 17 mm) with "Spherical" and "Tip" grasps. The object was used also during the training session.

Three force thresholds were established at 30% (low), 60% (medium) and 90% (high) of the sum of all force contributions recorded from FSR sensors. Three force bands were defined as follows to reduce the difficulty to perform a punctual value of force: the low-level was fixed between the $\pm$15% of the lowest threshold (i.e. 30%), the medium level was fixed as $\pm$15% of the medium threshold (i.e. 60%), while the high level starts from -15% of the highest threshold (i.e. 90%) and continued until the maximum value. These bands were used to give visual feedback to the subject during the recording of "Spherical" and "Tip" gestures.

4.2.2.2 Results and discussion

The results of the "hand/wrist gestures classifier" are reported in Table 4.2 in terms of the average accuracy and F1Score.

Table 4.2 Mean value and standard deviation of F1Score and Accuracy of the "hand/wrist gestures classifier" calculated for 31 healthy subjects

Hand/Wrist gestures Classifier				
Classes	**F1_Score**		**Accuracy**	
	Mean (%)	**Dev_std**	**Mean (%)**	**Dev_std**
Rest	98,25	4,05	99,50	1,24
Spherical	95,63	6,22	98,71	1,94
Tip	95,56	4,93	98,69	1,55
Platform	95,97	6,58	98,86	1,84
Point	92,69	9,25	97,63	3,58
Wrist supination	95,70	6,70	98,64	2,26
Wrist pronation	98,20	4,93	99,41	1,7

Table 4.3 Mean value and standard deviation of F1Score and Accuracy of the "Spherical force classifier" calculated for 31 healthy subjects

Spherical Force Classifier				
Classes	**F1_Score**		**Accuracy**	
	Mean (%)	**Dev_std**	**Mean (%)**	**Dev_std**
Low	97,49	4,84	98,35	3,13
Medium	97,43	4,21	98,25	2,86
High	99.69	1,2	99,80	0,78

The results of the two force classifiers, "Spherical force classifier" and "Tip force classifier" are shown, respectively, in Table 4.3 and Table 4.4, in terms of the average F1Score and accuracy. The average classification accuracy for "hand/wrist gestures classifier", "Spherical and Tip force classifiers" are respectively equals to 98.78%, 98.80%, 96.09%.

Table 4.4 Mean value and standard deviation of F1Score and Accuracy of the "Tip force classifier" calculated for 31 healthy subjects

Tip Force Classifier				
Classes	**F1_Score**		**Accuracy**	
	Mean (%)	**Dev_std**	**Mean (%)**	**Dev_std**
Low	91,54	8,61	94,46	5,42
Medium	91,56	8,24	94,36	5,14
High	99.03	1,96	99,26	1,31

Figure 4.9 shows the average confusion matrix when testing the "hand/wrist gestures classifier". Figure 4.10 and Figure 4.11 show the average confusion matrix when testing the "Spherical force and Tip force classifiers", respectively.

In Figure 4.12 the average values of the sum of all the FSR measurements for 31 healthy subjects are showed.

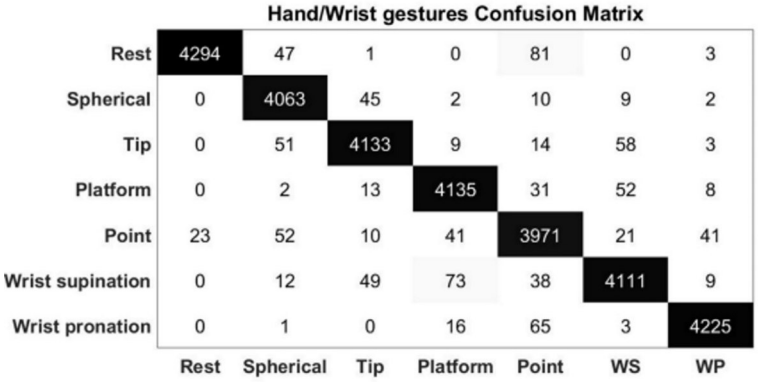

Figure 4.9 Confusion matrix of the "hand/wrist gestures classifier". On the main diagonal the cardinality of the correct classifications is reported; in the top left dial and bottom right dial, the cardinality of the misclassified data related to the 7 output classes representing the hand gestures are reported.

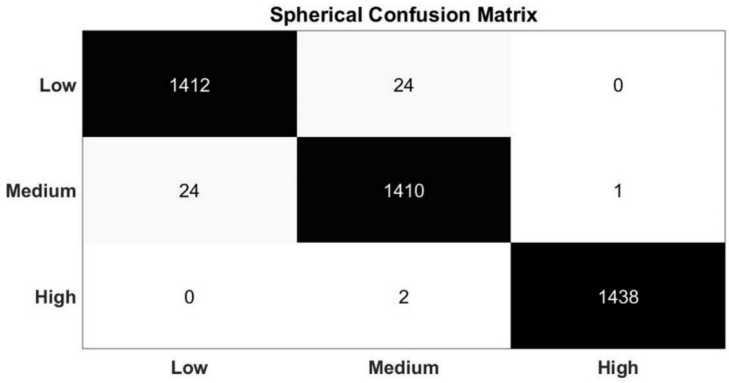

Figure 4.10 Confusion matrix of the "Spherical force classifier". The cardinality of the correct classifications is reported on the main diagonal; in the top left dial and bottom right dial, the cardinality of the misclassified data related to the 3 output classes that represented the force levels are reported.

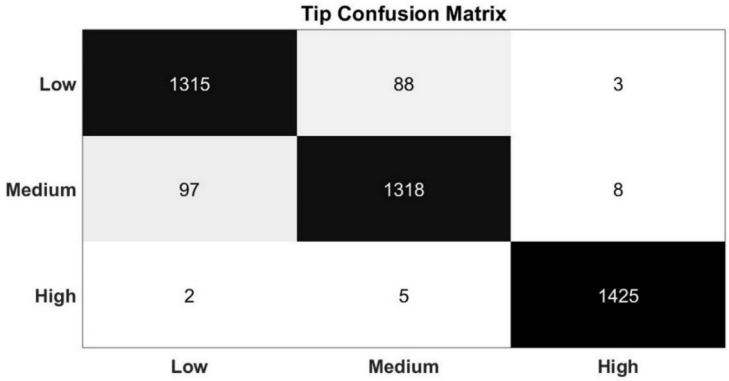

Figure 4.11 Confusion matrix of the "Tip force classifier". On the main diagonal the cardinality of the correct classifications is reported; in the top left dial and bottom right dial, the cardinality of the misclassified data related to the 3 output classes that represented the force levels are reported.

Almost all healthy subjects were able to modulate the force levels and fall into the range displayed by the visual feedback, without gener-

ating high variance values, as shown in Figure 4.12. Few subjects had difficulty reproducing forces values despite visual feedback as a reference. For instance, in Figure 4.12, the subjects 25 and 3 were not able to well differentiate between medium and high force levels during Tip grasp (represented as red and black points), while subject 28 performed the three force levels too closed during Tip grasp. This depended on the subject's difficulty to maintain the applied force within the force intervals.

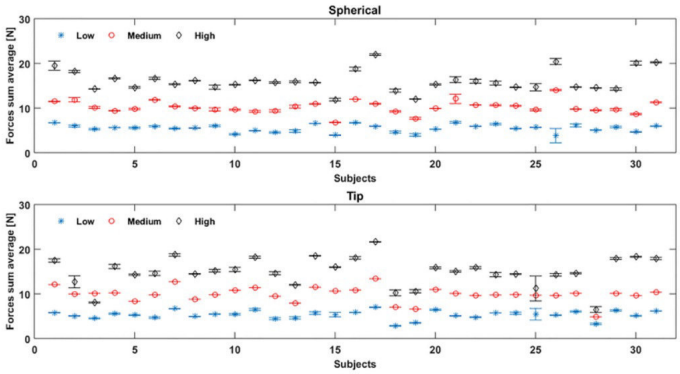

Figure 4.12 Force sum average values are obtained, by FSR measurements, for 31 healthy subjects during, respectively, the "Spherical" and "Tip" gestures, performed six times: the blue, red and black values represent the mean value and standard deviation of respectively low, medium and high force values performed by each subject.

The "Spherical force classifier" identified the force level reaching an average F1 score of 98.75% with NLR classifier, (Table 4.3). The "Tip force classifier" was able to define the force level with an average F1 score of 94.04% (Table 4.4). These results seem to be very promising if we consider that similar values of average F1Score were achieved only for gesture classification [186, 185]. Confusion matrices, reported in Figures 4.9, 4.10, confirmed the positive results of the accuracy parame-

ter. The cardinality of the correct classifications on the main diagonal underlined the high classification accuracy even if some misclassified data out of the main diagonal suggested a bit minus performance of "Tip force classifier" respect to "Spherical force classifier." This is due to the major difficulty encountered by a few subjects to modulate between low and medium force levels during a Tip grasp. The high force levels were always well discriminated at 99%.

4.2.2.3 Training environment for patient underwent to the Targeted Muscle Reinnervation

Upper-limb amputees need a prosthesis that replaces lost arm functionality. Active externally powered devices can be myoelectric or hybrid, but the first ones are most used [187]. Nevertheless, the abandonment factors for arm prosthesis are related to comfort and functionality, since amputees control the device in an unnatural way: with the co-contraction of two muscles to switch among DoF's groups (elbow, wrist, hand) [188] and with one muscle contraction to control each possible movement for that specific DoF's group (opening and closing for the elbow, pronation and supination for the wrist, opening and closing for the hand) [57].

In the last three decades, a new surgery technique was proposed by T. A. Kuiken: TMR [189, 190]. TMR is a surgical procedure that allows reinnervating, with residual nerve, target muscles that are no more used (Figure 4.13 [191]).

The residual nerves after an arm amputation are still functional up to the amputation site. It is possible to integrate these nerves into a different muscle to trigger a contraction. The original nerve is severed and surgically relocated to become incorporated into the muscle. This process is called targeted reinnervation. Training during the subsequent rehabilitation process allows the activation of the reinnervated muscles appropriately and selectively.

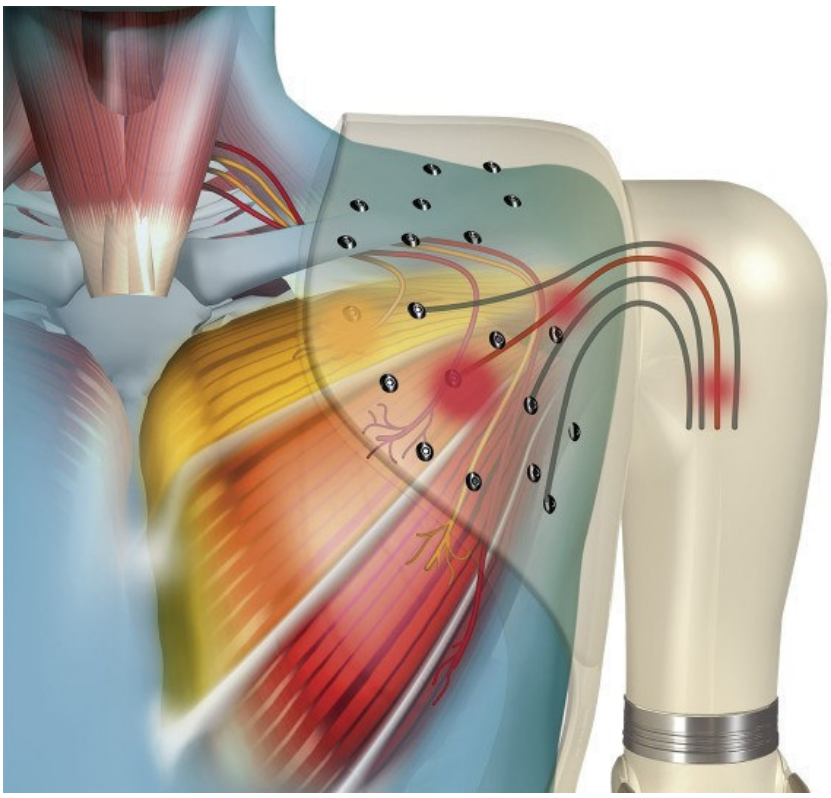

Figure 4.13 TMR example: the residual nerves of the arm are reinnervated in the pectoral muscle

In 1995 Kuiken examined muscle recovery and related changes in the motor unit population of "hyper-reinnervated" rat [189]; in 1998 the effect of long-term denervation on neuromuscular recovery in a rat hind limb model is presented [192]. We need to wait until 2004 for the first TMR surgery on human [190]. The idea was that muscle reinnervation allows users to more intuitively control prosthesis and simply perform ADL with sEMG.

When the EMG signals are available to be acquired from the sensors ($\sim$ 6 months after surgical [193]), amputee patient needs training before

using the prosthetic arm. Virtual realities (VR) are simple solutions to allow safe training for amputees [194, 195]. In this manner, the first phase with an ON/OFF control would be useful to the user to feel natural muscle contraction lost with the arm amputation.

Figure 4.14 Avatar of a human arm in ad-hoc developed virtual reality

To give a young woman, who underwent the TMR, the possibility of learning how to control a real arm prosthesis, a VR (Figure 4.14) reproducing the subject right arm and controlled by means of sEMG acquired from the reinnervated areas was developed in this thesis. The volunteer participant is a 27 years old right-handed woman with a right shoulder disarticulation. The patient, after the surgical procedure, was trained to use the reinnervated areas to control a real arm prosthesis.

A software ad-hoc (Figure 4.15) developed for the EMG signals management allows: i) the detection of a threshold (built on the 30% of the maximum contraction for that signal) for each sEMG sensor positioned on the reinnervated areas, ii) the acquisition and ii) the recording of the signals.

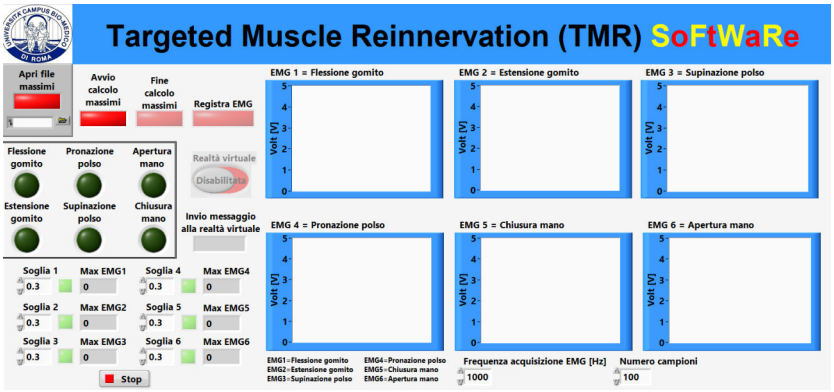

Figure 4.15 Graphic interface of the software developed to acquire, to manage and to record EMG signals

When each signal overcomes the threshold, a signal equal to 1 was sent to the VR to move the corresponding virtual arm DoF (6 movements for 6 reinnervated areas of the arm: opening and closing of the elbow, pronation and supination of the wrist, opening and closing of the hand). Preliminary results are shown in Figure 4.16 where, for the wrist supination movement, is evident that only after 17 days (in Figure 4.16) the others signals not associated to that DoF are lower than the corresponding threshold (in particular, the elbow flexion signal is lower than the corresponding threshold but also the elbow extension signal and the wrist pronation signal have a low amplitude in B) than to A)). This means that appropriate training lets the user learn how to selectively activate the reinnervated muscles.

4.3 Conclusions

A hand force-and-slippage control for the prosthetic hand was proposed and preliminarily tested on a poliarticulated prosthetic hand. The strategy is divided into 3 phases: a low-level, for the management of force and slippage information, and for the voluntary force increase; a medium

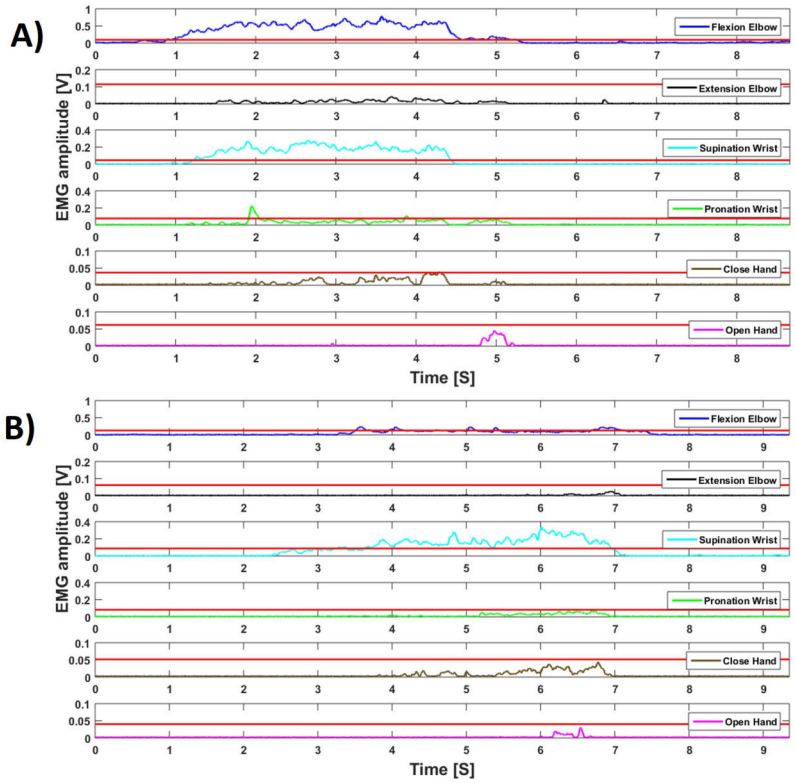

Figure 4.16 EMG signals for wrist supination. A) Training performed on 11/02/19. B) Training performed on 28/02/19.

level, for the pre-shaping and the reaching; and a high-level, for the user biological signal management. Furthermore, an approach for controlling the fingers in a coordinated manner was developed by means of the virtual finger concept.

FSR sensors positioned on the prosthetic hand fingertips was adopted for measuring the grasping forces. The slippage detection algorithm described in Chapter 3 was introduced in the low-level of the control strategy. Furthermore, an approach for controlling the fingers in a coordinated manner on the basis of the virtual finger concept was adopted.

Information about the forces applied on the objects during grasping, the slippage events, the joint angles were recorded during the trials in order to demonstrate the feasibility of the combined use of the force-and-slippage control with the touch-and-slippage detection algorithm, and have shown that the prosthetic hand is able to perform stable grasps of different objects guaranteeing fingers coordination. The combined use of the force-and-slippage control with the touch-and-slippage detection algorithm led to a success rate (i.e. n° of compensated slippage event/n° of trials) of 100%. Preliminary results have been obtained for the pinch and the power grasp of several objects, but the approach is easily extendable to the other grasp configurations.

In the high-level, a hierarchical classification approach was developed and tested to discriminate both hand/wrist gestures and force levels applied during grasping tasks. The method employed three different classifiers to discriminate both desired gestures and forces. The NLR algorithm was adopted for implementing the hierarchical classification approach and comparative analysis among the performance of these two algorithms was done. The force classifiers were able to robustly discriminate the same class of movement performed at different muscle contractions because they were trained with data containing the modulation of different force levels. A new potential strategy should be introduced for mitigating the effect of different exerted forces within a given movement class. Another innovative contribution is represented by the use of FSM theory for the management of three classifiers. This strategy avoids to resolve a seven multi-class problem using a single classifier and it makes the system controllability less complex by activating the force classifiers only when the "hand/wrist gestures classifier" returns an output class belonging to a closure hand gesture. This classification approach, implemented with the NLR algorithm, has obtained positive results and seems to be very promising for identifying simultaneously

desired gestures and force levels. In conclusion, the proposed method allowed to extract from EMG signals all the valuable information regarding not only muscle contractions related to hand/wrist motions but also the changes of muscle activation patterns depending on the influence of different force levels. This approach will allow to improve the performance of the currently adopted prosthesis EMG control architectures thanks to the possibility to manage desired gestures and force levels in a more natural way.

Chapter 5

Real-time force-and-slippage closed-loop control in one amputee subject

Abstract

Dexterity and manipulations skills in humans are allowed by complex biomechanics of the hand and a control loop based on a bidirectional communication with the brain, thanks to a sophisticated sensory system. Restoring of the bidirectional communication with the Peripheral Nervous System (PNS) in amputees through neural electrodes in the upper-limb nerves is a great challenge. Over the years, several studies were performed in order to restore a bidirectional communication in amputee to control a prosthesis but there are no examples of the use of the routed sensory information to finely control a prosthetic hand in complex grasp and manipulation tasks.

The developed arguments described in the previous chapters have contributed to restoring a real-time closed-loop control of bionic hands in tasks of fine grasp and manipulation. The strategy is similar to the one previous described, but each part was adapted to the specific need of the amputee. Force and slippage sensations were elicited in an amputee by means of biologically inspired slippage detection and encoding algorithms, supported by a stick-slip model of the performed grasp. A combination of the cuff and intraneural electrodes was implanted for 11 weeks in a young woman with a hand amputation. Evidence is provided about the improvement of the participant's grasping and manipulation capabilities over time resulting from neural feedback. The elicited tactile sensations enabled the successful fulfilment of fine grasp and manipulation tasks with increasing complexity. Grasp performance was quantitatively assessed by means of a purposely developed metrics. Closed-loop control capabilities enabled by the neural feedback were compared with those achieved without feedback.

5.1 Introduction

Hand loss is a dramatic event that changes the quality of life. Simple ADLs become difficult challenges. Although myoelectric prostheses are available for amputees, their abandonment caused by the unnatural perception of the device is common [56–58]. The lack of sensations due to interaction with the environment makes the prosthesis a simple device not felt as a part of the body.

Restoring the bidirectional communication with the PNS in amputees through neural electrodes in the upper-limb nerves is a great challenge.

Over the years, several studies were performed in order to restore a bidirectional communication in amputee to control a prosthesis.

The first attempt of a bidirectional control of a prosthetic hand through the use of intraneural electrodes has been developed in [196]. In this work, the possibility of using implanted peripheral nerve electrodes for the production of discrete touch and movement sensations and for the motor neuron activity recording has been demonstrated, without exploring the closed-loop control of the prosthesis. On the other hand, in [197] this aspect has been shown. A hand prosthesis control has been established by means of the neural signal directly extracted from median and ulnar nerves of an amputee while sensory feedback has been elicited by using afferent neural stimulation. In [198] the bidirectional control of a prosthetic hand was developed and used to recognize object features and positions during grasp. In [199] the improvement of hand controllability using implanted EMG sensors has been demonstrated.

Progress beyond the SoA The contribution of this thesis is to show the possibility of enabling real-time closed-loop control of bionic hands in tasks of fine grasp and manipulation, by using routed sensory information through neural electrodes implanted in an amputee. Close-to-natural

force and slippage sensations were elicited improving the participant's manipulative skills with the prosthesis.

The strategy described in the previous chapter was modified for the real need of the amputee.

High-level described in Section 4.1.2 was modified in order to classify five gestures: rest (relaxed hand), power (hand with all fingers closed), pinch (hand precision grasp with two fingers), open (hand with all fingers opened), and lateral (hand lateral configuration), and three levels of forces (high, medium, low).

Low-level described in Section 4.1.1 is not automatic in this Section because force and slippage sensations were elicited in the participant's nerves in order to allow her to actively control the prosthesis to regulate force and to manage the slippage.

As described in Section 3.2.3, stick-slip model, present in literature, was extended to simulate the more realistic situation of a multi-fingered grasp of an object; this model well describes the slippage phenomenon that generates movement of the grasped object relative to the skin of the fingers that are involved in grasping. For this reason, ten healthy subjects were recruited to perform grasp tasks: when the object was firmly grasped in the hand, a mass was added to cause the slippage. Information about forces and displacement were recorded and used in the model to validate it. The same tasks were performed by the amputee. The developed model causes a change in the contact area of the object with the fingers and that the object displacement involves two fingers, the index and middle fingers, in contact with the object. Therefore, slippage information was packaged into spatiotemporally discrete patterns and delivered sequentially to two adjacent fingers involved in grasping to produce a sensation similar to natural behaviour.

Force and slippage information were translated into electrical stimuli; this allowed the amputee participant to actively control the grasp stability,

modulate the force level, and hinder the object's fall by a myoelectric control of the prosthesis and elicited force-and-slippage sensations.

Closed-loop control capabilities enabled by the neural feedback were compared with those achieved without feedback. Force-and-slippage closed-loop control was replicated with both a research robotic hand prototype and a commercial prosthesis, showing that the performances were independent of the adopted prosthesis.

5.2 The proposed approach

5.2.1 Stick-slip model of multi-fingered grasp

The stick-slip model in the literature (Section 3.2.3) was extended to simulate the more realistic situation of a multi-fingered grasp of an object under gravity conditions. In Figure 5.1, F_{n1} and F_n are the forces applied by the thumb and by all the others fingers, respectively (i.e., $F_n = F_{n1} + F_{n2} + F_{n3}$ in Figure 5.1).

F_{t1}, F_{t2}, and F_{t3} are the force tangential components related to the normal components through the coefficient of kinetic friction μ. F_p models the load force, F_e is the elastic force generated by the skin elasticity modeled with a spring. F_s is the external disturbance that causes slippage modeled as a step function ($F_s = Fu(t)$). When a force F_s is applied to the spring, it will store elastic energy, and an increasing force will be exerted on the object that is opposed by the frictional force $F_t = F_{t1} + F_{t2} + F_{t3}$. When $F_t \geq F_p - F_e + F_s$, the object sticks; on the other hand, when $Ft < F_p - F_e + F_s$, the object slips. The equilibrium can be written as

$$Ft = F_p - F_e + m\ddot{x} - F_s \tag{5.1}$$

where m is the mass of the object and $\ddot{x}$ is the object acceleration. The object displacement induced by the external force F_s can be computed as

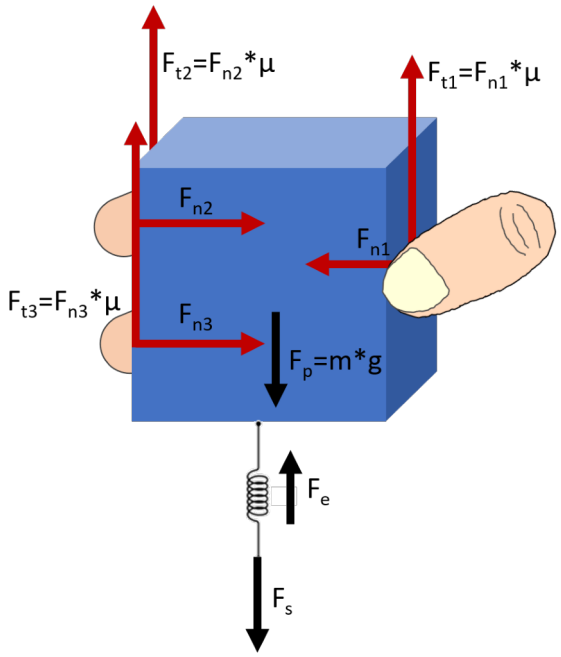

Figure 5.1 A tridigital grasp of an object is shown but the model can describe the mechanism of stick-slip during grasps involving from two to five fingers.

$$x(t) = \frac{a_0}{\omega_n^2}(u(t) - cos(\omega_n^2)) \tag{5.2}$$

where

$$\omega_n^2 = \frac{k}{m}; a_0 = \frac{1}{m}(\mu F_n - mg - F) \tag{5.3}$$

and k is skin stiffness.

5.2.2 Real-time force-and-slippage closed-loop control strategy

The real-time force-and-slippage closed-loop control strategy presented in Figure 1.2 is based on the subdivision of the prehension in the brain. The functioning of the strategy is shown in Figure 5.2.

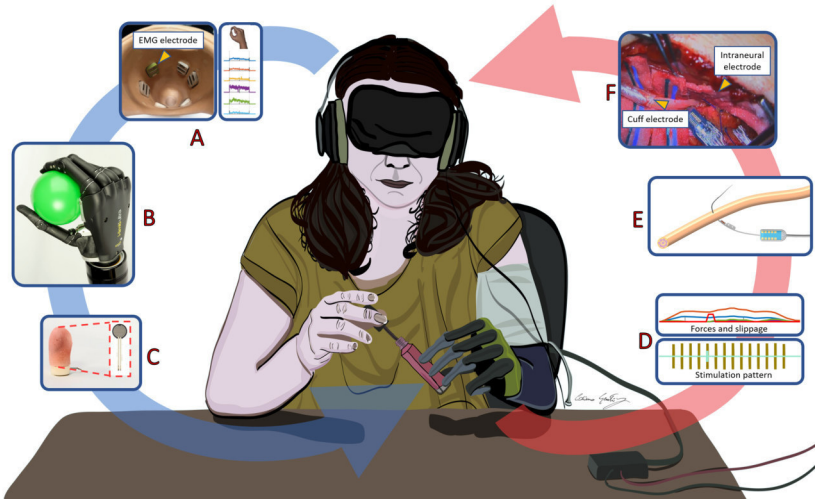

Figure 5.2 Real-time force-and-slippage closed-loop control strategy of hand prosthesis with neural feedback

High-level starts from the (A) in Figure 5.2, where hand movement intention of the participant was decoded by the muscular contraction by using sEMG sensors placed in the socket. Gestures and force levels were classified with a pattern recognition algorithm described in Section 4.1.2. The algorithm was adapted to classify five gestures and three force levels: rest, power, pinch, open, lateral and three levels of forces (high, medium, low). After the gesture was obtained, in the pre-shaping phase (B) the involved fingers were chosen and the participant can actively control the biomechatronic prosthetic hand, reaching the object thanks to the position control implemented on (middle-level in Figure 1.2). (C) Fingertips of the hand were equipped with FSR sensors to read the grasped force and to use this information to detect slippage events with the algorithm developed in [151]. The high-level was modified because (D) the measured grasped force and the information obtained about the slippage are encoded in relative stimulation patterns (D) delivered to the

participant by means (E, F) cuff and intraneural electrodes implanted in ulnar and median nerves. In this manner, the amputee subject can actively control the prosthesis: after the high-level where the subject decides the movement class, he/she position-controls the prosthesis to accomplish the desired grasp; when the touch is achieved, the subject is able to regulate the grasp force and autonomously increase or decrease it thanks to elicited sensations of force and slippage and the pattern recognition algorithm.

5.3 Experimental validation

Two experimental sessions were carried out to validate the proposed approach.

In the first experimental session, the stick-slip model was used to predict object displacement during slippage. In particular, ten healthy subjects performed grasp tasks: when the object was firmly grasped in the hand, a mass was added to cause the slippage. Information about forces and displacement were recorded and used in the model to validate it. The same tasks were performed by the amputee. The developed model causes a change in the contact area of the object with the fingers and the object displacement involves two fingers, the index and middle fingers, in contact with the object. This laid the foundations of the stimulation strategy adopted for eliciting slippage sensations.

In the second experimental session, force and slippage sensations were elicited in an amputee by means a combination of the cuff and intraneural electrodes implanted for 11 weeks, to provide close-to-natural force and slippage sensations. Closed-loop force-and-slippage control based on the elicited sensations was carried by the amputee out in four categories of tasks with increasing complexity.

In the following, each experimental session is described in detail.

5.3.1 Experimental session 1

5.3.1.1 Experimental setup and protocol

The main purpose of the stick-slip model is to analyze in-depth the slippage mechanism in healthy participants and then deduce the slippage stimulation strategy for the amputee participant.

Ten healthy subjects (seven males and three females, mean age (± s.d.): 26 ± 4 years) volunteered to participate in this study. All the participants received detailed instructions and familiarized with tasks before starting the acquisitions. They were comfortably seated at a desk with the arm sustained by support.

Each subject was blindfolded and acoustically shielded. Then, he/she was asked to grasp an object placed close to the fingers and lift it. Ten random repetitions ware performed for a power grasp and for a tridigital grasp. Two objects were adopted for this validation: BP for the power grasp and SP for the tridigital grasp (these objects are described in Section 4.2.1.1). The objects were equipped with FSR sensors [171] for recording the applied normal forces and reflective markers for monitoring the object displacement, as described in Section 3.3.2.1. One marker was placed at the upper extremity and two markers were at the lower extremity of the object. Moreover, an M-IMU was located at the top of the object to record object acceleration and orientation.

To generate a repeatable perturbation (i.e. F_s in the model), an additional mass was linked to the object and released when the object was lifted by the subject (Figure 5.3). For the power grasp, the additional mass was of the same weight of the object, while for the tridigital grasp the mass was twice the object weight. The weight of the additional masses was empirically chosen to be sure to induce slippage and obtain an observable object displacement.

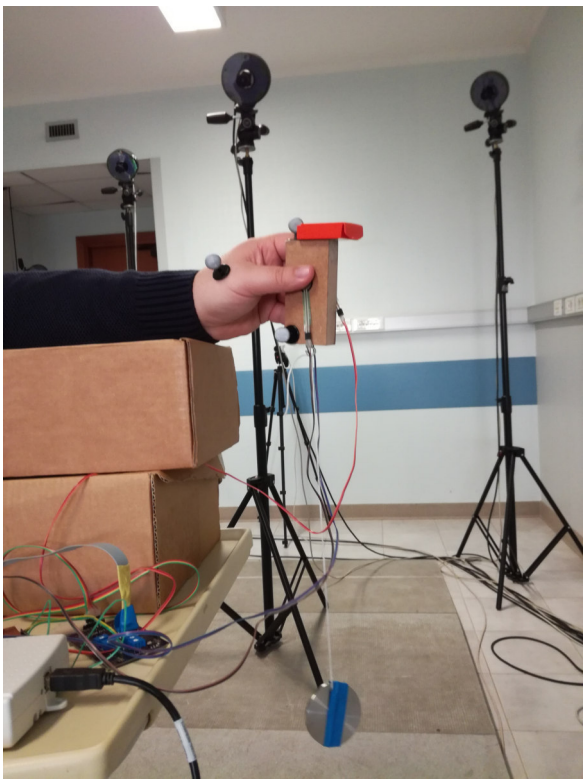

Figure 5.3 Setup for the stick-slip model validation

The same experimental setup and the same experimental conditions were reproduced with the amputee participant for the experiment of force-and-slippage closed-loop control with neural feedback.

5.3.1.2 Results and discussion

The object displacement computed by the model as 26.41 ± 10.22 mm was comparable with the measured one, given as 28.12 ± 8.95 mm (P = 0.84, Wilcoxon signed-rank test). Moreover, all the participants referred that, during slippage, they felt the object flowing along with the index and middle fingers because of the object displacement. This was also

supported by the data because the measured object displacement was comparable with the sum of the two fingers sizes in the slippage direction (i.e., 32.20 ± 4.76 mm; Figure 5.4). This achievement represented the key element of the adopted slippage stimulation strategy: i.e., slippage sensation was delivered with electrical stimulation that flowed along with the index and middle fingers in contact with the object.

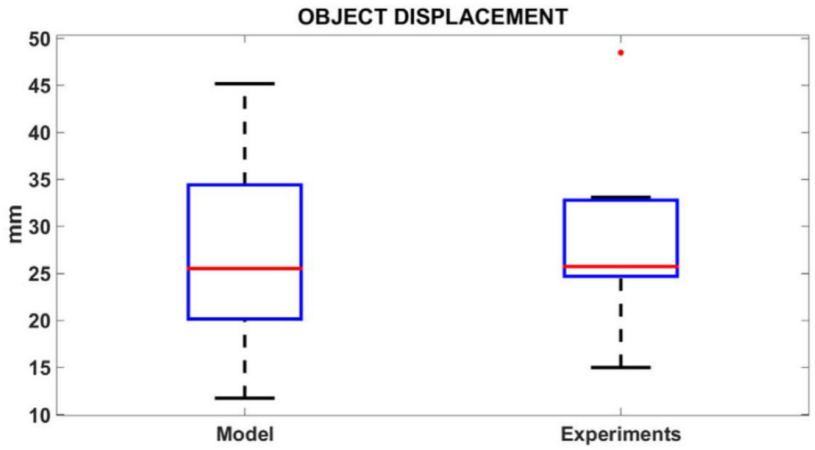

Figure 5.4 The object displacement caused by disturbance F_s and computed by the stick-slip model, and the displacement measured by the sensors on the object. The difference between the measured object displacement and the computed object displacement is not statistically significant (P = 0.84). The red horizontal lines show the medians, box limits indicate the 25^{th} and 75^{th} percentiles, and the whiskers extend to the most extreme data points (i.e., maximum and minimum).

For the amputee participant, slippage was detected through the induced vibrations, as described in [151], and encoded as trains of cathodic rectangular biphasic electrical current pulses with fixed parameters sequentially injected on two adjacent fingers (i.e., index and middle fingers) to deliver a sensation that integrated signals across the skin area of the fingers in contact with the object.

Figure 5.5 shows the total force applied by the amputee participant in power and precision grasps performed with neural feedback; it was comparable to the total force obtained by the model adapted to the amputee participant. In both cases, slippage was hindered and the object was stably grasped. The displacement of the object on the prosthesis fingers induced by the slippage was given by 26.36 ± 7.43 mm.

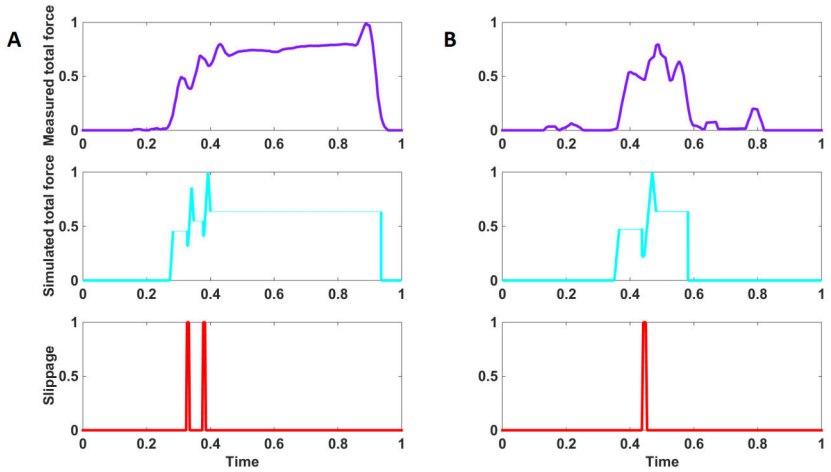

Figure 5.5 Closed-loop control with neural feedback in power (A) and precision (B) grasps. The measured normal component of the force, the normal force extracted from the model under the same perturbation condition and the processed slippage signal are shown in violet, light blue and red, respectively. The force level was modulated by the participant after feeling slippage through neural stimulation, achieving a stable grasp. All traces were normalized with respect to the maximum forces exerted by the hand (i.e., 7.33 N for power grasp and 3.96 N for precision grasp) and to maximum time duration (i.e., 26.90 s for power grasp and 19.35 s for precision grasp).

Figure 5.5 shows the total force applied by the amputee participant in power and precision grasps performed with neural feedback; it was comparable with the total force obtained by the model adapted to the amputee participant. In both cases, slippage was hindered and the object

was stably grasped. The displacement of the object on the prosthesis fingers induced by the slippage was given by 26.36 ± 7.43 mm.

The results demonstrated that slippage causes a change in the contact area of the object with the fingers and that the object displacement involves two fingers, the index and middle fingers, in contact with the object. This laid the foundations of the stimulation strategy adopted for eliciting slippage sensations.

5.3.2 Experimental session 2

5.3.2.1 Experimental setup and protocol

This study was conducted at Campus Bio-Medico University Hospital of Rome in accordance with the Declaration of Helsinki and following amendments and was approved by the local ethics committee and the assigned office of the Italian Ministry of Health. The volunteer participant signed an informed consent form.

The volunteer participant is right-handed and 40 years old at the time of the experiment, with a transradial left upper limb amputation. Details about the surgical procedure to implant electrodes are described in [34].

Two robotic hands, the IH2 Azzurra (research prototype [175]) and the RoboLimb (commercial prosthesis [200]) were used and both equipped with FSR [171] for the grasp force measuring mounted on an ad-hoc socket developed by INAIL (Italian Institute for Insurance against Accidents at Work) Prosthetic Center; six active sEMG sensors (Ottobock 13E200 = 50) were embedded into the socket to decode the movement and grasping force, classified from the muscular activity.

To electrically restore tactile sensation to ulnar and median nerves, intraneural [201] and cuff electrodes (Ardiem Medical Inc.) were implanted in the amputee's residuum for 11 weeks. The stimulation pattern was sent to the electrodes by using the Multi-Channel System STG4008 stimulator.

The sensory output produced by the biomechatronics hand during the tasks was delivered to the participant to evoke real-time close-to-natural force-and-slippage feedback like to her missing hand.

In particular, when the slippage was detected, the corresponding sensation was delivered to the subject to allow her a corrective action. For this reason, the grasping force was proportionally modulated with the EMG signal to oppose slippage. Details about the stimulation are available in [34].

The participant, blindfolded and acoustically shielded, was asked to perform different tasks under two conditions: with and without neural feedback. It is expected that in a real context of everyday life with visual and auditory feedback, the improvement of the participant's grasp and manipulation capabilities enabled by the delivered force and slippage sensory feedback could be even more evident.

Four categories of tasks were tested: lateral grasp of large and small objects, pick and place of large objects with a power grasp, pick and place objects with a precision grasp, and manipulation tasks of pouring water from a bottle to a cup and shape sorter with small cylinders and discs. Objects of different shapes (e.g. cylinder, parallelepiped, disk, cube and triangle), volume ($2.54x10^3mm^3 \div 2.65x10^3mm^3$), and weight ($18.28g \div 198.65g$) were used in different tasks (grasping, e.g. pick and place; manipulation, e.g. pouring, shape and sorter).

The extension of the contact area between the object and the hand is considered as the complexity of the grasp. Indeed, a lower contact area, typical of precision and manipulation tasks, requires more efficient control of grasping stability.

Three performance indicators (i.e. weighted success, force index, and execution time) were introduced to measure grasp and dexterity performance [34].

5.3.2.2 Results and discussion

In Figure 5.6 and Figure 5.7, two cases of use of neural feedback and absence of feedback are shown.

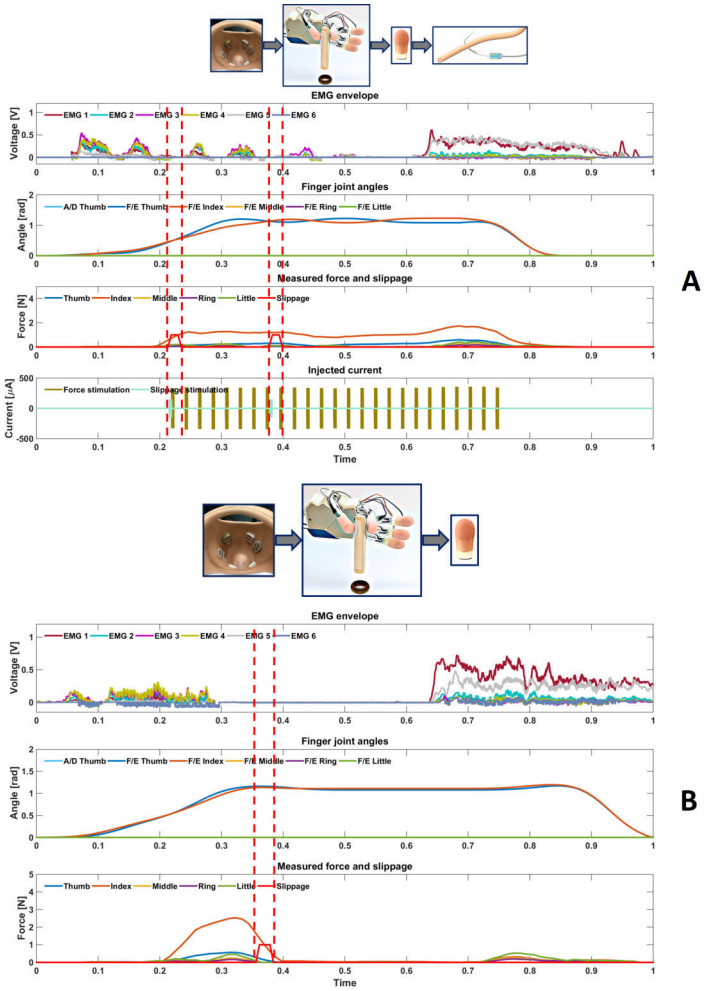

Figure 5.6 Real-time force-and-slippage control of a manipulation task. (A) With neural feedback. The participant performed a manipulation task of shape sorter of a small cylindrical object with a pinch gesture. Once the object was touched, force feedback was provided. The slippage event was felt by the participant, who closed the hand and actively tuned the level of force by producing a variation in the EMG signal. Grasp stability was reached up to the end of the trial. Hence, the open hand gesture was classified and the prosthetic hand reopened. (B) The same task, without feedback. The amputee participant was not able to feel the detected slippage event and, consequently, the object fell.

In the case of neural feedback, when the object is touched, the participant actively controls hand closing with the desired level of force, by producing a variation in the EMG signal related to the perceived force and slippage sensations. Otherwise, without neural feedback, the object can fall because slippage and forces information can not be managed by the participant.

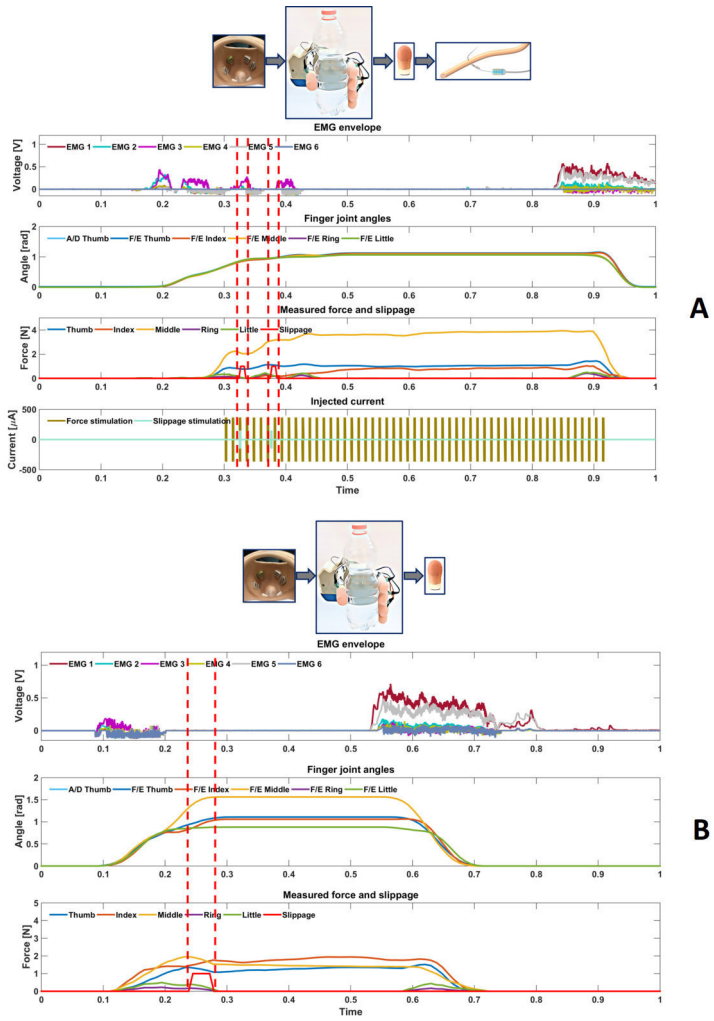

Figure 5.7 Real-time force-and-slippage control of a power grasp. (A) With neural feedback. The participant performed a power grasp. Once the object was touched, force feedback was provided. The slippage event was felt by the participant, who closed the hand and actively tuned the level of force by producing a variation in the EMG signal. Grasp stability was reached up to the end of the trial. Hence, the open hand gesture was classified and the prosthetic hand reopened. (B) The same task, without feedback. The amputee participant was not able to feel the detected slippage event and, consequently, the object fell.

The time employed by the algorithm in [151] to detect slippage starting from the measured applied force was about 50 ms. The hand controller acquired a new class from the classifier, including corrective actions due to slippage, every 100 ms. This time is compatible with the time delays in human sensorimotor control loops engaged in corrective actions ($\sim$ 100 ms) [82–87]. The amputee participant needed an overall time around 500 ms to decode the intended gesture, control the hand, provide the sensory feedback, and apply a corrective action to avoid slippage.

In order to monitor how the participant's ability to grasp and manipulate objects with and without neural feedback improve over time, three times were chosen: after the first week of training with the closed-loop control (i.e., week 4, named T_0), in the middle of the training period (i.e., week 7, named T_1), and at the end of the experimental study (i.e., week 10, named T_2). The participant was asked to perform a total number of 96 trials, 24 for each of the four above-described categories of tasks at each time point.

The comparative analysis of the performance achieved with neural feedback and without any feedback showed that the difference achieved with neural feedback and without any feedback was statistically significant for lateral (P = 0.0062) and power (P = 0.015) categories at T_0 and for precision (P = 0.0045) and manipulation (P = 0.0009) categories at T_2 (Figure 5.8).

In absence of feedback, the participant showed a relevant increase in performance with learning, probably because she did not use a myoelectric prosthesis before this study. She started from very low performance at T_0 and improved over time. The difference was statistically significant (i) for lateral grasp between T_0 and T_1 (P = 0.002) and between T_0 and T_2 (P = 0.002), (ii) for power grasp between T_0 and T_2 (P = 0.015), and (iii) for manipulation tasks between T_0 and T_2 (P = 0.0078).

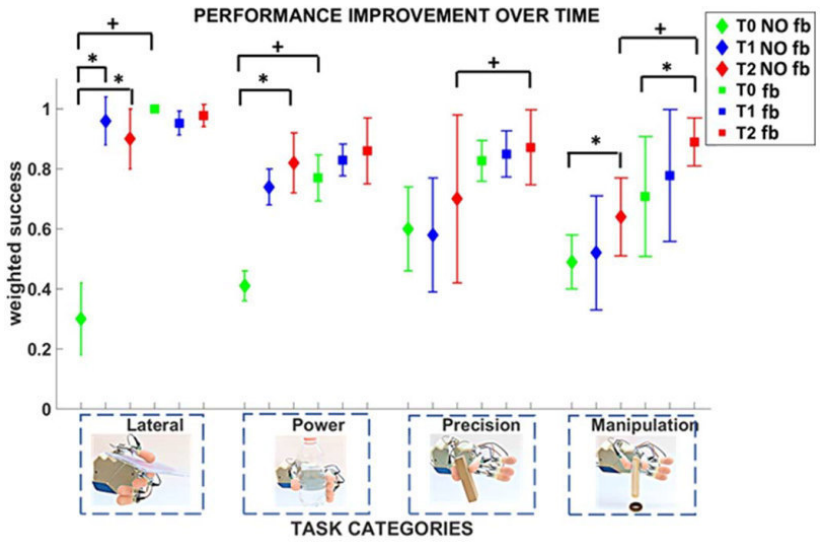

Figure 5.8 Temporal evolution of grasp performance without feedback and with neural feedback. The participant's grasp performance was measured through weighted success and monitored over time. Four categories of tasks (lateral, power, precision, and manipulation) were performed at T_0, T_1, and T_2. Mean value and SD of the weighted success index are shown for each time point. Statistical significance for the three time points is indicated with *P < 0.016 (Friedman nonparametric tests, Wilcoxon post hoc test, Bonferroni correction). Statistical significance between neural feedback (fb) and no feedback (NO fb) is indicated with +P < 0.05 (Wilcoxon signed-rank test).

In case of real-time force-and-slippage closed-loop control strategy with neural feedback, high performances were achieved by the participant already from the first time point, except for manipulation (which was more complex than the other tasks). For the manipulation category, performance improved over time up to a value of 0.89 ± 0.08 at T_2, which was significantly different with respect to the value achieved at T_0 ($P = 0.015$).

The advantage of using neural feedback to improve dexterity at time T_2 was also investigated in depth.

Figure 5.9 shows that grasp fundamental abilities were stable overtime during the 11 weeks of experiments, whereas manipulative skills gradually increased and significantly improved by 25.7% at T_2. The performance was shown to improve with continuous usage as the participant learned how to incorporate sensory feedback. Performance with neural feedback was always better than without feedback; the difference became statistically significant at T_2 for precision and manipulation tasks. For fundamental grasp categories (i.e., lateral and power grasps), performance improved over time also without feedback, probably because the participant had never used a myoelectric hand before the study.

The comparative analysis at T_2 showed that neural feedback allowed achieving good manipulative skills. The participant performed all task categories with higher forces and shorter execution times when neural feedback was provided. The difference became significant for manipulation tasks. This can be newly justified by the paramount role played by sensory feedback in more complex tasks. In the power grasp, the object stability can be easily achieved also by applying lower grasp force because of the wide contact area between the prosthetic hand and the object. This explains why power and lateral grasps can also be successfully performed when no feedback is provided. Precision and manipulation tasks are characterized by a reduction of the contact area

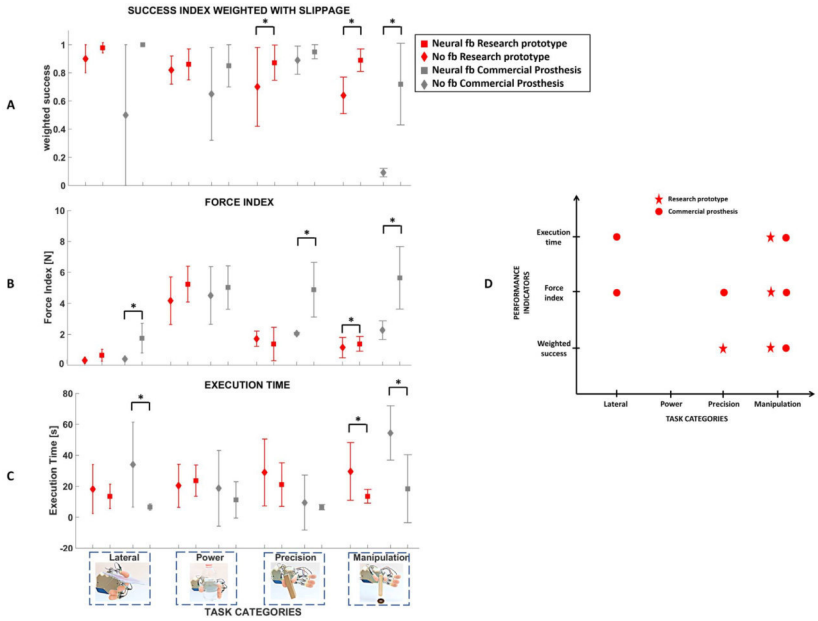

Figure 5.9 Grasp and dexterity assessment without feedback and with neural feedback and two different prosthetic hands. The participant's grasp performance and dexterity were measured through the weighted success, the force index, and the execution time for the two cases of no feedback and neural feedback and two different prosthetic hands (a research prototype and a commercial hand). Statistical significance between neural feedback and no feedback is indicated with *P <0.05 (Wilcoxon signed-rank test). (A) Weighted success. (B) Force index. (C) Execution time. (D) Statistically significant differences between no feedback and neural feedback for the three indices and the two prosthetic hands. A significant improvement of grasp performance and dexterity was achieved in manipulation tasks, resulting from neural feedback, independently of the adopted prosthetic hand.

between the object and the prosthetic hand. Then, mastered control of the applied forces to ensure stability is needed. It seems that the neural stimulation provides rapid and effective sensory feedback, which allows finely tuning the applied forces and reduce the execution time.

Both a research prototype and a commercial prosthesis were adopted to assess the interoperability of the developed closed-loop control and the robustness of the achieved results. The participant achieved globally comparable performances with the two prosthetic hands (Figure 5.9). The weighted success in the absence of feedback was always lower than the success rate achieved with neural feedback (Figure 5.9). For precision and manipulation tasks, the difference was statistically significant ($P = 0.0045$ and $P = 0.0009$) for the research prototype; the difference was statistically significant for manipulation tasks ($P = 0.015$) with the commercial hand. Similarly, the total applied force with no feedback was on average lower than with neural feedback (Figure 5.9). For the research prototype, the difference became significant for manipulation tasks ($P = 0.0023$), whereas for the commercial prosthesis, the difference was significant for lateral grasp ($P = 0.002$), precision grasp ($P = 0.02$), and manipulation ($P = 0.002$). Moreover, the participant, in general, took more time to complete the tasks when no feedback was provided (Figure 5.9). The difference was statistically significant in manipulation tasks (research prototype, $P = 0.006$; commercial hand, $P = 0.015$) and lateral grasp performed with the commercial hand ($P = 0.019$).

5.4 Conclusions

Dexterity and manipulations skills in humans are allowed by complex biomechanics of the hand and a control loop based on a bidirectional communication with the brain, thanks to a sophisticated sensory system. Differently from the previous automatic strategy, the restoration of

sensory information, through neural electrodes, to the amputee allows a physiological motor control of the hand prosthesis.

A real-time force-and-slippage closed-loop control strategy that i) includes an amputee subject in the control loop through invasive neural electrodes, ii) provides close-to-natural force and slippage sensations to improve manipulative skills for the amputee during the prosthesis use, modulating the grasping force level and preventing the object fall with a myoelectric control of the prosthesis, was presented.

Force and slippage sensations were elicited in an amputee by means of biologically inspired slippage detection and encoding algorithms, supported by a stick-slip model of the performed grasp. A combination of the cuff and intraneural electrodes was implanted for 11 weeks in a young woman with a hand amputation. Evidence is provided about the improvement of the participant's grasping and manipulation capabilities over time resulting from neural feedback. The elicited tactile sensations enabled the successful fulfilment of fine grasp and manipulation tasks with increasing complexity. Grasp performance was quantitatively assessed by means of instrumented objects and purposely developed metrics. Closed-loop control capabilities enabled by the neural feedback were compared with those achieved without feedback.

Chapter 6

Conclusions and future work

The main objective addressed in this thesis is the development of a control strategy able to improve grasp and manipulation capabilities of prosthesis based on the tactile sensorization and on the use of this information in the control strategy, inspired to the human hand [27].

To achieve this objective, it was necessary: i) to sensorize an active prosthetic hand in order to use this information ii) to detect touch and slippage information during the whole grasp, iii) useful to manage force and slippage during the grasp by using a force-and-slippage control law strategy; iv) to coordinate fingers during the grasp with a strategy based on the virtual finger concept; iv) to classify both gestures and forces by using EMG signal with a hierarchical classification approach with the aim to assess the desired hand/wrist gestures, as well as the desired force levels to exert during grasping tasks.

The proposed strategy presents 3 levels: high-level, to decode the biological human signals in movements and force levels, middle-level, to manage the pre-shaping and the fingers reaching to the object, low-level to regulate force and slippage during the whole grasp. Each level was developed and tested and carefully described in the previous chapters.

In Chapter 2, the evolution of controls for robotic hands is shown. This overview has demonstrated the importance of prostheses to have controls inspired by the human hand.

In Chapter 3, a touch-and-slippage detection algorithm for robotic or prosthetic hands was presented and experimentally validated since force information is not sufficient to control a prosthesis to avoid the object falling. The proposed approach relies only on the normal force component (or on the corresponding voltage raw signal) to detect the slippage events. The touch with the object surface has been also computed and

adopted as a trigger to start the slippage detection. The results have verified that: i) the signal variation produces an output only in presence of a tangential force component; ii) the ROC curve is useful to detect the threshold in order to generate a value equal to 1 only in presence of the slippage; iii) the number of slips is dependent on the change of the force applied on the sensor and on the sliding velocity of the probe then it is independent by them.

In Chapter 4, in the high-level of the strategy, a hierarchical classification system is used to discriminate simultaneously hand/wrist gestures and desired force levels. The NLR algorithm was adopted for implementing the hierarchical classification approach and comparative analysis among the performance of these two algorithms was done. The force classifiers were able to robustly discriminate the same class of movement performed at different muscle contractions because they were trained with data containing the modulation of different force levels. Another innovative contribution is represented by the use of FSM theory for the management of three classifiers, that avoids to face a more seven multi-class problem using a single classifier and make the system controllability less complex by activating the force classifiers only when the "hand/wrist gestures classifier" returns an output class belonging to a closure hand gesture. This classification approach has obtained positive results and seems to be very promising for identifying simultaneously desired gestures and force levels. This approach will allow improving the performance of the currently adopted prosthesis EMG control architectures thanks to the possibility to manage desired gestures and force levels in a more natural way.

To decrease the attention level and the cognitive burden for the user during grasp tasks, an automatic strategy is necessary. A force-and-slippage control strategy able to i) regulate the grasping force, ii) prevent the slippage events, iii) coordinate fingers for replicating a human-like

behaviour on the prosthetic system. Real-time reaction to slippage events and finger coordination have been achieved by means of i) a force control with inner position loop, ii) a sensorization system giving information about the applied normal forces, and iii) an approach for controlling the fingers in a coordinated manner on the basis of the virtual finger concept is developed and tested on a poliarticulated prosthetic hand. The slippage detection algorithm described in Chapter 3 and the hierarchical classification system was introduced in the control strategy. Preliminary results have been obtained for the pinch and the power grasp of several objects, but the approach is easily extendable to the other grasp configurations. The results obtained with the prosthetic hand, the high success rate in terms of both detected slippage events (99.4%) and compensated slippage events (100%) make the approach feasible for online application on a prosthetic hand controlled by an amputee.

In Chapter 5, real-time closed-loop control of bionic hands in tasks of fine grasp and manipulation is presented. Starting from the previous described strategy, each part was adapted to the specific need of the amputee. Force and slippage sensations were elicited in an amputee by means of biologically inspired slippage detection and encoding algorithms, supported by a stick-slip model of the performed grasp. The elicited tactile sensations enabled the successful fulfilment of fine grasp and manipulation tasks with increasing complexity. Grasp performance was quantitatively assessed by means of instrumented objects and purposely developed metrics. Closed-loop control capabilities enabled by the neural feedback were compared with those achieved without feedback.

The strategy proposed in this thesis could be used to perform complex manipulation tasks, expanding the coordination among the fingers, already discussed in Section 4.1.1, and adapting it for each specific task.

Moreover, the study of the functioning of the whole human arm would lead to the development of a control strategy to be used with people affected by shoulder disarticulation and/or transhumeral amputation who underwent the TMR surgical procedure. TMR allows users to control prosthesis more intuitively and simply perform ADL with sEMG. Hierarchical or parallel classification systems (as described in Section 4.1.2), where each DoF (elbow, wrist, hand) is individually managed, could improve the control to obtain a behaviour like the human one, increasing the acceptability to the amputees.

References

[1] A. Provenzale, F. Cordella, L. Zollo, A. Davalli, R. Sacchetti, and E. Guglielmelli. A grasp synthesis algorithm based on postural synergies for an anthropomorphic arm-hand robotic system. In *5th IEEE RAS/EMBS International Conference on Biomedical Robotics and Biomechatronics*, pages 958–963. IEEE, 2014.

[2] C. Laschi, P. Dario, M. C. Carrozza, E. Guglielmelli, G. Teti, D. Taddeucci, F. Leoni, B. Massa, M. Zecca, and R. Lazzarini. Grasping and manipulation in humanoid robotics. *Scuola Superiore Sant Anna, Italia*, 2000.

[3] B. A Kent, N. Karnati, and E. D. Engeberg. Electromyogram synergy control of a dexterous artificial hand to unscrew and screw objects. *Journal of neuroengineering and rehabilitation*, 11(1):41, 2014.

[4] R. M. Scott. Biomedical engineering in upper-limb prosthetics. chapter 12, the comprehensive management of the upper-limb amputee. dj atkins and rh meier, editors, 1988.

[5] M. C. Carrozza, B. Massa, S. Micera, R. Lazzarini, M. Zecca, and P. Dario. The development of a novel prosthetic hand-ongoing research and preliminary results. *IEEE/Asme Transactions on Mechatronics*, 7(2):108–114, 2002.

[6] P. J. Kyberd, O. E Holland, P. H. Chappell, S. Smith, R. Tregidgo, P. J. Bagwell, and M. Snaith. Marcus: A two degree of freedom hand prosthesis with hierarchical grip control. *IEEE Transactions on Rehabilitation Engineering*, 3(1):70–76, 1995.

[7] P. J. Kyberd, D. Gow, H. Scott, M. Griffiths, L. Sperling, L. Sandsjo, C. Almstrom, C. Wartenberg, and S. Jonsson. A comparison of upper limb prostheses users in europe. In *Myoelectr. Controls Symp. Fredericton*, 1999.

[8] R. B. Woodward and L. J. Hargrove. Adapting myoelectric control in real-time using a virtual environment. *Journal of neuroengineering and rehabilitation*, 16(1):11, 2019.

[9] M. LeBlanc. Give hope-give a hand-the ln-4 prosthetic hand [internet], 2008.

[10] W. R Frontera and J. K. Silver. *Fondamenti di medicina fisica e riabilitativa*. Verduci, 2004.

[11] F. Cordella, A. L. Ciancio, R. Sacchetti, A. Davalli, A. G. Cutti, E. Guglielmelli, and L. Zollo. Literature review on needs of upper limb prosthesis users. *Frontiers in neuroscience*, 10:209, 2016.

[12] L. L. Salisbury and A. B. Colman. A mechanical hand with automatic proportional control of prehension. *Medical and biological engineering*, 5(5):505–511, 1967.

[13] J. C. Baits, R. W. Todd, and J. M. Nightingale. Paper 10: The feasibility of an adaptive control scheme for artificial prehension. In *Proceedings of the Institution of Mechanical Engineers, Conference Proceedings*, volume 183, pages 54–59. SAGE Publications Sage UK: London, England, 1968.

[14] D. S. Childress. Closed-loop control in prosthetic systems: historical perspective. *Annals of biomedical engineering*, 8(4):293–303, 1980.

[15] R. D. Codd, J. M. Nightingale, and R. W. Todd. An adaptive multifunctional hand prosthesis. *The Journal of physiology*, 232(2):55P, 1973.

[16] J. M. Nightingale. Microprocessor control of an artificial arm. *Journal of microcomputer applications*, 8(2):167–173, 1985.

[17] P. H. Chappell and P. J. Kyberd. Prehensile control of a hand prosthesis by a microcontroller. *Journal of biomedical engineering*, 13(5):363–369, 1991.

[18] P. J. Kyberd and P. H. Chappell. The southampton hand: an intelligent myoelectric prosthesis. *Journal of rehabilitation Research and Development*, 31(4):326, 1994.

[19] C. Cipriani, F. Zaccone, G. Stellin, L. Beccai, G. Cappiello, M. C. Carrozza, and P. Dario. Closed-loop controller for a bio-inspired multi-fingered underactuated prosthesis. In *Proceedings 2006 IEEE International Conference on Robotics and Automation, 2006. ICRA 2006.*, pages 2111–2116. IEEE, 2006.

[20] M. R. Cutkosky et al. On grasp choice, grasp models, and the design of hands for manufacturing tasks. *IEEE Transactions on robotics and automation*, 5(3):269–279, 1989.

[21] C. F. Pasluosta and A. W. L. Chiu. Evaluation of a neural network-based control strategy for a cost-effective externally-powered prosthesis. *Assistive Technology*, 24(3):196–208, 2012.

[22] C. Quinayás, A. Ruiz, L. Torres, and C. Gaviria. Hierarchical-architecture oriented to multi-task planning for prosthetic hands controlling. In *International Work-Conference on the Interplay Between Natural and Artificial Computation*, pages 157–166. Springer, 2017.

[23] C. A. Quinayás-Burgos and C. A. G. López. Sistema de identificación de intención de movimiento para el control mioeléctrico de una prótesis de mano robótica. *Ingeniería y universidad*, 19(1):27–50, 2015.

[24] T. Iberall. The nature of human prehension: Three dextrous hands in one. In *Proceedings. 1987 IEEE International Conference on Robotics and Automation*, volume 4, pages 396–401. IEEE, 1987.

[25] C. M. Light, P. H. Chappell, B. Hudgins, and K. Engelhart. Intelligent multifunction myoelectric control of hand prostheses. *Journal of medical engineering & technology*, 26(4):139–146, 2002.

[26] G. Zhu, X. Duan, and H. Deng. Hybrid force-position fuzzy control for a prosthetic hand. In *International Conference on Intelligent Robotics and Applications*, pages 415–426. Springer, 2013.

[27] S. Jacobs, C. Danielmeier, and S. H. Frey. Human anterior intraparietal and ventral premotor cortices support representations of grasping with the hand or a novel tool. *Journal of Cognitive Neuroscience*, 22(11):2594–2608, 2010.

[28] P. J. Kyberd, C. Wartenberg, L. Sandsjö, S. Jönsson, D. Gow, J. Frid, C. Almström, and L. Sperling. Survey of upper-extremity prosthesis users in sweden and the united kingdom. *JPO: Journal of Prosthetics and Orthotics*, 19(2):55–62, 2007.

[29] M. A. Arbib. Coordinated control programs for movements of the hand. *Experimantal Brain Research*, 10:111–129, 1985.

[30] A. Muzumdar. *Powered Upper Limb Prostheses: Control, Implementation and Clinical Application; 11 Tables*. Springer Science & Business Media, 2004.

[31] F. Leone, C. Gentile, A. L. Ciancio, E. Gruppioni, A. Davalli, R. Sacchetti, E. Guglielmelli, and L. Zollo. Simultaneous semg classification of wrist/hand gestures and forces. *Frontiers in neurorobotics*, 13:42, 2019.

[32] C. Gentile, F. Cordella, C. Ramos Rodrigues, and L. Zollo. Touch-and-slippage detection algorithm for prosthetic hands. *Mechatronics (submitted)*, 2020.

[33] F. Cordella, C. Gentile, L. Zollo, R. Barone, R. Sacchetti, A. Davalli, B. Siciliano, and E. Guglielmelli. A force-and-slippage control strategy for a poliarticulated prosthetic hand. In *2016 IEEE International Conference on Robotics and Automation (ICRA)*, pages 3524–3529. IEEE, 2016.

[34] L. Zollo, G. Di Pino, A. L. Ciancio, F. Ranieri, F. Cordella, C. Gentile, E. Noce, E. A. Romeo, A. Dellacasa Bellingegni, G. Vadalà, et al. Restoring tactile sensations via neural interfaces for real-time force-and-slippage closed-loop control of bionic hands. *Science Robotics*, 4(27):eaau9924, 2019.

[35] W. Ogle et al. *Aristotle: on the parts of animals*. K. Paul, French & Company, 1882.

[36] C. Bell. *The hand: its mechanism and vital endowments, as evincing design*, volume 4. Bell & Daldy, 1865.

[37] F. W. Jones. *The principles of anatomy: As seen in the hand*. Bailliere, Tindall & Cox, 1944.

[38] J. R. Napier. Studies of the hands of living primates. In *Proceedings of the Zoological Society of London*, volume 134, pages 647–657. Wiley Online Library, 1960.

[39] P. Lemelin and D. Schmitt. On primitiveness, prehensility, and opposability of the primate hand: the contributions of frederic

wood jones and john russell napier. In *The Evolution of the Primate Hand*, pages 5–13. Springer, 2016.

[40] P. Hernigou. Ambroise paré iv: the early history of artificial limbs (from robotic to prostheses). *International orthopaedics*, 37(6):1195–1197, 2013.

[41] T. L. Wellerson. Historical development of upper extremity prosthetics. *Orthop Prosthet Appl J*, 11(3):73–77, 1957.

[42] J. Bostock, H. T. Riley, et al. *The natural history of Pliny*, volume 2. G. Bell, 1900.

[43] G. Schlesinger. Der mechanische aufbau der künstlichen glieder. In *Ersatzglieder und Arbeitshilfen*, pages 321–661. Springer, 1919.

[44] R. Reiter. Eine neue electro kunsthand. *Grenzgebiete der Medizin*, 4:133–135, 1948.

[45] R. N. Scott. Myoelectric control of prostheses: A brief history. In *Proceedings of the 1992 MyoElectric Controls/Powered Prosthetics Symposium, Fredericton, NB, Canada*, volume 1, 1992.

[46] M. Zecca, S. Micera, M. C. Carrozza, and P. Dario. Control of multifunctional prosthetic hands by processing the electromyographic signal. *Critical Reviews™ in Biomedical Engineering*, 30(4-6), 2002.

[47] R. N. Scott and P. A. Parker. Myoelectric prostheses: state of the art. *Journal of medical engineering & technology*, 12(4):143–151, 1988.

[48] B. Popov. The bio-electrically controlled prosthesis. *The Journal of bone and joint surgery. British volume*, 47(3):421–424, 1965.

[49] C. J. De Luca. The use of surface electromyography in biomechanics. *Journal of applied biomechanics*, 13(2):135–163, 1997.

[50] M. A. Oskoei and H. Hu. Myoelectric control systems—a survey. *Biomedical signal processing and control*, 2(4):275–294, 2007.

[51] G. N. Saridis and T. P. Gootee. Emg pattern analysis and classification for a prosthetic arm. *IEEE Transactions on Biomedical Engineering*, (6):403–412, 1982.

[52] C. I. Christodoulou and C. S. Pattichis. Unsupervised pattern recognition for the classification of emg signals. *IEEE Transactions on Biomedical engineering*, 46(2):169–178, 1999.

[53] S. H. Park and S. P. Lee. Emg pattern recognition based on artificial intelligence techniques. *IEEE transactions on Rehabilitation Engineering*, 6(4):400–405, 1998.

[54] M. Markovic, M. A. Schweisfurth, L. F. Engels, D. Farina, and S. Dosen. Myocontrol is closed-loop control: incidental feedback is sufficient for scaling the prosthesis force in routine grasping. *Journal of neuroengineering and rehabilitation*, 15(1):81, 2018.

[55] C. Cipriani, F. Zaccone, S. Micera, and M. C. Carrozza. On the shared control of an emg-controlled prosthetic hand: analysis of user–prosthesis interaction. *IEEE Transactions on Robotics*, 24(1):170–184, 2008.

[56] E. Biddiss, D. Beaton, and T. Chau. Consumer design priorities for upper limb prosthetics. *Disability and Rehabilitation: Assistive Technology*, 2(6):346–357, 2007.

[57] E. Biddiss and T. Chau. Upper-limb prosthetics: critical factors in device abandonment. *American journal of physical medicine & rehabilitation*, 86(12):977–987, 2007.

[58] A. L. Ciancio, F. Cordella, R. Barone, R. A. Romeo, A. Dellacasa Bellingegni, R. Sacchetti, A. Davalli, G. Di Pino, F. Ranieri, V. Di Lazzaro, et al. Control of prosthetic hands via the peripheral nervous system. *Frontiers in neuroscience*, 10:116, 2016.

[59] R. A. Roeschlein and E. Domholdt. Factors related to successful upper extremity prosthetic use. *Prosthetics and orthotics international*, 13(1):14–18, 1989.

[60] J. T. Belter, J. L. Segil, A. M. Dollar, and R. F. Weir. Mechanical design and performance specifications of anthropomorphic prosthetic hands: A review. *Journal of Rehabilitation Research & Development*, 50(5), 2013.

[61] L. E. Rodriguez-Cheu and A. Casals. Sensing and control of a prosthetic hand with myoelectric feedback. In *The First IEEE/RAS-EMBS International Conference on Biomedical*

Robotics and Biomechatronics, 2006. BioRob 2006., pages 607–612. IEEE, 2006.

[62] H. A. Ernst. Mh-1, a computer-operated mechanical hand. In *Proceedings of the May 1-3, 1962, spring joint computer conference*, pages 39–51. ACM, 1962.

[63] R. Tomovic and G. Boni. An adaptive artificial hand. *IRE Transactions on Automatic Control*, 7(3):3–10, 1962.

[64] J. R. Napier. The prehensile movements of the human hand. *The Journal of bone and joint surgery. British volume*, 38(4):902–913, 1956.

[65] J. M. F. Landsmeer. Power grip and precision handling. *Annals of the rheumatic diseases*, 21(2):164, 1962.

[66] N. Kamakura, M. Matsuo, H. Ishii, F. Mitsuboshi, and Y. Miura. Patterns of static prehension in normal hands. *American Journal of Occupational Therapy*, 34(7):437–445, 1980.

[67] T. Iberall. Grasp planning from human prehension. In *IJCAI*, volume 87, pages 1153–1157. Citeseer, 1987.

[68] T. Yamashita. Engineering approaches to function of fingers. *Report of the Institute of Industrial Science the Univ. of Tokyo*, 13(3):60–110, 1963.

[69] P. Michelman. Precision object manipulation with a multifingered robot hand. *IEEE Transactions on Robotics and Automation*, 14(1):105–113, 1998.

[70] T. Okada. Computer control of multijointed finger system for precise object-handling. *IEEE Transactions on Systems, Man, and Cybernetics*, 12(3):289–299, 1982.

[71] M. H. Raobert. Hybrid position/force control of manipulator. *IEEE Trans, ASME, J, Dyn, Sys, Meas, Control*, 102:126, 1981.

[72] N. Hogan. Impedance control: An approach to manipulation. In *1984 American control conference*, pages 304–313. IEEE, 1984.

[73] Y. Nakamura, K. Nagai, and T. Yoshikawa. Dynamics and stability in coordination of multiple robotic mechanisms. *The International Journal of Robotics Research*, 8(2):44–61, 1989.

[74] P. R Pagilla and M. Tomizuka. Adaptive control of two robot arms carrying an unknown object. In *Proceedings of 1995 IEEE International Conference on Robotics and Automation*, volume 1, pages 597–602. IEEE, 1995.

[75] H. van Duinen and S. C. Gandevia. Constraints for control of the human hand. *The Journal of physiology*, 589(23):5583–5593, 2011.

[76] M. Santello, M. Flanders, and J. F. Soechting. Postural hand synergies for tool use. *Journal of Neuroscience*, 18(23):10105–10115, 1998.

[77] R. Ozawa and K. Tahara. Grasp and dexterous manipulation of multi-fingered robotic hands: a review from a control view point. *Advanced Robotics*, 31(19-20):1030–1050, 2017.

[78] Y. Li, J. L. Fu, and N. S. Pollard. Data-driven grasp synthesis using shape matching and task-based pruning. *IEEE Transactions on Visualization and Computer Graphics*, 13(4):732–747, 2007.

[79] F. Cordella, L. Zollo, A. Salerno, D. Accoto, E. Guglielmelli, and B. Siciliano. Human hand motion analysis and synthesis of optimal power grasps for a robotic hand. *International Journal of Advanced Robotic Systems*, 11(3):37, 2014.

[80] H. P. Huang, Y. H. Liu, W. C. Lee, J. Y. Kuan, and T. H. Huang. Rehabilitation robotic prostheses for upper extremity. *Contemporary Issues in Systems Science and Engineering*, pages 661–697, 2015.

[81] D. S. Naidu, C. H. Chen, A. Perez, and M. P. Schoen. Control strategies for smart prosthetic hand technology: An overview. In *2008 30th Annual International Conference of the IEEE Engineering in Medicine and Biology Society*, pages 4314–4317. IEEE, 2008.

[82] M. Dafotakis, R. Sparing, S. B. Eickhoff, G. R. Fink, and D. A. Nowak. On the role of the ventral premotor cortex and anterior intraparietal area for predictive and reactive scaling of grip force. *Brain research*, 1228:73–80, 2008.

[83] G. Prabhu, M. Voss, T. Brochier, L. Cattaneo, P. Haggard, and R. Lemon. Excitability of human motor cortex inputs prior to grasp. *The Journal of physiology*, 581(1):189–201, 2007.

[84] M. N. Loh, L. Kirsch, J. C. Rothwell, R. N. Lemon, and M. Davare. Information about the weight of grasped objects from vision and internal models interacts within the primary motor cortex. *Journal of Neuroscience*, 30(20):6984–6990, 2010.

[85] R. S. Johansson and G. Westling. Signals in tactile afferents from the fingers eliciting adaptive motor responses during precision grip. *Experimental brain research*, 66(1):141–154, 1987.

[86] R. S. Johansson and J. R. Flanagan. Coding and use of tactile signals from the fingertips in object manipulation tasks. *Nature Reviews Neuroscience*, 10(5):345, 2009.

[87] J. R. Flanagan and A. M. Wing. Modulation of grip force with load force during point-to-point arm movements. *Experimental Brain Research*, 95(1):131–143, 1993.

[88] F. J. Valero-Cuevas and M. Santello. On neuromechanical approaches for the study of biological and robotic grasp and manipulation. *Journal of neuroengineering and rehabilitation*, 14(1):101, 2017.

[89] S. Faugier-Grimaud, C. Frenois, and D. G. Stein. Effects of posterior parietal lesions on visually guided behavior in monkeys. *Neuropsychologia*, 16(2):151–168, 1978.

[90] A. C. Roy, Y. Paulignan, A. Farne, C. Jouffrais, and D. Boussaoud. Hand kinematics during reaching and grasping in the macaque monkey. *Behavioural brain research*, 117(1-2):75–82, 2000.

[91] M. I. Christel and A. Billard. Comparison between macaques' and humans' kinematics of prehension: the role of morphological differences and control mechanisms. *Behavioural brain research*, 131(1-2):169–184, 2002.

[92] P. T. Fox and M. E. Raichle. Focal physiological uncoupling of cerebral blood flow and oxidative metabolism during somatosensory stimulation in human subjects. *Proceedings of the National Academy of Sciences*, 83(4):1140–1144, 1986.

[93] P. A. Bandettini, A. Jesmanowicz, E. C. Wong, and J. S. Hyde. Processing strategies for time-course data sets in functional mri of the human brain. *Magnetic resonance in medicine*, 30(2):161–173, 1993.

[94] N. K. Logothetis, J. Pauls, M. Augath, T. Trinath, and A. Oeltermann. Neurophysiological investigation of the basis of the fmri signal. *Nature*, 412(6843):150, 2001.

[95] A. Pascual-Leone, V. Walsh, and J. Rothwell. Transcranial magnetic stimulation in cognitive neuroscience–virtual lesion, chronometry, and functional connectivity. *Current opinion in neurobiology*, 10(2):232–237, 2000.

[96] J. C. Culham, C. Cavina-Pratesi, and A. Singhal. The role of parietal cortex in visuomotor control: what have we learned from neuroimaging? *Neuropsychologia*, 44(13):2668–2684, 2006.

[97] U. Castiello. The neuroscience of grasping. *Nature Reviews Neuroscience*, 6(9):726, 2005.

[98] G. Kroliczak, T. D. McAdam, D. .J Quinlan, and J. C. Culham. The human dorsal stream adapts to real actions and 3d shape processing: a functional magnetic resonance imaging study. *Journal of neurophysiology*, 100(5):2627–2639, 2008.

[99] C. Grefkes and G. R. Fink. The functional organization of the intraparietal sulcus in humans and monkeys. *Journal of anatomy*, 207(1):3–17, 2005.

[100] E. Tunik, N. J. Rice, A. Hamilton, and S. T. Grafton. Beyond grasping: representation of action in human anterior intraparietal sulcus. *Neuroimage*, 36:T77–T86, 2007.

[101] G. J. P. Savelsbergh, B. Steenbergen, and J. Van der Kamp. The role of fragility information in the guidance of the precision grip. *Human Movement Science*, 15(1):115–127, 1996.

[102] R. J. Bootsma, R. G. Marteniuk, C. L. MacKenzie, and F. T. J. M. Zaal. The speed-accuracy trade-off in manual prehension: effects of movement amplitude, object size and object width on kinematic characteristics. *Experimental brain research*, 98(3):535–541, 1994.

[103] P. L. Weir, C. L. MacKenzie, R. G. Marteniuk, and S. L. Cargoe. Is object texture a constraint on human prehension!: Kinematic evidence. *Journal of Motor Behavior*, 23(3):205–210, 1991.

[104] P. L. Weir, C. L. MacKenzie, R. G. Marteniuk, S. L. Cargoe, and M. B. Frazer. The effects of object weight on the kinematics of prehension. *Journal of Motor Behavior*, 23(3):192–204, 1991.

[105] R. S. Johansson and G. Westling. Coordinated isometric muscle commands adequately and erroneously programmed for the weight during lifting task with precision grip. *Experimental brain research*, 71(1):59–71, 1988.

[106] A. M. Gordon, H. Forssberg, R. S. Johansson, and G. Westling. Visual size cues in the programming of manipulative forces during precision grip. *Experimental brain research*, 83(3):477–482, 1991.

[107] C. Ansuini, M. Santello, S. Massaccesi, and U. Castiello. Effects of end-goal on hand shaping. *Journal of neurophysiology*, 95(4):2456–2465, 2006.

[108] C. Ansuini, L. Giosa, L. Turella, G. Altoè, and U. Castiello. An object for an action, the same object for other actions: effects on hand shaping. *Experimental Brain Research*, 185(1):111–119, 2008.

[109] R. G. Cohen and D. A. Rosenbaum. Where grasps are made reveals how grasps are planned: generation and recall of motor plans. *Experimental Brain Research*, 157(4):486–495, 2004.

[110] C. Armbrüster and W. Spijkers. Movement planning in prehension: do intended actions influence the initial reach and grasp movement? *Motor control*, 10(4):311–329, 2006.

[111] K. L. Moore, A. F. Dalley, and A. M. R. Agur. *Clinically oriented anatomy*. Lippincott Williams & Wilkins, 2013.

[112] M. A. Baumann, M. C. Fluet, and H. Scherberger. Context-specific grasp movement representation in the macaque anterior intraparietal area. *Journal of Neuroscience*, 29(20):6436–6448, 2009.

[113] G. Rizzolatti, R. Camarda, L. Fogassi, M. Gentilucci, G. Luppino, and M. Matelli. Functional organization of inferior area 6 in the macaque monkey. *Experimental brain research*, 71(3):491–507, 1988.

[114] M. C. Fluet, M. A Baumann, and H. Scherberger. Context-specific grasp movement representation in macaque ventral premotor cortex. *Journal of Neuroscience*, 30(45):15175–15184, 2010.

[115] U. Castiello and C. Begliomini. The cortical control of visually guided grasping. *The Neuroscientist*, 14(2):157–170, 2008.

[116] A. Bosco, R. Breveglieri, E. Chinellato, C. Galletti, and P. Fattori. Reaching activity in the medial posterior parietal cortex of monkeys is modulated by visual feedback. *Journal of Neuroscience*, 30(44):14773–14785, 2010.

[117] P. B. Johnson, S. Ferraina, L. Bianchi, and R. Caminiti. Cortical networks for visual reaching: physiological and anatomical organization of frontal and parietal lobe arm regions. *Cerebral Cortex*, 6(2):102–119, 1996.

[118] R. Caminiti, P. B. Johnson, C. Galli, S. Ferraina, and Y. Burnod. Making arm movements within different parts of space: the premotor and motor cortical representation of a coordinate system for reaching to visual targets. *Journal of Neuroscience*, 11(5):1182–1197, 1991.

[119] M. Davare, A. Kraskov, J. C. Rothwell, and R. N. Lemon. Interactions between areas of the cortical grasping network. *Current opinion in neurobiology*, 21(4):565–570, 2011.

[120] L. Turella and A. Lingnau. Neural correlates of grasping. *Frontiers in human neuroscience*, 8:686, 2014.

[121] K. L. Macuga and S. H. Frey. Neural representations involved in observed, imagined, and imitated actions are dissociable and hierarchically organized. *Neuroimage*, 59(3):2798–2807, 2012.

[122] G. Rizzolatti and G. Luppino. The cortical motor system. *Neuron*, 31(6):889–901, 2001.

[123] F. Filimon. Human cortical control of hand movements: parietofrontal networks for reaching, grasping, and pointing. *The Neuroscientist*, 16(4):388–407, 2010.

[124] R. S. Johansson and G. Westling. Roles of glabrous skin receptors and sensorimotor memory in automatic control of precision grip when lifting rougher or more slippery objects. *Experimental brain research*, 56(3):550–564, 1984.

[125] A. W. Goodwin, P. Jenmalm, and R. S. Johansson. Control of grip force when tilting objects: effect of curvature of grasped surfaces and applied tangential torque. *Journal of Neuroscience*, 18(24):10724–10734, 1998.

[126] A. M. Wing and S. J. Lederman. Anticipatory load torques produced by voluntary movements. *Journal of Experimental Psychology: Human Perception and Performance*, 24(6):1571, 1998.

[127] R. S. Johansson, J. L. Backlin, and Magnus K. O. Burstedt. Control of grasp stability during pronation and supination movements. *Experimental Brain Research*, 128(1-2):20–30, 1999.

[128] J. R. Flanagan and A. M. Wing. The stability of precision grip forces during cyclic arm movements with a hand-held load. *Experimental brain research*, 105(3):455–464, 1990.

[129] J. R. Flanagan and J. R. Tresilian. Grip-load force coupling: a general control strategy for transporting objects. *Journal of Experimental Psychology: Human Perception and Performance*, 20(5):944, 1994.

[130] R. S. Johansson and G. Westling. Programmed and triggered actions to rapid load changes during precision grip. *Experimental brain research*, 71(1):72–86, 1988.

[131] A. G. Witney, S. J. Goodbody, and D. M. Wolpert. Predictive motor learning of temporal delays. *Journal of Neurophysiology*, 82(5):2039–2048, 1999.

[132] J. R. Flanagan and A. M. Wing. The role of internal models in motion planning and control: evidence from grip force adjustments during movements of hand-held loads. *Journal of Neuroscience*, 17(4):1519–1528, 1997.

[133] J. R. Flanagan, P. Vetter, R. S. Johansson, and D. M. Wolpert. Prediction precedes control in motor learning. *Current Biology*, 13(2):146–150, 2003.

[134] G. Cadoret and A. M. Smith. Friction, not texture, dictates grip forces used during object manipulation. *Journal of Neurophysiology*, 75(5):1963–1969, 1996.

[135] P. Jenmalm and R. S. Johansson. Visual and somatosensory information about object shape control manipulative fingertip forces. *Journal of Neuroscience*, 17(11):4486–4499, 1997.

[136] P. Jenmalm, S. Dahlstedt, and R. S. Johansson. Visual and tactile information about object-curvature control fingertip forces and grasp kinematics in human dexterous manipulation. *Journal of neurophysiology*, 84(6):2984–2997, 2000.

[137] Y. Bekiroglu, C. Smith, Y. Karayiannidis, D. Kragic, et al. Predicting slippage and learning manipulation affordances through gaussian process regression. In *2013 13th IEEE-RAS International Conference on Humanoid Robots (Humanoids)*, pages 462–468. IEEE, 2013.

[138] P. Dzitac, A. M. Mazid, M. Y. Ibrahim, G. K. Appuhamillage, and T. A. Choudhury. Optimal sensing requirement for slippage prevention in robotic grasping. In *2015 IEEE International Conference on Industrial Technology (ICIT)*, pages 373–378. IEEE, 2015.

[139] G. De Maria, P. Falco, C. Natale, and S. Pirozzi. Integrated force/tactile sensing: The enabling technology for slipping detection and avoidance. In *2015 IEEE International Conference on Robotics and Automation (ICRA)*, pages 3883–3889. IEEE, 2015.

[140] E. Moreira, L. F. Rocha, A. M. Pinto, A. P. Moreira, and G. Veiga. Assessment of robotic picking operations using a 6 axis force/torque sensor. *IEEE Robotics and Automation Letters*, 1(2):768–775, 2016.

[141] S. Teshigawara, T. Tsutsumi, S. Shimizu, Y. Suzuki, A. Ming, M. Ishikawa, and M. Shimojo. Highly sensitive sensor for detection of initial slip and its application in a multi-fingered robot

hand. In *2011 IEEE International Conference on Robotics and Automation*, pages 1097–1102. IEEE, 2011.

[142] Y. Ma, Y. Huang, L. Mao, P. Liu, C. Liu, and Y. Ge. Pre-sliding detection in robot hand grasping based on slip-tactile sensor. In *2015 IEEE International Conference on Robotics and Biomimetics (ROBIO)*, pages 2603–2608. IEEE, 2015.

[143] E. D. Engeberg and S. G. Meek. Adaptive object slip prevention for prosthetic hands through proportional-derivative shear force feedback. In *2008 IEEE/RSJ International Conference on Intelligent Robots and Systems*, pages 1940–1945. IEEE, 2008.

[144] M. T. Francomano, D. Accoto, and E. Guglielmelli. Artificial sense of slip—a review. *IEEE Sensors Journal*, 13(7):2489–2498, 2013.

[145] E. D. Engeberg and S. G. Meek. Adaptive sliding mode control for prosthetic hands to simultaneously prevent slip and minimize deformation of grasped objects. *IEEE/ASME Transactions on Mechatronics*, 18(1):376–385, 2011.

[146] S. Qiao, D. M. Beloiu, and R. A. Ibrahim. Deterministic and stochastic characterization of friction-induced vibration in disc brakes. *Nonlinear dynamics*, 36(2-4):361–378, 2004.

[147] M. Stachowsky, T. Hummel, M. Moussa, and H. A. Abdullah. A slip detection and correction strategy for precision robot grasping. *IEEE/ASME Transactions on Mechatronics*, 21(5):2214–2226, 2016.

[148] J. A. Fishel, V. J. Santos, and G. E. Loeb. A robust micro-vibration sensor for biomimetic fingertips. In *2008 2nd IEEE RAS & EMBS International Conference on Biomedical Robotics and Biomechatronics*, pages 659–663. IEEE, 2008.

[149] N. Wettels, V. J. Santos, R. S. Johansson, and G. E. Loeb. Biomimetic tactile sensor array. *Advanced Robotics*, 22(8):829–849, 2008.

[150] A. Ajoudani, E. Hocaoglu, A. Altobelli, M. Rossi, E. Battaglia, N. Tsagarakis, and A. Bicchi. Reflex control of the pisa/iit softhand during object slippage. In *2016 IEEE International Con-*

ference on Robotics and Automation (ICRA), pages 1972–1979. IEEE, 2016.

[151] R. A. Romeo, C. Oddo, M. C. Carrozza, E. Guglielmelli, and L. Zollo. Slippage detection with piezoresistive tactile sensors. *Sensors*, 17(8):1844, 2017.

[152] Y. Cheng, C. Su, Y. Jia, and N. Xi. Data correlation approach for slippage detection in robotic manipulations using tactile sensor array. In *2015 IEEE/RSJ International Conference on Intelligent Robots and Systems (IROS)*, pages 2717–2722. IEEE, 2015.

[153] Y. Zhang, X. G. Duan, G. Zhong, and H. Deng. Initial slip detection and its application in biomimetic robotic hands. *IEEE Sensors Journal*, 16(19):7073–7080, 2016.

[154] P. L. Ko, M. C. Taponat, and R. Pfaifer. Friction-induced vibration—with and without external disturbance. *Tribology international*, 34(1):7–24, 2001.

[155] W. S. Owen and E. A. Croft. The reduction of stick-slip friction in hydraulic actuators. *IEEE/ASME transactions on mechatronics*, 8(3):362–371, 2003.

[156] G. Sriram, A. N. Jensen, and S. C. Chiu. Slippage control for a smart prosthetic hand prototype via modified tactile sensory feedback. In *IEEE international conference on electro/information technology*, pages 225–230. IEEE, 2014.

[157] K. F. Anderson. The new current loop: An instrumentation and measurement circuit topology. *IEEE transactions on instrumentation and measurement*, 46(5):1061–1067, 1997.

[158] J. Zhao, L. Jiang, S. Shi, H. Cai, H. Liu, and G. Hirzinger. A five-fingered underactuated prosthetic hand system. In *2006 International Conference on Mechatronics and Automation*, pages 1453–1458. Ieee, 2006.

[159] A. B. Ajiboye and R. F. Weir. A heuristic fuzzy logic approach to emg pattern recognition for multifunctional prosthesis control. *IEEE Transactions on Neural Systems and Rehabilitation Engineering*, 13(3):280–291, 2005.

[160] K. F. Anderson. Nasa's anderson loop. *IEEE Instrumentation & Measurement Magazine*, 1(1):5–15, 1998.

[161] W. W. T. G. Peterson, T. Birdsall, and W. Fox. The theory of signal detectability. *Transactions of the IRE professional group on information theory*, 4(4):171–212, 1954.

[162] P. Wan, C. Wu, Y. Lin, and X. Ma. On-road experimental study on driving anger identification model based on physiological features by roc curve analysis. *IET Intelligent Transport Systems*, 11(5):290–298, 2017.

[163] J. A. Hanley and B. J. McNeil. The meaning and use of the area under a receiver operating characteristic (roc) curve. *Radiology*, 143(1):29–36, 1982.

[164] J. A. Swets. Measuring the accuracy of diagnostic systems. *Science*, 240(4857):1285–1293, 1988.

[165] F. P. Bowden and D. Tabor. Friction and lubrication. 1956.

[166] E. Rabinowicz. Stick and slip. *Scientific American*, 194(5):109–118, 1956.

[167] E. Rabinowicz. The intrinsic variables affecting the stick-slip process. *Proceedings of the Physical Society*, 71(4):668, 1958.

[168] F. di Liberto, E. Balzano, M. Serpico, and F. Peruggi. Dinamica stick-slip: Oscillazioni con attrito, 2007.

[169] C. Schwarz. The slip hypothesis: tactile perception and its neuronal bases. *Trends in neurosciences*, 39(7):449–462, 2016.

[170] J. C. Butcher. *Numerical methods for ordinary differential equations*. John Wiley & Sons, 2016.

[171] FSR Datasheet. Model 400. interlink electronics.

[172] JR3 Inc. Datasheet. Model jr3 multi - axis force - torque sensor.

[173] A. Albu-Schäffer, S. Haddadin, C. Ott, A. Stemmer, T. Wimböck, and G. Hirzinger. The dlr lightweight robot: design and control concepts for robots in human environments. *Industrial Robot: an international journal*, 34(5):376–385, 2007.

[174] R. A. Romeo, F. Cordella, L. Zollo, D. Formica, P. Saccomandi, E. Schena, G. Carpino, A. Davalli, R. Sacchetti, and E. Guglielmelli. Development and preliminary testing of an instrumented object for force analysis during grasping. In *2015 37th Annual International Conference of the IEEE Engineering in Medicine and Biology Society (EMBC)*, pages 6720–6723. IEEE, 2015.

[175] Prensilia s.r.l Datasheet. *IH2 Azzurra robotic hand*.

[176] L. Zollo, S. Roccella, E. Guglielmelli, M. C. Carrozza, and P. Dario. Biomechatronic design and control of an anthropomorphic artificial hand for prosthetic and robotic applications. *IEEE/ASME Transactions On Mechatronics*, 12(4):418–429, 2007.

[177] M. J. Adams, S. A Johnson, P. Lefèvre, V. Lévesque, V. Hayward, T. André, and J. L. Thonnard. Finger pad friction and its role in grip and touch. *Journal of The Royal Society Interface*, 10(80):20120467, 2013.

[178] J. M. Romano, K. Hsiao, G. Niemeyer, S. Chitta, and K. J. Kuchenbecker. Human-inspired robotic grasp control with tactile sensing. *IEEE Transactions on Robotics*, 27(6):1067–1079, 2011.

[179] D. Goeger, N. Ecker, and H. Woern. Tactile sensor and algorithm to detect slip in robot grasping processes. In *2008 IEEE International Conference on Robotics and Biomimetics*, pages 1480–1485. IEEE, 2009.

[180] J. Jo, S. K. Kim, Y. Oh, and S. R. Oh. Contact force control of a robotic hand using f/t sensory feedback with a rigid object. In *2012 IEEE International Conference on Automation Science and Engineering (CASE)*, pages 436–441. IEEE, 2012.

[181] M. R. Cutkosky and R. D. Howe. Human grasp choice and robotic grasp analysis. In *Dextrous robot hands*, pages 5–31. Springer, 1990.

[182] N. Morita, H. Nogami, E. Higurashi, and R. Sawada. Grasping force control for a robotic hand by slip detection using developed micro laser doppler velocimeter. *Sensors*, 18(2):326, 2018.

[183] Z. Ding, N. Paperno, K. Prakash, and A. Behal. An adaptive control-based approach for 1-click gripping of novel objects using a robotic manipulator. *IEEE Transactions on Control Systems Technology*, 27(4):1805–1812, 2018.

[184] F. Riillo, L. R. Quitadamo, F. Cavrini, E. Gruppioni, C. A. Pinto, N. C. Pastò, L. Sbernini, L. Albero, and G. Saggio. Optimization of emg-based hand gesture recognition: Supervised vs. unsupervised data preprocessing on healthy subjects and transradial amputees. *Biomedical Signal Processing and Control*, 14:117–125, 2014.

[185] A. Dellacasa Bellingegni, E. Gruppioni, G. Colazzo, A. Davalli, R. Sacchetti, W. Guglielmelli, and L. Zollo. Nlr, mlp, svm, and lda: a comparative analysis on emg data from people with transradial amputation. *Journal of neuroengineering and rehabilitation*, 14(1):82, 2017.

[186] F. Duan, L. Dai, W. Chang, Z. Chen, C. Zhu, and W. Li. semg-based identification of hand motion commands using wavelet neural network combined with discrete wavelet transform. *IEEE Trans. Industrial Electronics*, 63(3):1923–1934, 2016.

[187] P. Geethanjali. Myoelectric control of prosthetic hands: state-of-the-art review. *Medical Devices (Auckland, NZ)*, 9:247, 2016.

[188] T. A. Kuiken, G. A. Dumanian, R. D. Lipschutz, L. A. Miller, and K. A. Stubblefield. Targeted muscle reinnervation for improved myoelectric prosthesis control. In *Conference Proceedings. 2nd International IEEE EMBS Conference on Neural Engineering, 2005.*, pages 396–399. IEEE, 2005.

[189] T. A. Kuiken, D. S. Childress, and W. Z. Rymer. The hyper-reinnervation of rat skeletal muscle. *Brain research*, 676(1):113–123, 1995.

[190] T. A. Kuiken, G. A. Dumanian, L. A. Lipschutz, R. D.and Miller, and KA Stubblefield. The use of targeted muscle reinnervation for improved myoelectric prosthesis control in a bilateral shoulder disarticulation amputee. *Prosthetics and orthotics international*, 28(3):245–253, 2004.

[191] Ottobock. https://bit.ly/36vsxph.

[192] J. Kobayashi, O. Mackinnon, S. E.and Watanabe, X. Ball, D. J.and Ming Gu, and W. M. Hunter, D. A.and Kuzon Jr. The effect of duration of muscle denervation on functional recovery in the rat model. *Muscle & Nerve: Official Journal of the American Association of Electrodiagnostic Medicine*, 20(7):858–866, 1997.

[193] Y. Xu, D. Zhang, Y. Wang, J. Feng, and W. Xu. Two ways to improve myoelectric control for a transhumeral amputee after targeted muscle reinnervation: a case study. *Journal of neuroengineering and rehabilitation*, 15(1):37, 2018.

[194] T. A. Kuiken, G. Li, B. A. Lock, R. D. Lipschutz, L. A. Miller, K. A. Stubblefield, and Kevin B Englehart. Targeted muscle reinnervation for real-time myoelectric control of multifunction artificial arms. *Jama*, 301(6):619–628, 2009.

[195] A. M. Simon, L. J. Hargrove, B. A. Lock, and T. A. Kuiken. The target achievement control test: Evaluating real-time myoelectric pattern recognition control of a multifunctional upper-limb prosthesis. *Journal of rehabilitation research and development*, 48(6):619, 2011.

[196] G. S. Dhillon and K. W. Horch. Direct neural sensory feedback and control of a prosthetic arm. *IEEE transactions on neural systems and rehabilitation engineering*, 13(4):468–472, 2005.

[197] P. M. Rossini, S. Micera, A. Benvenuto, J. Carpaneto, G. Cavallo, L. Citi, C. Cipriani, L. Denaro, V. Denaro, G. Di Pino, et al. Double nerve intraneural interface implant on a human amputee for robotic hand control. *Clinical neurophysiology*, 121(5):777–783, 2010.

[198] S. Raspopovic, M. Capogrosso, F. M. Petrini, M. Bonizzato, J. Rigosa, G. Di Pino, J. Carpaneto, M. Controzzi, T. Boretius, E. Fernandez, et al. Restoring natural sensory feedback in real-time bidirectional hand prostheses. *Science translational medicine*, 6(222):222ra19–222ra19, 2014.

[199] M. Ortiz-Catalan, B. Håkansson, and R. Brånemark. An osseointegrated human-machine gateway for long-term sensory feedback and motor control of artificial limbs. *Science translational medicine*, 6(257):257re6–257re6, 2014.

[200] Touch Bionics s.r.l. Datasheet. *RoboLimb robotic hand*.

[201] W. Poppendieck, S. Muceli, J. Dideriksen, E. Rocon, J. L. Pons, D. Farina, and K. P. Hoffmann. A new generation of double-sided intramuscular electrodes for multi-channel recording and stimulation. In *2015 37th Annual International Conference of the IEEE Engineering in Medicine and Biology Society (EMBC)*, pages 7135–7138. IEEE, 2015.